Numerical methods for mass transport equations in two-phase incompressible flows

Von der Fakultät für Mathematik, Informatik und Naturwissenschaften der RWTH Aachen University zur Erlangung des akademischen Grades eines Doktors der Naturwissenschaften genehmigte Dissertation

vorgelegt von

Master of Science Trung Hieu Nguyen

aus Hanoi, Vietnam

Berichter: Universitätsprofessor Dr. Arnold Reusken
Universitätsprofessor Dr. Siegfried Müller

Tag der mündlichen Prüfung: 08. Dezember 2009

Acknowledgements

First of all, I would like to express my gratitude to my advisor Prof. Arnold Reusken, for his invaluable support, guidance and patience during the course of this work. I sincerely thank my second referee Prof. Siegfried Müller for taking a thorough reading of this thesis and for his many valuable comments.

Many thanks to my colleagues at the IGPM for the great working atmosphere. I am grateful to Jörg Grande, Sven Groß, Volker Reichelt, Maxim Larin, Eva Loch and Patrick Esser for many valuable ideas, suggestions and helps. Thank you Jörg for your willingness to help at any time. I thank Evangelos Bertakis at the Chair of Thermal Process Engineering for the helpfull discussions on the topic of mass transport process and for kindly providing me the simulation data and figures in Chapter 4.

Finally and foremost, I wish to express my deepest gratitude to my parents and my brother for their love, understanding and support throughout my life. Special thanks go to my wife Hong Nhung and our children Duc and Thanh for your love, patience and encouragement as well as for the sacrifices you made to support and accompany me during my PhD in Aachen.

Abstract

In this thesis, we presented numerical methods for discretizing and solving the mass transport problem in two-phase flows. The level set method is used for capturing the time-dependent interface. The motion of the fluid is described by the two-phase Navier-Stokes equations. For the spatial discretization of these equations we use the known methods in the literature, namely the *improved* Laplace-Beltrami discretization for the surface force and the extended finite element (XFEM) for the pressure approximation. The combination of these methods delivers optimal error bounds when the surface tension coefficient is constant. For the general case with a variable surface tension coefficient, we introduce a new discretization of the localized surface force term.

The solution of the mass transport equation must satisfy certain interface conditions, which imply that in general both the concentration and its derivatives are discontinuous across the interface. A simple transformation is often used in the literature to eliminate the discontinuity of the solution, which, however, results in a suboptimal approximation error bound $\mathcal{O}(h^{\frac{1}{2}})$ in the L^2 norm for the finite element discretization. We use the Nitsche-XFEM method to handle the Henry condition and obtain an optimal error estimate $\mathcal{O}(h^2)$ in the L^2-norm for the spatial discretization in the case of a *stationary* interface. The semi-discretization resulting from the Nitsche-XFEM method is combined with the standard θ-scheme and an optimal time discretization error bound is also obtained. This method can also be applied for problem with moving interface but a full error analysis is not available.

Finally, we performed numerical simulations of the coupled two-phase Navier-Stokes and mass transport equations for rising droplet problems for both cases of constant and concentration-dependent surface tension coefficients. For the latter case, different phenomena were observed, such as the occurrence of the so-called *stagnant cap* in the velocity field and a significant

change in the droplet rising velocity. Due to the absence of a stabilization method for the discretization of the mass transport problem, we restrict ourselves to the case of medium diffusivity instead of the physically correct (much smaller) diffusivity. Effects of the initial concentration and the size of the convection (relative to the diffusion) on the droplet rising velocity and the droplet concentration at steady state are investigated.

Zusammenfassung

In der vorliegenden Doktorarbeit präsentieren wir numerische Methoden, um das Stofftransportproblems bei Zweiphasenströmungen zu diskretisieren und zu lösen. Zur Beschreibung der zeitabhängigen Grenzfläche wird die Levelsetmethode verwendet. Die Bewegung des Fluids wird mit Hilfe der zweiphasigen Navier-Stokes-Gleichungen beschrieben. Für die räumliche Diskretisierung benutzen wir in der Literatur bekannte Methoden aus *verbesserter* Laplace-Beltrami-Diskretisierung der Grenzflächenspannung und erweiterten finiten Elementen (XFEM) für den Druck. Diese Kombination liefert im Fall eines konstanten Grenzflächenspannungkoeffizienten optimale Fehlerschranken. Im allgemeinen Fall eines variablen Grenzflächenspannungkoeffizienten stellen wir eine neue Diskretisierung des lokalen Grenzflächenkraftterms vor.

Die Lösung der Stofftransportgleichung genügt zwei Bedingungen, die dazu führen, dass im allgemeinen sowohl die Konzentration als auch ihre Ableitung an der Grenzfläche unstetig sind. In Methoden aus der Literatur wird häufig eine einfache Transformation verwendet, um die Unstetigkeit zu eliminieren. Diese Transformation führt bei der Finite-Elemente-Diskretisierung zu einer suboptimalen Approximationsfehlerschranke $\mathcal{O}(h^{\frac{1}{2}})$ in der L^2-Norm. Wir setzen die Nitsche-XFEM-Methode ein, um die Henry-Bedingung zu erfüllen. Deshalb erhalten wir im Fall einer *stationären* Grenzfläche für die räumliche Diskretisierung eine optimale Fehlerschranke $\mathcal{O}(h^2)$ in der L^2-Norm. Die aus der Nitsche-XFEM-Methode resultierende Semidiskretisierung wird mit einem Standard-θ-Schema kombiniert. Wir zeigen eine optimale Fehlerschranke für die Zeitdiskretisierung. Die Methode kann auf Probleme mit beweglicher Grenzfläche angewendet werden, jedoch ist in diesem Fall keine vollständige Fehleranalyse verfügbar.

Abschließend führen wir numerische Simulationen mit den gekoppelten zweiphasigen Navier-Stokes- und Stofftransportgleichungen durch. Ein aufsteigender Tropfen wird sowohl mit konstantem als auch mit konzentrations-

abhängigem Grenzflächenspannungskoeffizienten simuliert. Im letzteren Fall treten im Vergleich zum ersteren neue Phänomene auf, zum Beispiel eine *starre Kappe* im Geschwindigkeitsfeld und eine signifikante Änderung der Aufstiegsgeschwindigkeit des Tropfens. Da keine Stabilisierung für die Diskretisierung des Stofftransportproblems implementiert wurde, beschränken wir uns auf den Fall mittlerer Diffusivität. Die physikalisch korrekte Diffusivität ist viel kleiner. In weiteren Simulationen wird der Effekt der Anfangskonzentration und der Konvektionsstärke (relativ zur Diffusion) auf die Aufstiegsgeschwindigkeit des Tropfens und auf die Stoffkonzentration im Tropfen im Gleichgewichtszustand untersucht.

Table of Contents

Chapter 1

Introduction

In recent years, the numerical simulation of two-phase flows, in which two immiscible fluids with different physical properties are separated by an interface, is a topic of growing interest in computational fluid dynamics. The motion of the flows is governed by the incompressible Navier-Stokes equations combined with coupling conditions at the interface. Several difficulties, which are absent in one-phase flows, arise when solving the two-phase flow problem, for example:

- The interface, which defines the two phases, is unknown and must be determined together with the flow variables.
- The surface tension force only acts at the interface.
- Due to the surface tension, the pressure usually has a jump at the interface, which requires special treatment.
- The coefficients of the Navier-Stokes (viscosity and density) are discontinuous across the interface.

As a consequence, numerical algorithms developed for one-phase flows cannot be directly applied for the simulation of two-phase flow problems.

Many methods have been used to describe the moving interface, most of which can be classified as either front-tracking or front-capturing techniques. In the front-tracking approach, the interface is often described explicitly, using a global moving grid or an additional mesh for the interface. Although the interface can be represented very accurately, this approach is ineffective for problems with large topological changes (break up or merging).

Frequent remeshing is also required to prevent deterioration of the moving mesh. Therefore, this approach is mainly used for one-phase flows with a slowly varying free boundary, cf. [Smo01]. In the front-capturing approach the interface is implicitly described by some phase indicator function. In this approach, a fixed unfitted mesh is used and the interface can be reconstructed from the indicator function if needed. The most popular methods are the volume-of-fluids (VOF) cf. [HN81, GW01] and the level set method cf. [OS88, Set96b]. The VOF method characterizes the interface using a volume fraction function of one certain phase in a volume cell. An nice property of this method is, that if it is combined with a conservative finite volume method, then mass is conserved. In the level set method, which is used in this thesis, the interface is determined by the zero level of a continuous scalar function in the computational domain. This method, as well as the VOF method, is capable of handling complicated topological changes. Disadvantages of the level set method are the deterioration of shape of the level set function during the advection of the interface and the relatively poor (compared to VOF) mass conservation properties. These require additional techniques such as, for example, reparametrization, to obtain a good approximation of the interface cf. [Set99, SSO94, KS98].

The local surface tension force depends on the curvature of the interface, and this involves second order derivatives. An accurate discretization of this force term using the finite element method is not straightforward. In the literature [Dzi91, GRR06, GR07a], a variational Laplace-Beltrami method has been presented in which only (tangential) first derivatives are required for the representation of the surface tension force. This representation requires a careful discretization as is shown in [GR07a]. The combination of the *improved* Laplace-Beltrami discretization for the surface force in [GR07a] and the extended finite element (XFEM) for the pressure approximation in [GR07b] delivers optimal error bound for the case of constant surface tension coefficient. Numerical simulations in [BGG$^+$08, EGR08] show the superiority of the XFEM method to the standard finite element one. For an overview of the finite element discretizations for the two-phase Navier-Stokes equations using level set methods, we refer to [GRR06, Gro08, Reu09].

In this thesis, we study the *instationary* two-phase Navier-Stokes equations *combined with mass transport* due to diffusion and convection of a third component between the two phases. One typical example is the mass transport from a droplet in the ambient fluid, which has many applications in chemical engineering, cf. [Gro08]. In the fluid dynamics combined with mass

transport model additional difficulties occur, such as

- the discontinuity of the diffusion coefficients in the mass transport equation due to the different phases,
- the solution of the mass transport equation must satisfy certain interface conditions, which imply that in general both the concentration and its derivatives are discontinuous across the interface,
- in many applications, the mass transport is dominated by convection, which requires stabilization techniques. Moreover, small values of the diffusion coefficients lead to very thin boundary layers. Thus a high resolution near the interface is needed.
- the surface tension coefficient may depend on the mass concentration in the vicinity of the interface, cf. [MBS85], which in turn affects the flow and the shape of the interface, resulting in a strongly nonlinear coupling between the Navier-Stokes and the mass transport equations *in both directions.*

A common technique to handle the jump of the concentration due to the so-called Henry's condition is to use a transformation, using the Henry's constant [YM05, WLW$^+$08, BKWW03, KAT07, WFW$^+$07] such that, a continuous transformed concentration is obtained. Then, however, the corresponding transformed velocity is discontinuous across the interface and a subdomain-dependent coefficient in front of the time derivative appears. The transformed problem is often discretized using a finite volume or finite difference method combined with some stabilization method such as e. g. WENO, Power-law methods..., cf. [YM05, WLW$^+$08]. In [KAT07], a standard finite element method is used to discretize the transformed problem. When the discrete solution of the derived problem is transformed back to the original variable, a suboptimal approximation error bound $\mathcal{O}(h^{\frac{1}{2}})$ in the L^2 norm is obtained. Thus there is a demand for improved finite element discretization methods for this type of problems. In this thesis such methods will be presented.

Simulations for static or moving droplets with mass transport can be found in the literature, e. g.[BKWW03, YM05, PW06, WFW$^+$07, WLW$^+$08]. However, most of these simulations use strongly simplifying assumptions. In [YM05], the mass transfer is only considered when the droplet already

reaches the steady state, i. e. the transport in the deformation stage is not considered. In [PW06, WFW$^+$07], the droplet is assumed to be spherical, which is only reasonable for sufficiently small droplets.

In [JL04, MC04, WFW$^+$07], simulations of two-phase flow problems with a concentration-dependent surface tension coefficient are carried out and Marangoni effects are investigated. Effects of the variable surface tension on the droplet terminal velocity and mass transport are investigated using numerical simulations and qualitatively validated by experiments. To our knowledge, numerical simulations with a variable surface tension coefficient based on finite element techniques are not known in the literature.

In this thesis, we focus on the following topics:

- The finite element discretization of the surface tension force with a *variable* surface tension coefficient.

- The Nitsche-XFEM discretization of the two-phase mass transport problem.

Starting from the *improved* Laplace-Beltrami technique presented in [GR07a] for the case of *constant* surface tension we develop a discretization of the localized surface force for the general case. Although no error analysis of the discretization has been obtained, the simulation in [EGR08] with a simple model of the variable surface tension coefficient using our implementation shows good agreement with experimental data from [ASB05].

The main topic of this thesis is a detailed study of the Nitsche-XFEM method for the discretization of the mass transport equation. Both theoretical analysis and applications of this method will be presented. The extended finite element method (cf. [MDB99, BMUP01]) is used to represent the discontinuity of the concentration while interface conditions are weakly enforced in the weak formulation using Nitsche's method. The Nitsche-XFEM combination has been used in [HH02] for a *stationary* pure diffusion problem in which the solution is continuous but has a kink at the interface. We extend the results in this paper for an *instationary* convection-diffusion problem with a discontinuous solution at the interface. For the case of a *stationary* interface, we obtain an optimal spatial discretization error bound $\mathcal{O}(h^2)$, cf. [RN09]. The semi-discretization resulting from the Nitsche-XFEM method is combined with the standard θ-scheme and an optimal time discretization error bound is also obtained. When applied to the reaction-convection-diffusion

problem resulting from the Rothe approach (time discretization before spatial discretization) for the case of a *moving* interface, the Nitsche-XFEM discretization results in a spatial discretization error bound which is only optimal in the H^1-norm. An error analysis for the full discretization is a topic of future research. In this thesis we study a Nitsche-XFEM method that is suitable for *diffusion-dominated* problems. When the diffusivity is very small (relative to the convection), as in many real processes, a stabilization technique is needed. For the Nitsche-XFEM discretization, such a stabilization is not available, yet.

The thesis is organized as follows. In Chapter 2, we introduce the governing equations for the two-phase flow and mass transport problems. The level set technique for capturing the interface is discussed. Spatial and time discretizations for the two-phase Navier-Stokes and level set equations are addressed in Chapter 3. In Chapter 4 we collect some main results from [GR07a] and present the new discretization for the surface tension force with a *variable* surface tension coefficient. The main results of the thesis are presented in Chapter 5, in which the mass transport problem with a *stationary* interface is analyzed. An error analysis for the full discretization (method of lines: semi-discretization combined with a θ-scheme time discretization) is obtained, with optimal bounds both for the spatial and time discretization error. The case of a moving interface is considered in Chapter 6. An analysis for the spatial discretization of a time-discretized problem (Rothe method) is given. In Chapter 7 we conduct several numerical simulations of the coupled two-phase Navier-Stokes and mass transport problem for rising droplet problems. Due to the absence of a stabilization method for the discretization of the mass transport problem and the limitations of memory and computation time, we restrict ourselves to the case of medium diffusivity instead of the physically correct (much smaller) diffusivity. Simulations with both constant and variable surface tension coefficients are considered to qualitatively investigate the Marangoni effect. A summary and outlook is presented in Chapter 8.

Chapter 2

Model for two-phase flow with mass transport

2.1 Two-phase flow Navier-Stokes equations

Let $\Omega \subset \mathbb{R}^d$, $d = 2, 3$, be a polygonal domain that contains two different immiscible incompressible phases. The (in general time dependent) subdomains containing the two phases are denoted by Ω_1, Ω_2, with $\bar{\Omega} = \bar{\Omega}_1 \cup \bar{\Omega}_2$. The interface $\Gamma = \Gamma(t)$ between the two phases $(\partial\Omega_1 \cap \partial\Omega_2)$ is assumed to be sufficiently smooth. We assume that the density ρ_i and the viscosity μ_i, $i = 1, 2$ are constant in each phase.

Let $\mathbf{u}(\mathbf{x}, t)$ and $p(\mathbf{x}, t)$ be the velocity and pressure. The conservation of mass and momentum leads to the Navier-Stokes equations in each phase Ω_i, $i = 1, 2$

$$\begin{cases} \rho_i\big(\frac{\partial \mathbf{u}}{\partial t} + (\mathbf{u}\cdot\nabla)\mathbf{u}\big) = -\nabla p + \rho_i \mathbf{g} + \operatorname{div}(\mu_i \mathbf{D}(\mathbf{u})) & \text{in } \Omega_i \\ \operatorname{div} \mathbf{u} = 0 & \text{in } \Omega_i \end{cases} \quad \text{for } i = 1, 2,$$

where $\mathbf{g}$ is an external force and $\mathbf{D}(\mathbf{u}) = \nabla\mathbf{u} + (\nabla\mathbf{u})^T$ is the deformation tensor.

We define the jump $[f]_\Gamma$ of a function f over the interface Γ by

$$[f]_\Gamma(x) = \lim_{h \downarrow 0} \big(f(x - h\mathbf{n}) - f(x + h\mathbf{n})\big) \quad x \in \Gamma$$

with $\mathbf{n} = \mathbf{n}_\Gamma$ the unit normal at the interface (pointing from Ω_1 in Ω_2). To model the forces at the interface we make the standard assumption that the

surface tension balances the jump of the normal stress on the interface, i. e., we have a free boundary condition

$$[\boldsymbol{\sigma}\mathbf{n}]_\Gamma = \tau\kappa\mathbf{n} - \nabla_\Gamma\tau,$$

with τ the surface tension coefficient , $\kappa = -\nabla\cdot\mathbf{n}$ the curvature of Γ and $\boldsymbol{\sigma}$ the stress tensor, i. e., $\boldsymbol{\sigma} = -p\mathbf{I} + \mu\mathbf{D}(\mathbf{u})$. The notation $\nabla_\Gamma = P\nabla$, with $P = I - \mathbf{n}\mathbf{n}^T$, is used for the tangential gradient. If the surface tension coefficient τ is assumed to be constant, the second term in the right hand side vanishes. In each phase Ω_i, $i = 1, 2$ the Navier-Stokes equations are obtained from the conservations of mass and momentum.

The continuum surface force (CSF) model [BKZ92, OS88] expresses the free boundary condition for the surface tension as a localized volume force f_Γ at the interface

$$f_\Gamma = \tau\kappa\delta_\Gamma\mathbf{n}_\Gamma \ .$$

Here δ_Γ is a Dirac δ-function with support on Γ. Its action on a smooth test function ψ is given by

$$\int_\Omega \delta_\Gamma(x)\psi(x)\,dx = \int_\Gamma \psi(s)\,ds \ .$$

Using this approach, we can derive the Navier-Stokes equations in the whole domain Ω.

Let the density ρ and viscosity μ be the piecewise constant coefficients, which equal ρ_i and μ_i in Ω_i, $i = 1, 2$, respectively. The Navier-Stokes equations can be written as follows

$$\begin{aligned} \rho\Big(\frac{\partial\mathbf{u}}{\partial t} + (\mathbf{u}\cdot\nabla)\mathbf{u}\Big) &= -\nabla p + \rho\mathbf{g} + \operatorname{div}(\mu\mathbf{D}(\mathbf{u})) + f_\Gamma \quad \text{in } \Omega \\ \operatorname{div}\mathbf{u} &= 0 \quad \text{in } \Omega \end{aligned} \tag{2.1}$$

This model should be interpreted in a suitable weak sense, cf. [Reu09]. In [Gro08], it is shown that the CSF model can be derived from conservation of momentum and mass in Ω.

Furthermore, we need boundary conditions on the boundary $\partial\Omega$ and an initial condition at $t = 0$. We assume that $\partial\Omega$ consists of two separated parts

$\partial\Omega = \partial\Omega_D \cup \partial\Omega_N$ with $\partial\Omega_D \cap \partial\Omega_N = \emptyset$. On the Dirichlet boundary $\partial\Omega_D$ we have the essential condition $\mathbf{u}(x,t) = \mathbf{u}_D(x,t)$. On the Neumann part $\partial\Omega_N$ the natural boundary condition has the form $\boldsymbol{\sigma}\mathbf{n}_\Omega = -p_{ext}\mathbf{n}_\Omega$, with $\mathbf{n}_\Omega$ the outward pointing normal vector on $\partial\Omega$ and p_{ext} a given external pressure. If $p_{ext} = 0$ we have a homogeneous Neumann boundary condition on $\partial\Omega_N$.

2.2 Mass transport of a dissolved species

In this section, we consider a model for the transport of a dissolved species in the two-phase flow. Let $c(x,t)$ denote the concentration of the species. In each phase the concentration is the solution of a standard parabolic convection-diffusion equation of the form:

$$\frac{\partial c_i}{\partial t} + \mathbf{u}\cdot\nabla c_i - \operatorname{div}(\alpha_i \nabla c_i) = 0 \quad \text{in } \Omega_i,$$

where $\mathbf{u}$ is the velocity field resulting from the two-phase flow problem and α_i denotes the diffusion coefficient in $\Omega_i,\ i = 1,2$.

At the interface, the mass flux is assumed to be continuous. According to Fick's law, we have the first interface condition

$$[\alpha\nabla c\cdot\mathbf{n}]_\Gamma = 0.$$

The diffusion coefficient α is assumed to be piecewise constant:

$$\alpha = \alpha_i > 0 \quad \text{in } \Omega_i.$$

In general we have $\alpha_1 \neq \alpha_2$.

The second condition comes from continuity of chemical potentials at the interface and is known as the Henry condition, cf. [Ish75, Sla99, SAC97, BKWW03, BKW$^+$04]:

$$[\beta c]_\Gamma = 0$$

In this condition the coefficient β is strictly positive and piecewise constant:

$$\beta = \beta_i > 0 \quad \text{in } \Omega_i.$$

In general we have $\beta_1 \neq \beta_2$, since species concentration usually has a jump discontinuity at the interface due to different solubility within the respective fluid phases. Hence, the solution c is *discontinuous across the interface*.

We obtain the two-phase mass transport equations in the following form

$$\frac{\partial c}{\partial t} + \mathbf{u} \cdot \nabla c - \operatorname{div}(\alpha \nabla c) = 0 \quad \text{in } \Omega, \text{ for } t \in [0, T], \tag{2.2}$$

$$[\alpha \nabla c \cdot \mathbf{n}]_\Gamma = 0, \tag{2.3}$$

$$[\beta c]_\Gamma = 0, \tag{2.4}$$

with suitable initial and boundary conditions.

2.3 Level set function

In the above-mentioned models it is necessary that the (generally) time-dependent interface Γ can be determined at any time t. Different methods to describe the moving interface are available in the literature, most of which can be classified as either front-tracking, cf. [UT92, Bän01], or front-capturing techniques, cf. [HN81, GW01, OS88, Set96b]. The level set method, introduced by Sethian and Osher [OS88], is a very popular the numerical technique for capturing the interface.

In this method, the interface is implicitly represented as the zero level of a scalar function $\phi(\mathbf{x}, t)$, i. e.

$$\Gamma(t) = \{x \in \Omega | \, \phi(\mathbf{x}, t) = 0\},$$

while the phases are indicated by the sign of this function. We make the convention that

$$\phi(\mathbf{x}, t) = \begin{cases} < 0 & \text{for } \mathbf{x} \text{ in } \Omega_1, \\ > 0 & \text{for } \mathbf{x} \text{ in } \Omega_2, \\ = 0 & \text{at the interface} \end{cases}$$

Assume that at $t = 0$, the interface and the two phases are described by the initial value of the level set $\phi(\mathbf{x}, 0) = \phi_0(\mathbf{x})$. We consider a single particle at the position $\mathbf{x}(0) = \mathbf{x}_0$ on the interface $\Gamma(0)$. As the interface evolves, at time $t > 0$, the particle still remains on the interface $\Gamma(t)$ and has the new position $\mathbf{x}(t)$. Thus we have $\phi(\mathbf{x}(t), t) = \phi(\mathbf{x}(0), 0) = 0$ for all $t \geq 0$. We extent this condition to the whole domain, i. e. $\phi(\mathbf{x}(t), t) = \phi(\mathbf{x}(0), 0) = const$ for all $\mathbf{x}$

in Ω and all $t \geq 0$. Differentiation yields

$$\begin{aligned} 0 &= \frac{d}{dt}\phi(\mathbf{x}(t), t) \\ &= \frac{\partial \phi}{\partial t}(\mathbf{x}(t), t) + \nabla \phi(\mathbf{x}, t) \cdot \frac{d\mathbf{x}}{dt}(t). \end{aligned}$$

As $\frac{d\mathbf{x}}{dt}(t) = \mathbf{u}(\mathbf{x}(t), t)$, the velocity of the particle at $(\mathbf{x}, t)$, we obtain the following level set equation

$$\frac{\partial \phi}{\partial t} + \mathbf{u} \cdot \nabla \phi = 0 \quad \text{in} \quad \Omega, \tag{2.5}$$

with initial condition $\phi(\mathbf{x}, 0) = \phi_0(\mathbf{x})$.

Note that the level set function ϕ is introduced for numerical purposes and has no physical meaning. Ideally, ϕ should be a signed distance function, i. e.

$$|\phi(\mathbf{x}, t)| = \text{dist}(\mathbf{x}, \Gamma(t))$$

which has the property $||\nabla \phi(\mathbf{x}, t)|| = 1$. However, a feasible form for such a function is not always available for a smooth initial interface $\Gamma(0)$. Hence, an approximation of the signed distance function will be used instead.

When the level set function is advanced, it will in general not remain close to the signed distance function and the norm of its gradient may become (very) different from 1. In this case, the level set function must be (frequently) replaced by a new approximate signed distance function with approximately the same zero level set. Different reparametrization methods can be used to stabilize the level set equation, for example the re-initialization method in [SSO94] and the Fast Marching Method, cf. [KS98, Set99]. Due to the reparametrization, the advection of the level set function according to (2.5) is used only in a short time interval. Thus, we can use the level set equation without any boundary condition. The finite element discretization of the level set equation is not mass-conserving. Additional techniques must be used to improve the mass conservation of the level set method.

Chapter 3

Discretization of the two-phase flow Navier-Stokes equations

In this chapter we present a discretization of the two-phase flow Navier-Stokes equations (2.1) combined with the level set equation (2.5), which is used to describe the interface. In Section 3.2 we consider the spatial discretization using the finite element method. Due to the discontinuity of the pressure across the interface, a special finite element space has to be employed to obtain an optimal approximation property. The hyperbolic level set equation is stabilized by the streamline diffusion technique. The discretization of the localized surface force is discussed in Chapter 4. The discretization methods in this chapter can be found in the literature [Gro08, RFG$^+$, Reu09].

3.1 Weak formulations

We consider the combination of the two-phase flow Navier-Stokes equations (2.1) and the level set equation (2.5) in Chapter 2

$$\begin{aligned} \rho(\phi)\Big(\frac{\partial \mathbf{u}}{\partial t} + (\mathbf{u}\cdot\nabla)\mathbf{u}\Big) &= -\nabla p + \rho(\phi)\mathbf{g} + \operatorname{div}(\mu(\phi)\mathbf{D}(\mathbf{u})) + f_\Gamma \\ \operatorname{div}\mathbf{u} &= 0 \\ \frac{\partial \phi}{\partial t} + \mathbf{u}\cdot\nabla\phi &= 0 \end{aligned} \tag{3.1}$$

with suitable boundary conditions and an initial condition for the Navier-Stokes equations and the level set equation. The coefficients ρ and μ are defined as

$$\begin{aligned} \rho(\phi) &:= \rho_1 + (\rho_2 - \rho_1)H(\phi), \\ \mu(\phi) &:= \mu_1 + (\mu_2 - \mu_1)H(\phi), \end{aligned} \tag{3.2}$$

with $H : \mathbb{R} \to \mathbb{R}$ is the Heaviside function:

$$H(\zeta) = 0 \quad \text{for} \;\; \zeta < 0 \;, \qquad H(\zeta) = 1 \quad \text{for} \;\; \zeta > 0 \;,$$

and $H(0) = \frac{1}{2}$ for convenience.

We introduce the following Hilbert spaces

$$\begin{aligned} \mathbf{V} &:= (H^1(\Omega))^3, \\ \mathbf{V}_0 &:= \{\, \mathbf{v} \in \mathbf{V} : \, \mathbf{v} = 0 \text{ on } \partial\Omega_D \,\}, \\ \mathbf{V}_D &:= \{\, \mathbf{v} \in \mathbf{V} : \, \mathbf{v} = \mathbf{u}_D \text{ on } \partial\Omega_D \,\}, \\ Q &:= L^2_0(\Omega) = \{\, q \in L^2(\Omega) : \, \int_\Omega q \, dx = 0 \,\}, \\ V &:= \{v \in L^2(\Omega) : \mathbf{u} \cdot \nabla v \in L^2(\Omega)\} \end{aligned}$$

and define the bilinear forms

$$\begin{aligned} m : L^2(\Omega)^3 \times L^2(\Omega)^3 \to \mathbb{R} \;\; : \quad & m(\mathbf{u}, \mathbf{v}) = \int_\Omega \rho(\phi)\, \mathbf{u} \cdot \mathbf{v} \, dx, \\ a : \mathbf{V} \times \mathbf{V} \to \mathbb{R} \;\; : \quad & a(\mathbf{u}, \mathbf{v}) = \frac{1}{2} \int_\Omega \mu(\phi) \; \mathrm{tr}\left(\mathbf{D}(\mathbf{u})\mathbf{D}(\mathbf{v})\right) \, dx, \\ b : \mathbf{V} \times Q \to \mathbb{R} \;\; : \quad & b(\mathbf{u}, q) = \int_\Omega q \, \mathrm{div}\, \mathbf{u} \, dx, \end{aligned}$$

and the trilinear form

$$c : \mathbf{V} \times \mathbf{V} \times \mathbf{V} \to \mathbb{R} \;\; : \quad c(\mathbf{u}; \mathbf{v}, \mathbf{w}) = \int_\Omega \rho(\phi) \, (\mathbf{u} \cdot \nabla \mathbf{v}) \cdot \mathbf{w} \, dx.$$

We consider the following weak formulation of (3.1):

Find $\mathbf{u}(t) \in \mathbf{V}_D, p(t) \in Q$ and $\phi(t) \in V$ such that

$$\begin{aligned} m(\frac{\partial \mathbf{u}(t)}{\partial t}, \mathbf{v}) + a(\mathbf{u}(t), \mathbf{v}) + c(\mathbf{u}(t); \mathbf{u}(t), \mathbf{v}) - b(\mathbf{v}, p(t)) & \\ = m(\mathbf{g}, \mathbf{v}) + f_\Gamma(\mathbf{v}) \quad \text{for all } v \in \mathbf{V}_0 & \\ b(\mathbf{u}(t), q) = 0 \quad \text{for all } q \in Q & \qquad (3.3) \\ (\frac{\partial \phi(t)}{\partial t}, v)_0 + (\mathbf{u}(t) \cdot \nabla \phi(t), v)_0 = 0 \quad \text{for all } v \in L^2(\Omega) & \end{aligned}$$

with

$$f_\Gamma(\mathbf{v}) = \int_\Omega \left(\tau\kappa\delta_\Gamma \mathbf{n}_\Gamma - \nabla_\Gamma \tau \delta_\Gamma\right) \cdot \mathbf{v}\, dx = \int_\Gamma \left(\tau\kappa \mathbf{n}_\Gamma - \nabla_\Gamma \tau\right) \cdot \mathbf{v}\, ds. \quad (3.4)$$

The time derivatives $\frac{\partial \mathbf{u}}{\partial t}$ and $\frac{\partial \phi}{\partial t}$ should be interpreted in a suitable weak sense, cf. [Reu09]. Here δ_Γ denotes a Dirac distribution and ∇_Γ denotes the tangential gradient.

3.2 Spatial discretization

3.2.1 Multilevel triangulation

The finite element discretization of the Navier-Stokes and level set equations (3.1) in this section is based on a multilevel grid hierarchy, which is convenient for local refinement and coarsening as well as for multigrid methods to solve the resulting linear system. Below we present some basic definitions from [GR05]. For more details on multilevel refinement (and coarsening) strategies, we refer to the literature [BSW83, Bas96, BBJ+97, Bey95, GR05]. We assume that the domain Ω is polyhedral.

Definition 3.1 (Triangulation)**.** A finite collection $\mathcal{T} = \{T\}$ of tetrahedra $T \subset \overline{\Omega}$ is called a *triangulation* of Ω if the following holds:

1. $\text{vol}(T) > 0$ for all $T \in \mathcal{T}$,
2. $\bigcup_{T \in \mathcal{T}} T = \overline{\Omega}$,
3. $\text{int}(S) \cap \text{int}(T) = \emptyset$ for all $S, T \in \mathcal{T}$ with $S \neq T$.

Definition 3.2 (Consistency)**.** A triangulation $\mathcal{T}$ is called *consistent* if the intersection of any two tetrahedra in $\mathcal{T}$ is either empty, a common face, a common edge or a common vertex.

Definition 3.3 (Stability)**.** A sequence of triangulations $\mathcal{T}_0, \mathcal{T}_1, \mathcal{T}_2, \ldots$ is called *stable* if all angles of all tetrahedra in this sequence are uniformly bounded away from zero.

Definition 3.4 (Refinement)**.** For a given tetrahedron T a triangulation $\mathcal{K}(T)$ of T is called a *refinement* of T if $|\mathcal{K}(T)| \geq 2$ and any vertex of any tetrahedron $T' \in \mathcal{K}(T)$ is either a vertex or an edge midpoint of T. In this case T' is called a child of T and T is called the parent of T'. A triangulation $\mathcal{T}_{k+1}$ is called *refinement* of a triangulation $\mathcal{T}_k \neq \mathcal{T}_{k+1}$ if for every $T \in \mathcal{T}_k$ either $T \in \mathcal{T}_{k+1}$ or $\mathcal{K}(T) \subset \mathcal{T}_{k+1}$ for some refinement $\mathcal{K}(T)$ of T.

Definition 3.5 (Multilevel triangulation)**.** A sequence of consistent triangulations $\mathcal{M} = (\mathcal{T}_0, \ldots, \mathcal{T}_J)$ is called a *multilevel triangulation* of Ω if the following holds:

1. For $0 \leq k < J$: $\mathcal{T}_{k+1}$ is a refinement of $\mathcal{T}_k$.

2. For $0 \leq k < J$: $T \in \mathcal{T}_k \cap \mathcal{T}_{k+1} \Rightarrow T \in \mathcal{T}_J$.

3.2.2 Galerkin finite element discretization

Let $\mathcal{M} = (\mathcal{T}_0, \ldots, \mathcal{T}_J)$ be a multilevel triangulation of Ω. With each triangulation $\mathcal{T}_k$ $(0 \leq k \leq J)$ we associate a mesh size parameter $h = h_k$. Let $\mathbf{V}_h \subset \mathbf{V}_0$, $\mathbf{V}_h^D \subset \mathbf{V}_D$, $Q_h \subset L_0^2(\Omega)$ and $V_h \subset V$ be finite element spaces corresponding to the triangulation $\mathcal{T}_k$. The pair $(\mathbf{V}_h, Q_h)$ is assumed to be LBB stable, i. e. the following Ladyshenskaja-Babuska-Brezzi condition is fulfilled

$$\exists\, \hat{\beta} > 0 \;:\quad \sup_{\mathbf{u}_h \in \mathbf{V}_h} \frac{b(\mathbf{u}_h, q_h)}{\|\mathbf{u}_h\|_1} \geq \hat{\beta} \|q_h\|_{L^2} \quad \text{for all} \;\; q_h \in Q_h, \tag{3.5}$$

with $\hat{\beta}$ independent of h.

The Galerkin discretization of (3.1) is as follows:

Find $\mathbf{u}_h(t) \in \mathbf{V}_h^D$, $p_h(t) \in Q_h$ and $\phi_h(t) \in V_h$ such that for $t \in [0,T]$:

$$\begin{aligned} m(\frac{\partial \mathbf{u}_h(t)}{\partial t}, \mathbf{v}_h) + a(\mathbf{u}_h(t), \mathbf{v}_h) + c(\mathbf{u}_h(t); \mathbf{u}_h(t), \mathbf{v}_h) - b(\mathbf{v}_h, p_h(t)) \\ = m(\mathbf{g}, \mathbf{v}_h) + f_{\Gamma_h}(\mathbf{v}_h) \quad \forall \mathbf{v}_h \in \mathbf{V}_h \end{aligned} \tag{3.6}$$

$$b(\mathbf{u}_h(t), q_h) = 0 \quad \forall q_h \in Q_h \tag{3.7}$$

$$(\frac{\partial \phi_h(t)}{\partial t}, v_h)_0 + (\mathbf{u}_h(t) \cdot \nabla \phi_h(t), v_h)_0 = 0 \quad \forall v_h \in V_h. \tag{3.8}$$

Here $f_{\Gamma_h}(\mathbf{v}_h)$ is a suitable approximation of the surface force $f_\Gamma(\mathbf{v}_h)$, cf. Section 4.

The discretization (3.8) of the hyperbolic level set equation is unstable. In [Reu09], an analysis for a simple one-dimensional problem shows that the inf-sup constant of the corresponding bilinear form tends to 0 when the mesh size h decreases. We consider the streamline diffusion stabilization to improve the stability of (3.8), cf. [Reu09]. For each tetrahedron $T \in \mathcal{T}_k$ and each $v_h \in V_h$ we define a test function $\hat{v}_h \in L^2(\Omega)$ as follows

$$\hat{v}_h(x) = v_h(x) + \delta_T \mathbf{u}_h(x,t) \cdot \nabla v_h(x), \quad x \in T, \quad T \in \mathcal{T}_h.$$

where $\delta_T \geq 0$ is a stabilization parameter, which depends on the mesh size h and the local velocity $\mathbf{u}_h$ on T. An analysis of the streamline diffusion method and reasonable choices for the stabilization parameter δ_T can be found in [Reu09]. This leads to the stabilized variant of (3.8):

$$\sum_{T \in \mathcal{T}_k} (\frac{\partial \phi_h}{\partial t}(t) + \mathbf{u}_h(t) \cdot \nabla \phi_h(t), v_h + \delta_T \mathbf{u}_h(t) \cdot \nabla v_h)_T = 0 \qquad \forall v_h \in V_h. \tag{3.9}$$

Here $(\cdot,\cdot)_T$ denotes the L^2-scalar product over the domain T.

Let $\{\boldsymbol{\xi}_j\}_{1 \leq j \leq N}$, $\{\psi_j\}_{1 \leq j \leq K}$ and $\{\chi_j\}_{1 \leq j \leq L}$ be (nodal) bases of $\mathbf{V}_h$, Q_h and V_h, respectively. Then we can represent the solutions $\mathbf{u}_h(t) \in \mathbf{V}_h^D$, $p_h(t) \in Q_h$ and $\phi_h(t) \in V_h$ in these bases as:

$$\mathbf{u}_h(t) = \sum_{j=1}^{N} u_j(t) \boldsymbol{\xi}_j, \quad \vec{\mathbf{u}}(t) := (u_1(t), \ldots, u_N(t))$$

$$p_h(t) = \sum_{j=1}^{K} p_j(t) \psi_j, \quad \vec{\mathbf{p}}(t) := (p_1(t), \ldots, p_K(t))$$

$$\phi_h(t) = \sum_{j=1}^{L} \phi_j(t) \chi_j, \quad \vec{\boldsymbol{\phi}}(t) := (\phi_1(t), \ldots, \phi_L(t)).$$

For $\phi_h \in V_h$ and $\mathbf{u}_h \in \mathbf{V}_h$ we introduce the following matrices:

$$\begin{aligned}
\mathbf{M}(\phi_h) \in \mathbb{R}^{N\times N}, &\quad \mathbf{M}(\phi_h)_{ij} = \int_\Omega \rho(\phi_h)\boldsymbol{\xi}_i \cdot \boldsymbol{\xi}_j \; dx \\
\mathbf{A}(\phi_h) \in \mathbb{R}^{N\times N}, &\quad \mathbf{A}(\phi_h)_{ij} = \frac{1}{2}\int_\Omega \mu(\phi_h)\,\mathrm{tr}\left(\mathbf{D}(\boldsymbol{\xi}_i)\mathbf{D}(\boldsymbol{\xi}_j)\right) \; dx \\
\mathbf{B} \in \mathbb{R}^{K\times N}, &\quad \mathbf{B}_{ij} = -\int_\Omega \psi_i \,\mathrm{div}\,\boldsymbol{\xi}_j \; dx \\
\mathbf{N}(\phi_h,\mathbf{u}_h) \in \mathbb{R}^{N\times N}, &\quad \mathbf{N}(\phi_h,\mathbf{u}_h)_{ij} = \int_\Omega \rho(\phi_h)(\mathbf{u}_h\cdot\nabla\boldsymbol{\xi}_j)\cdot\boldsymbol{\xi}_i \; dx \\
\mathbf{E}(\mathbf{u}_h) \in \mathbb{R}^{L\times L}, &\quad \mathbf{E}(\mathbf{u}_h)_{ij} = \sum_{T\in\mathcal{T}_k}\int_T \chi_j(\chi_i + \delta_T\mathbf{u}_h\cdot\nabla\chi_i) \; dx \\
\mathbf{H}(\mathbf{u}_h) \in \mathbb{R}^{L\times L}, &\quad \mathbf{H}(\mathbf{u}_h)_{ij} = \sum_{T\in\mathcal{T}_k}\int_T (\mathbf{u}_h\cdot\nabla\chi_j)(\chi_i + \delta_T\mathbf{u}_h\cdot\nabla\chi_i) \; dx.
\end{aligned}$$

We also use the following notations

$$\begin{aligned}
\mathbf{M}(\vec{\boldsymbol{\phi}}(t)) &= \mathbf{M}(\phi_h) \\
\mathbf{A}(\vec{\boldsymbol{\phi}}(t)) &= \mathbf{A}(\phi_h) \\
\mathbf{N}(\vec{\boldsymbol{\phi}}(t),\vec{\mathbf{u}}(t)) &= \mathbf{N}(\phi_h,\mathbf{u}_h) \\
\mathbf{E}(\vec{\mathbf{u}}(t)) &= \mathbf{E}(\mathbf{u}_h) \\
\mathbf{H}(\vec{\mathbf{u}}(t)) &= \mathbf{H}(\mathbf{u}_h).
\end{aligned}$$

to emphasize the dependence of these matrices on the *time-dependent* vectors $\vec{\mathbf{u}}(t)$ and $\vec{\boldsymbol{\phi}}(t)$.

Using this notation we obtain the following equivalent formulation of the coupled system of ordinary differential equations (3.6), (3.7), (3.9): Find $\vec{\mathbf{u}}(t) \in \mathbb{R}^N$, $\vec{\mathbf{p}}(t) \in \mathbb{R}^K$ and $\vec{\boldsymbol{\phi}}(t) \in \mathbb{R}^L$ such that for all $t \in [0,T]$

$$\begin{aligned}
\mathbf{M}(\vec{\boldsymbol{\phi}}(t))\frac{d\vec{\mathbf{u}}}{dt}(t) + \mathbf{A}(\vec{\boldsymbol{\phi}}(t))\vec{\mathbf{u}}(t) + \mathbf{N}(\vec{\boldsymbol{\phi}}(t),\vec{\mathbf{u}}(t))\vec{\mathbf{u}}(t) + \mathbf{B}^T\vec{\mathbf{p}}(t) & \\
= \vec{\mathbf{g}}(\vec{\boldsymbol{\phi}}(t)) + \vec{\mathbf{f}}_{\Gamma_h}(\vec{\boldsymbol{\phi}}(t)) & \quad (3.10)\\
\mathbf{B}\vec{\mathbf{u}}(t) = 0 & \quad (3.11)\\
\mathbf{E}(\vec{\mathbf{u}}(t))\frac{d\vec{\boldsymbol{\phi}}}{dt}(t) + \mathbf{H}(\vec{\mathbf{u}}(t))\vec{\boldsymbol{\phi}}(t) = 0. & \quad (3.12)
\end{aligned}$$

The vectors in the right-hand side are defined as

$$\vec{\mathbf{g}}(\phi_h) \in \mathbb{R}^N, \quad \vec{\mathbf{g}}(\phi_h)_i = \int_\Omega \rho(\phi_h)\mathbf{g}\cdot\boldsymbol{\xi}_i \, dx,$$
$$\vec{\mathbf{f}}_{\Gamma_h}(\phi_h) \in \mathbb{R}^N, \quad \vec{\mathbf{f}}_{\Gamma_h}(\phi_h)_i = f_{\Gamma_h}(\boldsymbol{\xi}_i).$$

3.2.3 Extended finite element space for the pressure

We introduce the spaces of piecewise polynomial functions of degree $k \in \mathbb{N}$ on the triangulation $\mathcal{T}_h$

$$\mathbb{X}_h^k := \{\, v \in C(\bar{\Omega}) \mid v_{|T} \in \mathcal{P}_k \ \text{ for all } \ T \in \mathcal{T}_h \,\}, \quad k \geq 1, \tag{3.13a}$$
$$\mathbb{X}_{h,0}^k := \mathbb{X}_h^k \cap H_0^1(\Omega), \quad k \geq 1. \tag{3.13b}$$

In the Galerkin discretization for the one-phase flow Navier-Stokes equations, the Hood-Taylor P_2-P_1 finite element pair $(\mathbf{V}_h, Q_h) := \big((\mathbb{X}_{h,0}^2)^3\,,\, \mathbb{X}_h^1 \cap L_0^2(\Omega)\big)$ is a standard choice because of its LBB-stability and optimal approximation properties, cf. [GR86]. For the two-phase flow problem, due to the appearance of the surface tension, the pressure p has a jump across the interface Γ. As the interface Γ is in general not aligned with the grid, the discontinuity of p lies inside the elements which contain Γ. Hence the standard finite element space $Q_h := \mathbb{X}_h^1 \cap L_0^2(\Omega)$ is no longer suitable to approximate the discontinuous pressure p. In practice, a piecewise planar approximation Γ_h is used for the reconstruction of the interface Γ. We refer to Section 3.2.4 for the definition of Γ_h. Thus, the subdomains Ω_1 and Ω_2 are approximated by two polyhedral subdomains $\Omega_{1,h}$ and $\Omega_{2,h}$ with respect to Γ_h. We define in these polyhedral subdomains the piecewise constant density ρ_h, such that $\rho_h = \rho_i$ in $\Omega_{i,h}$. In [GR07a], an approximation error bound for the numerical solution of a stationary two-phase flow Stokes equation (with a constant viscosity $\mu > 0$ in Ω) is derived. As a consequence of Strang's lemma, this error bound is of the form

$$\begin{aligned}\mu\|\mathbf{u}-\mathbf{u}_h\|_1 + \|p-p_h\|_{L^2} \leq c\big(&\mu \inf_{\mathbf{v}_h\in\mathbf{V}_h} \|\mathbf{u}-\mathbf{v}_h\|_1 + \inf_{q_h\in Q_h} \|q_h - p\|_{L^2} \\ &+ \sup_{\mathbf{v}_h\in\mathbf{V}_h} \frac{|(\rho\mathbf{g},\mathbf{v}_h) - (\rho_h\mathbf{g},\mathbf{v}_h)|}{\|\mathbf{v}_h\|_1} \\ &+ \sup_{\mathbf{v}_h\in\mathbf{V}_h} \frac{|f_\Gamma(\mathbf{v}_h) - f_{\Gamma_h}(\mathbf{v}_h)|}{\|\mathbf{v}_h\|_1}\big)\end{aligned} \tag{3.14}$$

It is shown that, cf. [GR07a], the quantity $\inf_{q_h \in Q_h} \|q_h - p\|_{L^2}$ has no better upper bound than $ch^{\frac{1}{2}}$. Thus, the best one can obtain are sub-optimal error bounds for the velocity $\|\mathbf{u} - \mathbf{u}_h\|_1 \leq ch^{\frac{1}{2}}$ and the pressure $\|p - p_h\|_{L^2} \leq ch^{\frac{1}{2}}$ respectively.

A much better approximation of the pressure is obtained by using the extended finite element method (XFEM), introduced by Belytschko et al. cf. [MDB99, BMUP01]. The idea of this method is that the standard finite element space is enriched by certain functions which can represent discontinuities across the interface

$$Q_h^\Gamma := \{\, v \in H^1(\Omega_1 \cup \Omega_2) : v_{|T_i} \text{ is linear for all } T \in \mathcal{T}_h,\ i = 1, 2. \,\}, \quad (3.15)$$

where $T_i = T \cap \Omega_i$.

We define the index set $\mathcal{I} = \{1, \ldots, K\}$, where $K = \dim \mathbb{X}_h^1$, and let $(\psi_i)_{i \in \mathcal{I}}$ be the nodal basis in $\mathbb{X}_h^1$. Let $\mathcal{I}_\Gamma := \{\, i \in \mathcal{I} : \ |\Gamma \cap \operatorname{supp}(\psi_i)| > 0 \,\}$ be the index set of those basis functions the support of which is intersected by Γ. The Heaviside function H_Γ has the values $H_\Gamma(x) = 0$ for $x \in \Omega_1$, $H_\Gamma(x) = 1$ for $x \in \Omega_2$. Using this, for $i \in \mathcal{I}_\Gamma$ we introduce a so-called *enrichment function*

$$\Phi_i(x) := H_\Gamma(x) - H_\Gamma(x_i),$$

where x_i is the vertex with index i. We introduce a new basis function

$$\psi_i^\Gamma := \psi_i \Phi_i, \quad i \in \mathcal{I}_\Gamma$$

and define the space

$$Q_h^\Gamma := Q_h \oplus \operatorname{span}\{\, \psi_i^\Gamma \mid i \in \mathcal{I}_\Gamma \,\}.$$

An illustration of the enrichment basis functions in the one-dimensional case is shown in Figure 3.1.

The following theorem from [Reu08] proves the optimal approximation property of the XFEM space Q_h^Γ

Theorem 3.1. For an integer $k \geq 0$ we define the space

$$H^k(\Omega_1 \cup \Omega_2) := \{\, p \in L_2(\Omega) : p_{|\Omega_i} \in H^k(\Omega_i),\ i = 1, 2 \,\}$$

with the norm $\|p\|^2_{k,\Omega_1 \cup \Omega_2} := \|p\|^2_{k,\Omega_1} + \|p\|^2_{k,\Omega_2}$. Then for integer l, m with $0 \leq l < m \leq 2$ the following holds:

$$\inf_{v \in Q_h^\Gamma} \|u - v\|_{l,\Omega_1 \cup \Omega_2} \leq c\, h^{m-l} \|u\|_{m,\Omega_1 \cup \Omega_2} \quad (3.16)$$

for all $u \in H^m(\Omega_1 \cup \Omega_2)$.

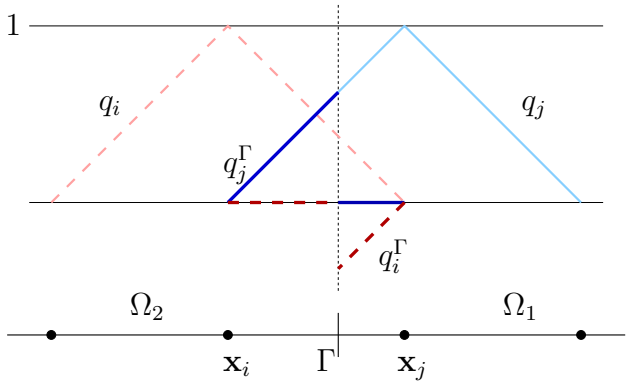

Figure 3.1: Extended finite element basis functions q_i, q_i^Γ (dashed) and q_j, q_j^Γ (solid) for 1D case.

In general, as the evolving interface is not aligned with the fixed grid, there are basis functions $\psi_i \in Q_h^\Gamma$ with very small support in the sense that

$$\frac{|\mathrm{supp}(\psi_i^\Gamma)|}{|\mathrm{supp}(\psi_i)|} \ll 1.$$

Such basis functions may lead to instability, for example if their contributions are dominated by rounding errors. In [Reu08] a modified XFEM space is introduced, in which basis functions from Q_h^Γ with very small support are deleted. Let $\alpha > 0$, $\tilde{c} \geq 0$ be given parameters. We denote by Ω_Γ the set of all tetrahedra intersected by Γ. Let $\mathcal{I}_\gamma \subset \mathcal{I}^\Gamma$ be the index set such that for all $i \in \mathcal{I}_\Gamma \setminus \mathcal{I}_\gamma$:

$$\frac{\|\psi_i\|_{l,T\cap\Omega_i}}{\|\psi_i\|_{l,T}} \leq \tilde{c}\, h_T^\alpha \quad \text{for all} \quad T \subset \big(\mathrm{supp}(\psi_i) \cap \Omega_\Gamma\big). \tag{3.17}$$

The values of $\tilde{c}$ is used to determine which basis functions are deleted. If $\tilde{c} = 0$, all the enrichment functions are included while a large value of $\tilde{c}$ would give the standard finite element space. In practice we choose $l = 0$. The choice of α will be addressed below.
The modified XFEM spaces Q_h^γ is defined by

$$Q_h^\gamma := Q_h \oplus \mathrm{span}\{\, \psi_i^\Gamma \mid i \in \mathcal{I}_\gamma \,\}.$$

For this space the following approximation property holds, cf. [Reu08]:

Theorem 3.2. *We assume $\{\mathcal{T}_h\}_{h>0}$ to be quasi-uniform. For $0 \le l < m \le 2$ the following holds:*

$$\inf_{v \in Q_h^\gamma} \|u - v\|_{l,\Omega_1 \cup \Omega_2} \le c\big(h^{m-l} + h^{\alpha-l}\big)\|u\|_{m,\Omega_1 \cup \Omega_2} \quad \textit{for all} \;\; u \in H^m(\Omega_1 \cup \Omega_2).$$

This means that the order of approximation of the modified space Q_h^γ is the same as that of Q_h^γ if we take $\alpha = m$. From the definition of Q_h^Γ, we choose $\alpha = m = 1$.

3.2.4 Implementation issues

We use the finite element pair $(\mathbf{V}_h, Q_h^\gamma)$ for the spatial discretization of the Navier-Stokes equations. For the discrete level set equation, piecewise quadratic finite elements with streamline diffusion stabilization are used to provide a good approximation ϕ_h of ϕ. We explain how a piecewise planar approximation Γ_h of Γ is reconstructed.

Let $\mathcal{T}_h$ be a shape regular tetrahedral triangulation of Ω. We introduce one further regular refinement of $\mathcal{T}_h$ denoted by $\mathcal{T}_h'$. Let $I_h(\phi_h)$ be the continuous piecewise *linear* function on $\mathcal{T}_h'$ which interpolates the piecewise quadratic function ϕ_h at the vertices of each tetrahedron in $\mathcal{T}_h'$, i. e.:

$$\forall \text{ vertices } \nu \text{ of } T' : \quad I_h(\phi_h)(\nu) = \phi_h(\nu).$$

Then Γ_h is defined as

$$\Gamma_h := \{\, x \in \Omega \mid I_h(\phi_h)(x) = 0 \,\}. \tag{3.18}$$

Note that Γ_h is easy to construct, since $I_h(\phi_h)$ is piecewise linear. Once Γ_h is known, we obtain the two polyhedral subdomains $\Omega_{1,h}$ and $\Omega_{2,h}$ as approximations for Ω_1 and Ω_2.

Let $\mathcal{T}_{\Gamma_h} := \{T \in \mathcal{T}_h \mid T \cap \Gamma_h \neq \emptyset\}$ denote the set of all tetrahedra which are intersected by the approximate interface Γ_h. For each $T \in \mathcal{T}_{\Gamma_h}$, let $T' \in \mathcal{T}_h'$ be one of the 8 regular children of T. We introduce the notations $T_i' := T' \cap \Omega_{i,h}$, $i = 1, 2$, and $\Gamma_{h,T'} = T' \cap \Gamma_h$, the restrictions of the subdomains and interface in T'. Then T_i' is either a tetrahedron or a prism, which can be subdivided into 3 subtetrahedra. The planar segment $\Gamma_{h,T'}$ is either a triangle or a quadrilateral, which can be subdivided into 2 triangles. Thus integrals over T_i' or $\Gamma_{h,T'}$ of smooth functions can be easily determined with high accuracy using standard (Gauss) quadrature.

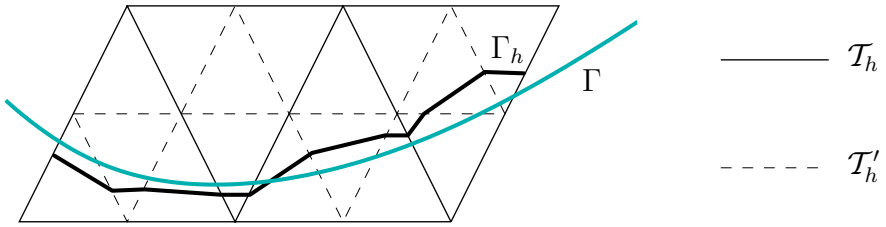

Figure 3.2: Construction of a piecewise linear interface for 2D case.

The matrices and vectors in (3.10)-(3.12) are assembled element-wise by summing the contributions from all tetrahedra T in $\mathcal{T}_h$. A Gauss quadrature of degree five in a tetrahedron is used to compute the local integrals. Note that the coefficients ρ and μ, appearing in $\mathbf{M}, \mathbf{A}, \mathbf{B}$ and $\vec{\mathbf{g}}$, are discontinuous in each tetrahedron $T \in \mathcal{T}_{\Gamma_h}$. In this case, as mentioned above, each regular child T' of T is partitioned into two polyhedral parts T_1' and T_2', in which the coefficients ρ and μ are constant. Then the same Gauss quadrature can be applied in the (at most three) subtetrahedra of T_i'. The sums of the results from all subtetrahedra give the local integrals of $\mathbf{M}, \mathbf{A}, \mathbf{B}$ and $\vec{\mathbf{g}}$ in T.

For the pressure we use the extended finite element space Q_h^γ, which contains discontinuous basis functions at the interface. Hence the local integrals $\int_{T\in\mathcal{T}_{\Gamma_h}} \psi_i^\Gamma \operatorname{div} \boldsymbol{\xi}_j \, dx$ that arise in the assembling process for the matrix $\mathbf{B}$ are treated in a similar way. From the definition of ψ_i^Γ we have

$$\operatorname{supp}(\psi_i^\Gamma)|_{T'} = \begin{cases} T_2' & \text{if } \; x_i \in \Omega_1 \\ T_1' & \text{if } \; x_i \in \Omega_2, \end{cases}$$

which can be determined from the sign of the level set function at the vertices. Thus we have

$$\int_{T'} \psi_i^\Gamma \operatorname{div} \boldsymbol{\xi}_j \, dx = \begin{cases} \int_{T_2'} \psi_i \operatorname{div} \boldsymbol{\xi}_j \, dx & \text{if } \; x_i \in \Omega_1, \\ -\int_{T_1'} \psi_i \operatorname{div} \boldsymbol{\xi}_j \, dx & \text{if } \; x_i \in \Omega_2, \end{cases}$$

which can be computed by applying the Gauss quadrature in the subtetrahedra of T_1' or T_2' and summing the results. If both T_1' and T_2' are non-tetrahedral, the integration in each part involves three subtetrahedra. In case one of these two parts is a tetrahedron, say T_1', it is more efficient to compute the integral in this tetrahedral part, since the integral in T_2' (for the

case $x_i \in \Omega_1$) can be deduced from

$$\int_{T_2'} \psi_i \operatorname{div} \boldsymbol{\xi}_j \, dx = \int_{T'} \psi_i \operatorname{div} \boldsymbol{\xi}_j \, dx - \int_{T_1'} \psi_i \operatorname{div} \boldsymbol{\xi}_j \, dx.$$

3.3 Time discretization

In the spatial discretization of the two-phase Navier-Stokes equations in Section 3.2.2, the mass matrix $\mathbf{M}$ (scaled by the discontinuous density $\rho(\phi_h(t))$ is in general time-dependent. If the extended finite element method is used for the pressure, the matrix $\mathbf{B}$ depends also on time, as the XFEM space changes with the evolution of the interface. In this section, we present the time integration for the Navier-Sokes equations (3.11) and the level set equation (3.12) from [Reu09] using the generalized θ-scheme. In subsection 3.3.2, a simple variant of the implicit Euler method cf. [Gro08] is discussed.

3.3.1 The generalized θ-scheme

For simplicity, we first restrict to the case with the matrix $\mathbf{B}$ independent of t. We consider the Navier-Stokes part in (3.10)-(3.11). We introduce the notation

$$\mathbf{G}(\vec{\mathbf{u}}, \vec{\boldsymbol{\phi}}, \vec{\mathbf{g}}, \vec{\mathbf{f}}_{\Gamma_h}) = \vec{\mathbf{g}}(\vec{\boldsymbol{\phi}}(t)) + \vec{\mathbf{f}}_{\Gamma_h}(\vec{\boldsymbol{\phi}}(t)) - \mathbf{A}(\vec{\boldsymbol{\phi}}(t))\vec{\mathbf{u}}(t) - \mathbf{N}(\vec{\boldsymbol{\phi}}(t), \vec{\mathbf{u}}(t))\vec{\mathbf{u}}(t).$$

For simplicity, we use the notations

$$\mathbf{M}(t) = \mathbf{M}(\vec{\boldsymbol{\phi}}(t)) \quad \text{and } \mathbf{G}(\vec{\mathbf{u}}, t) = \mathbf{G}(\vec{\mathbf{u}}, \vec{\boldsymbol{\phi}}, \vec{\mathbf{g}}, \vec{\mathbf{f}}_{\Gamma_h}).$$

Then the Navier-Stokes equations can be written as

$$\begin{aligned} \mathbf{M}(t)\frac{d\vec{\mathbf{u}}}{dt}(t) + \mathbf{B}^T\vec{\mathbf{p}}(t) &= \mathbf{G}(\vec{\mathbf{u}}, t) \\ \mathbf{B}\vec{\mathbf{u}}(t) &= 0, \end{aligned} \tag{3.19}$$

or, equivalently,

$$\begin{aligned} \frac{d\vec{\mathbf{u}}}{dt}(t) + \mathbf{M}(t)^{-1}\mathbf{B}^T\vec{\mathbf{p}}(t) &= \mathbf{M}(t)^{-1}\mathbf{G}(\vec{\mathbf{u}}, t) \\ \mathbf{B}\vec{\mathbf{u}}(t) &= 0. \end{aligned} \tag{3.20}$$

We define the projection $\mathbf{Q}(t) = I - \mathbf{M}(t)^{-1}\mathbf{B}^T\mathbf{S}(t)^{-1}\mathbf{B}$, where $\mathbf{S}(t) := \mathbf{B}\mathbf{M}(t)^{-1}\mathbf{B}^T$. From $\mathbf{B}\frac{d\vec{\mathbf{u}}}{dt}(t) = 0$ and substitution of $\frac{d\vec{\mathbf{u}}}{dt}(t)$ from the first equation we obtain

$$\mathbf{S}(t)\vec{\mathbf{p}}(t) = \mathbf{B}\mathbf{M}(t)^{-1}\mathbf{G}(\vec{\mathbf{u}}, t), \quad \mathbf{S}(t) := \mathbf{B}\mathbf{M}(t)^{-1}\mathbf{B}^T. \tag{3.21}$$

Using (3.21) we can eliminate $\vec{\mathbf{p}}(t)$ from the first equation in (3.20) resulting in

$$\begin{aligned}\frac{d\vec{\mathbf{u}}}{dt}(t) &= \big[\mathbf{I} - \mathbf{M}(t)^{-1}\mathbf{B}^T\mathbf{S}(t)^{-1}\mathbf{B}\big]\mathbf{M}(t)^{-1}\mathbf{G}(\vec{\mathbf{u}}, t)\\ &=: \mathbf{Q}(t)\mathbf{M}(t)^{-1}\mathbf{G}(\vec{\mathbf{u}}, t).\end{aligned} \tag{3.22}$$

The projection $\mathbf{Q}(t) = I - \mathbf{M}(t)^{-1}\mathbf{B}^T\mathbf{S}(t)^{-1}\mathbf{B}$ satisfies $\mathbf{B}\mathbf{Q}(t) = 0$. Given the initial condition $\mathbf{B}\vec{\mathbf{u}}(0) = 0$, the solution $\vec{\mathbf{u}}(t)$ of the ordinary differential equation (3.22) remains in the subspace $\mathrm{Ker}(\mathbf{B})$. The θ-scheme applied to (3.22) yields

$$\begin{aligned}\frac{\vec{\mathbf{u}}^{n+1} - \vec{\mathbf{u}}^n}{\Delta t} &= \theta\mathbf{Q}(t_{n+1})\mathbf{M}(t_{n+1})^{-1}\mathbf{G}(\vec{\mathbf{u}}^{n+1}, t_{n+1})\\ &\quad + (1-\theta)\mathbf{Q}(t_n)\mathbf{M}(t_n)^{-1}\mathbf{G}(\vec{\mathbf{u}}^n, t_n).\end{aligned} \tag{3.23}$$

We assume that for each n this system has a unique solution $\vec{\mathbf{u}}^{n+1}$ (which is the case for Δt sufficiently small). If $\mathbf{B}\vec{\mathbf{u}}^0 = 0$ then $\mathbf{B}\vec{\mathbf{u}}^n = 0$ for all $n \geq 1$. For implementation it is convenient to eliminate the projection $\mathbf{Q}$ by introducing a suitable Lagrange multiplier. Define $\vec{\mathbf{p}}^k := \mathbf{S}(t_k)^{-1}\mathbf{B}\mathbf{M}(t_k)^{-1}\mathbf{G}(\vec{\mathbf{u}}^k, t_k)$. Then (3.23) takes the form

$$\begin{aligned}\frac{\vec{\mathbf{u}}^{n+1} - \vec{\mathbf{u}}^n}{\Delta t} &= \theta\mathbf{M}(t_{n+1})^{-1}\big(\mathbf{G}(\vec{\mathbf{u}}^{n+1}, t_{n+1}) - \mathbf{B}^T\vec{\mathbf{p}}^{n+1}\big)\\ &\quad + (1-\theta)\mathbf{M}(t_n)^{-1}\big(\mathbf{G}(\vec{\mathbf{u}}^n, t_n) - \mathbf{B}^T\vec{\mathbf{p}}^n\big).\end{aligned} \tag{3.24}$$

Assume that $\vec{\mathbf{u}}^0$ is such that $\mathbf{B}\vec{\mathbf{u}}^0 = 0$. The sequence $(\vec{\mathbf{u}}^n)_{n\geq 0}$ defined by the θ-scheme (3.23) satisfies (3.24) and also $\mathbf{B}\vec{\mathbf{u}}^n = 0$ for all n. We use $\vec{\mathbf{p}}^k$ as a Lagrange multiplier to enforce $\mathbf{B}\vec{\mathbf{u}}^k = 0$ as follows. Given $\vec{\mathbf{u}}^0$ with $\mathbf{B}\vec{\mathbf{u}}^0 = 0$ define

$$\vec{\mathbf{p}}^0 := \mathbf{S}(t_0)^{-1}\mathbf{B}\mathbf{M}(t_0)^{-1}\mathbf{G}(\vec{\mathbf{u}}^0, t_0),$$

and for $n \geq 0$ let $\vec{\mathbf{u}}^{n+1}$, $\vec{\mathbf{p}}^{n+1}$ be such that

$$\begin{aligned}\frac{\vec{\mathbf{u}}^{n+1} - \vec{\mathbf{u}}^n}{\Delta t} &= \theta\mathbf{M}(t_{n+1})^{-1}\big(\mathbf{G}(\vec{\mathbf{u}}^{n+1}, t_{n+1}) - \mathbf{B}^T\vec{\mathbf{p}}^{n+1}\big)\\ &\quad + (1-\theta)\mathbf{M}(t_n)^{-1}\big(\mathbf{G}(\vec{\mathbf{u}}^n, t_n) - \mathbf{B}^T\vec{\mathbf{p}}^n\big) \qquad (3.25)\\ \mathbf{B}\vec{\mathbf{u}}^{n+1} &= 0 \qquad (3.26)\end{aligned}$$

holds. Due to (3.24) this system has a solution. If we assume that for each n the saddle point problem (3.25) has a unique solution (which is true for Δt sufficiently small) then this yields the solution of the θ-scheme in (3.23).

We consider $\theta \neq 0$, as the explicit Euler method ($\theta = 0$) is not stable. If we also have $\theta \neq 1$, in (3.25) inverses of both $\mathbf{M}(t_{n+1})$ and $\mathbf{M}(t_n)$ occur. Using an additional variable, we can avoid the inverse of $\mathbf{M}(t_n)$. Define

$$\vec{\mathbf{z}}^k := \mathbf{M}(t_k)^{-1}\big(\mathbf{G}(\vec{\mathbf{u}}^k, t_k) - \mathbf{B}^T\vec{\mathbf{p}}^k\big), \quad k \geq 0,$$

i.e.

$$\begin{aligned}\mathbf{M}(t_0)\vec{\mathbf{z}}^0 &= \mathbf{G}(\vec{\mathbf{u}}^0, t_0) - \mathbf{B}^T\vec{\mathbf{p}}^0\\ \theta\vec{\mathbf{z}}^{k+1} &= \frac{\vec{\mathbf{u}}^{k+1} - \vec{\mathbf{u}}^k}{\Delta t} - (1-\theta)\vec{\mathbf{z}}^k, \quad k \geq 0.\end{aligned}$$

Using this, (3.25) can be reformulated as

$$\begin{aligned}\mathbf{M}(t_{n+1})\frac{\vec{\mathbf{u}}^{n+1} - \vec{\mathbf{u}}^n}{\Delta t} + \theta\mathbf{B}^T\vec{\mathbf{p}}^{n+1} &= \theta\mathbf{G}(\vec{\mathbf{u}}^{n+1}, t_{n+1}) + (1-\theta)\mathbf{M}(t_{n+1})\vec{\mathbf{z}}^n\\ \mathbf{B}\vec{\mathbf{u}}^{n+1} &= 0\\ \theta\vec{\mathbf{z}}^{n+1} &= \frac{\vec{\mathbf{u}}^{n+1} - \vec{\mathbf{u}}^n}{\Delta t} - (1-\theta)\vec{\mathbf{z}}^n,\end{aligned} \tag{3.27}$$

for $n \geq 0$ and a starting value $\vec{\mathbf{z}}^0$ as defined above.

Application of the θ-scheme to the level set equation (3.12) results in

$$\frac{\vec{\boldsymbol{\phi}}^{n+1} - \vec{\boldsymbol{\phi}}^n}{\Delta t} = -\theta\mathbf{E}(\vec{\mathbf{u}}^{n+1})^{-1}\mathbf{H}(\vec{\mathbf{u}}^{n+1})\vec{\boldsymbol{\phi}}^{n+1} - (1-\theta)\mathbf{E}(\vec{\mathbf{u}}^n)^{-1}\mathbf{H}(\vec{\mathbf{u}}^n)\vec{\boldsymbol{\phi}}^n.$$

This can be reformulated using a new variable

$$\vec{\mathbf{w}}^k = -\mathbf{E}(\vec{\mathbf{u}}^k)^{-1}\mathbf{H}(\vec{\mathbf{u}}^k),$$

which satisfies (for $\theta \neq 0$)

$$\theta\vec{\mathbf{w}}^{n+1} = \frac{\vec{\boldsymbol{\phi}}^{n+1} - \vec{\boldsymbol{\phi}}^n}{\Delta t} - (1-\theta)\vec{\mathbf{w}}^n,$$

resulting in

$$\mathbf{E}(\vec{\mathbf{u}}^{n+1})\frac{\vec{\boldsymbol{\phi}}^{n+1} - \vec{\boldsymbol{\phi}}^n}{\Delta t} = -\theta\mathbf{H}(\vec{\mathbf{u}}^{n+1})\vec{\boldsymbol{\phi}}^{n+1} + (1-\theta)\mathbf{E}(\vec{\mathbf{u}}^{n+1})\vec{\mathbf{w}}^n. \tag{3.28}$$

Combining these results we obtain, for $\theta \neq 0$, the following coupled nonlinear system for $(\vec{\mathbf{u}}^n, \vec{\mathbf{p}}^n, \vec{\boldsymbol{\phi}}^n) \to (\vec{\mathbf{u}}^{n+1}, \vec{\mathbf{p}}^{n+1}, \vec{\boldsymbol{\phi}}^{n+1})$:

Given $\vec{\mathbf{u}}^0$, $\vec{\boldsymbol{\phi}}^0$, determine $\vec{\mathbf{z}}^0$ and $\vec{\mathbf{w}}^0$ as follows:

$$\begin{aligned}
\mathbf{G}(\vec{\mathbf{u}}^0, \vec{\boldsymbol{\phi}}^0, \vec{\mathbf{g}}, \vec{\mathbf{f}}_{\Gamma_h}) &= \vec{\mathbf{g}}(\vec{\boldsymbol{\phi}}^0) + \vec{\mathbf{f}}_{\Gamma_h}(\vec{\boldsymbol{\phi}}^0) - \mathbf{A}(\vec{\boldsymbol{\phi}}^0)\vec{\mathbf{u}}^0 - \mathbf{N}(\vec{\boldsymbol{\phi}}^0, \vec{\mathbf{u}}^0)\vec{\mathbf{u}}^0 \\
\mathbf{B}\mathbf{M}(\vec{\boldsymbol{\phi}}^0)^{-1}\mathbf{B}^T\vec{\mathbf{p}}^0 &= \mathbf{B}\mathbf{M}(\vec{\boldsymbol{\phi}}^0)^{-1}\mathbf{G}(\vec{\mathbf{u}}^0, \vec{\boldsymbol{\phi}}^0, \vec{\mathbf{g}}, \vec{\mathbf{f}}_{\Gamma_h}) \\
\mathbf{M}(\vec{\boldsymbol{\phi}}^0)\vec{\mathbf{z}}^0 &= \mathbf{G}(\vec{\mathbf{u}}^0, \vec{\boldsymbol{\phi}}^0, \vec{\mathbf{g}}, \vec{\mathbf{f}}_{\Gamma_h}) - \mathbf{B}^T\vec{\mathbf{p}}^0 \\
\mathbf{E}(\vec{\mathbf{u}}^0)\vec{\mathbf{w}}^0 &= \mathbf{H}(\vec{\mathbf{u}}^0)\vec{\boldsymbol{\phi}}^0
\end{aligned} \tag{3.29}$$

For $n \geq 0$:

$$\begin{aligned}
\mathbf{M}(\vec{\boldsymbol{\phi}}^{n+1})\frac{\vec{\mathbf{u}}^{n+1}}{\Delta t} &+ \theta\big[\mathbf{A}(\vec{\boldsymbol{\phi}}^{n+1})\vec{\mathbf{u}}^{n+1} + \mathbf{N}(\vec{\boldsymbol{\phi}}^{n+1}, \vec{\mathbf{u}}^{n+1})\vec{\mathbf{u}}^{n+1} - \vec{\mathbf{g}}(\vec{\boldsymbol{\phi}}^{n+1}) \\
&\quad - \vec{\mathbf{f}}_{\Gamma_h}(\vec{\boldsymbol{\phi}}^{n+1})\big] + \theta\mathbf{B}^T\vec{\mathbf{p}}^{n+1} \\
&= \mathbf{M}(\vec{\boldsymbol{\phi}}^{n+1})\frac{\vec{\mathbf{u}}^n}{\Delta t} + (1-\theta)\mathbf{M}(\vec{\boldsymbol{\phi}}^{n+1})\vec{\mathbf{z}}^n, \\
\mathbf{B}\vec{\mathbf{u}}^{n+1} &= 0 \\
\mathbf{E}(\vec{\mathbf{u}}^{n+1})\frac{\vec{\boldsymbol{\phi}}^{n+1}}{\Delta t} + \theta\mathbf{H}(\vec{\mathbf{u}}^{n+1})\vec{\boldsymbol{\phi}}^{n+1} &= \mathbf{E}(\vec{\mathbf{u}}^{n+1})\frac{\vec{\boldsymbol{\phi}}^n}{\Delta t} + (1-\theta)\mathbf{E}(\vec{\mathbf{u}}^{n+1})\vec{\mathbf{w}}^n \\
\theta\vec{\mathbf{z}}^{n+1} &= \frac{\vec{\mathbf{u}}^{n+1} - \vec{\mathbf{u}}^n}{\Delta t} - (1-\theta)\vec{\mathbf{z}}^n \\
\theta\vec{\mathbf{w}}^{n+1} &= \frac{\vec{\boldsymbol{\phi}}^{n+1} - \vec{\boldsymbol{\phi}}^n}{\Delta t} - (1-\theta)\vec{\mathbf{w}}^n.
\end{aligned} \tag{3.30}$$

Remark 3.1. For the case $\theta = 1$ the scheme takes a much simpler form. In particular the sequences for $\vec{\mathbf{z}}^n$ and $\vec{\mathbf{w}}^n$ are not needed. The resulting method is as follows:

Given $\vec{\mathbf{u}}^0,\ \vec{\boldsymbol{\phi}}^0$, determine for $n \geq 0$:

$$\begin{aligned}
\mathbf{M}(\vec{\boldsymbol{\phi}}^{n+1})\frac{\vec{\mathbf{u}}^{n+1}}{\Delta t} + \big[\mathbf{A}(\vec{\boldsymbol{\phi}}^{n+1})\vec{\mathbf{u}}^{n+1} + \mathbf{N}(\vec{\boldsymbol{\phi}}^{n+1}, \vec{\mathbf{u}}^{n+1})\vec{\mathbf{u}}^{n+1} - \vec{\mathbf{g}}(\vec{\boldsymbol{\phi}}^{n+1}) \\
- \vec{\mathbf{f}}_{\Gamma_h}(\vec{\boldsymbol{\phi}}^{n+1})\big] + \mathbf{B}^T\vec{\mathbf{p}}^{n+1} \\
= \mathbf{M}(\vec{\boldsymbol{\phi}}^{n+1})\frac{\vec{\mathbf{u}}^{n}}{\Delta t} \\
\mathbf{B}\vec{\mathbf{u}}^{n+1} = 0 \\
\mathbf{E}(\vec{\mathbf{u}}^{n+1})\frac{\vec{\boldsymbol{\phi}}^{n+1}}{\Delta t} + \mathbf{H}(\vec{\mathbf{u}}^{n+1})\vec{\boldsymbol{\phi}}^{n+1} = \mathbf{E}(\vec{\mathbf{u}}^{n+1})\frac{\vec{\boldsymbol{\phi}}^{n}}{\Delta t}.
\end{aligned} \tag{3.31}$$

3.3.2 An implicit Euler type of method

We present a variant of an implicit Euler method from [RFG+, Gro08] which is used in our experiments in Chapter 7 due to its simplicity. Starting point is the ODE system for the Navier-Stokes part in (3.22):

$$\frac{d\vec{\mathbf{u}}}{dt}(t) = \mathbf{Q}(t)\mathbf{M}(t)^{-1}\mathbf{G}(\vec{\mathbf{u}}, t).$$

For the discretization the projection operator $\mathbf{Q}(t)$ is treated explicitly, whereas the operator $\mathbf{G}(\vec{\mathbf{u}}, t)$ is treated semi-implicitly. Applying an implicit Euler method for the latter, we obtain the discretization

$$\frac{\vec{\mathbf{u}}^{n+1} - \vec{\mathbf{u}}^{n}}{\Delta t} = \mathbf{Q}(t_n)\mathbf{M}(t_n)^{-1}\mathbf{G}(\vec{\mathbf{u}}^{n+1}, t_n).$$

Using a Lagrange multiplier $\vec{\mathbf{p}}^{k+1} := \mathbf{S}(t_k)^{-1}\mathbf{B}\mathbf{M}(t_k)^{-1}\mathbf{G}(\vec{\mathbf{u}}^{k+1}, t_k)$ we obtain the saddle point form

$$\begin{aligned}
\frac{\vec{\mathbf{u}}^{n+1} - \vec{\mathbf{u}}^{n}}{\Delta t} &= \mathbf{M}(t_n)^{-1}\big(\mathbf{G}(\vec{\mathbf{u}}^{n+1}, t_n) - \mathbf{B}^T\vec{\mathbf{p}}^{n+1}\big) \\
\mathbf{B}\vec{\mathbf{u}}^{n+1} &= 0.
\end{aligned} \tag{3.32}$$

The same idea is applied to the level set equation and thus we get the following time integration scheme for the coupled problem

Given $\vec{\mathbf{u}}^0$, $\vec{\boldsymbol{\phi}}^0$, determine for $n \geq 0$:

$$\begin{aligned}
\mathbf{M}(\vec{\boldsymbol{\phi}}^n)\frac{\vec{\mathbf{u}}^{n+1}}{\Delta t} + \big[\mathbf{A}(\vec{\boldsymbol{\phi}}^n)\vec{\mathbf{u}}^{n+1} + \mathbf{N}(\vec{\boldsymbol{\phi}}^n, \vec{\mathbf{u}}^{n+1})\vec{\mathbf{u}}^{n+1} - \vec{\mathbf{g}}(\vec{\boldsymbol{\phi}}^n) \\
- \vec{\mathbf{f}}_{\Gamma_h}(\vec{\boldsymbol{\phi}}^n)\big] + \mathbf{B}^T\vec{\mathbf{p}}^{n+1} \\
= \mathbf{M}(\vec{\boldsymbol{\phi}}^n)\frac{\vec{\mathbf{u}}^n}{\Delta t} \qquad (3.33) \\
\mathbf{B}\vec{\mathbf{u}}^{n+1} = 0 \\
\mathbf{E}(\vec{\mathbf{u}}^n)\frac{\vec{\boldsymbol{\phi}}^{n+1}}{\Delta t} + \mathbf{H}(\vec{\mathbf{u}}^n)\vec{\boldsymbol{\phi}}^{n+1} = \mathbf{E}(\vec{\mathbf{u}}^n)\frac{\vec{\boldsymbol{\phi}}^n}{\Delta t}.
\end{aligned}$$

This scheme is similar to the one in Remark 3.1, but now the mass matrices $\mathbf{M}$ and $\mathbf{E}$ are treated explicitly (i.e. evaluated at t_n instead of t_{n+1}). Thus per time step there is a *decoupling* between the Navier-Stokes and level set equation.

Remark 3.2. In section 7.2.1 we will briefly discuss iterative methods for solving the nonlinear systems resulting from the time discretization schemes 3.3.1 and 3.33. The reparametrization method for maintaining the level set function is addressed in section 7.2.2.

Chapter 4

Treatment of variable surface tension

In this chapter we present the Laplace-Beltrami method for approximation of the localized surface tension force f_Γ. In section 4.1 we recall the discretization methods and results in [Bän01, Dzi91, GRR06, GR07b] for the case of a *constant* surface tension coefficient τ. For this case, an analysis of the Laplace-Beltrami discretization is given in [GR07b]. The *new* discretization for the case with *variable* surface tension coefficient is presented in Section 4.2.

4.1 Laplace-Beltrami method for discretization of the surface tension force

Let the interface Γ be defined on an open subset U of $\mathbb{R}^3$. We define the signed distance function

$$d : U \to \mathbb{R}, \qquad |d(x)| := \operatorname{dist}(x, \Gamma) \quad \text{for all } x \in U.$$

Thus Γ is the zero level set of d. We assume $d < 0$ in Ω_1 and $d > 0$ in Ω_2. We define $\mathbf{n}(x) := \nabla d(x)$ for all $x \in U$. Thus $\mathbf{n} = \mathbf{n}_\Gamma$ on Γ and $\|\mathbf{n}(x)\| = 1$ for all $x \in U$. We define the orthogonal projection on Γ

$$\mathbf{P}(x) := \mathbf{I} - \mathbf{n}(x)\,\mathbf{n}(x)^T, \quad x \in \Gamma,$$

and also the orthogonal projection on Γ_h, with Γ_h as in 3.2.4

$$\mathbf{P}_h(x) := \mathbf{I} - \mathbf{n}_h(x)\,\mathbf{n}_h(x)^T, \quad x \in \Gamma_h,\ x \text{ not on an edge},$$

where $\mathbf{n}_h$ denotes the unit normal on Γ_h.

For a sufficiently smooth function $u : U \to \mathbb{R}$ the tangential derivative of u is defined by projecting the derivative to the tangent space of Γ, i. e.

$$\nabla_\Gamma u := \mathbf{P}(x)\nabla u. \tag{4.1}$$

Similarly, we have the tangential derivative along Γ_h

$$\nabla_\Gamma u := \mathbf{P}_h(x)\nabla u. \tag{4.2}$$

We define the *Laplace-Beltrami operator* of f on Γ by

$$\Delta_\Gamma f(x) := \nabla_\Gamma \cdot \nabla_\Gamma f(x).$$

For vector valued functions $\mathbf{f}$, $\mathbf{g} : \Gamma \to \mathbb{R}^3$ we have

$$\Delta_\Gamma \mathbf{f} := (\Delta_\Gamma f_1, \Delta_\Gamma f_2, \Delta_\Gamma f_3)^T, \qquad \nabla_\Gamma \mathbf{f} \cdot \nabla_\Gamma \mathbf{g} := \sum_{i=1}^{3} \nabla_\Gamma f_i \cdot \nabla_\Gamma g_i \,.$$

The following basic result from differential geometry shows how curvature can be related to the Laplace-Beltrami operator and how partial integration can be applied.

Theorem 4.1. *Let* $\mathrm{id}_\Gamma : \Gamma \to \mathbb{R}^3$ *be the identity on* Γ, $\kappa = \kappa_1 + \kappa_2$ *the sum of the principal curvatures, and* $\mathbf{n}$ *the outward unit normal on* Γ. *Then for all sufficiently smooth vector functions* $\mathbf{v}$ *on* Γ *the following holds:*

$$\int_\Gamma \kappa\, \mathbf{n} \cdot \mathbf{v}\, ds = -\int_\Gamma (\Delta_\Gamma \,\mathrm{id}_\Gamma) \cdot \mathbf{v}\, ds = \int_\Gamma \nabla_\Gamma \,\mathrm{id}_\Gamma \cdot \nabla_\Gamma \mathbf{v}\, ds \,.$$

We construct a polygonal approximation Γ_h of the interface Γ as the approximate zero level of the piecewise *quadratic* discrete level set function ϕ_h.. The localized force term $f_\Gamma(\mathbf{v}_h)$ is approximated by

$$f_{\Gamma_h}(\mathbf{v}_h) := \tau \int_{\Gamma_h} \nabla_{\Gamma_h} \,\mathrm{id}_{\Gamma_h} \cdot \nabla_{\Gamma_h} \mathbf{v}_h\, ds, \qquad \mathbf{v}_h \in \mathbf{V}_h \tag{4.3}$$

where $\mathbf{V}_h$ is the finite element space defined in Section 3.2.2.

From the identity

$$\nabla_{\Gamma_h} \,\mathrm{id}_{\Gamma_h} = \mathbf{P}_h \nabla \,\mathrm{id}_{\Gamma_h} = (\mathbf{P}_h \mathbf{e}_1, \mathbf{P}_h \mathbf{e}_2, \mathbf{P}_h \mathbf{e}_3)^T$$

with $\mathbf{e}_i$ the i-th standard basis vector in $\mathbb{R}^3$, we obtain

$$\begin{aligned} f_{\Gamma_h}(\mathbf{v}_h) &= \tau \int_{\Gamma_h} \mathbf{P}_h \nabla \operatorname{id}_{\Gamma_h} \cdot \nabla_{\Gamma_h} \mathbf{v}_h \, ds \\ &= \tau \sum_{i=1}^{3} \int_{\Gamma_h} \mathbf{P}_h \mathbf{e}_i \cdot \nabla_{\Gamma_h} (\mathbf{v}_h)_i \, ds. \end{aligned} \tag{4.4}$$

The analysis in [GR07b] yields the following error bound

$$\sup_{\mathbf{v}_h \in \mathbf{V}_h} \frac{|f_\Gamma(\mathbf{v}_h) - f_{\Gamma_h}(\mathbf{v}_h)|}{\|\mathbf{v}_h\|_1} \leq c \sqrt{h_\Gamma}. \tag{4.5}$$

As mentioned in Section 3.2.3, the term $\sup_{\mathbf{v}_h \in \mathbf{V}_h} \frac{|f_\Gamma(\mathbf{v}_h) - f_{\Gamma_h}(\mathbf{v}_h)|}{\|\mathbf{v}_h\|_1}$ contributes to the upper bound for the discretization error. The estimate (4.5) states that the discretization (4.4) results in suboptimal bounds for $\|\mathbf{u} - \mathbf{u}_h\|_1$ and $\|p - p_h\|_{L^2}$. The numerical results in [GR07b, GMT07] also show that the bound in (4.5) is sharp.

The *improved Laplace-Beltrami discretization* in [GR07b] is introduced to overcome the poor approximation error bound (4.5) using the following improved projection $\tilde{\mathbf{P}}_h$

$$\tilde{\mathbf{P}}_h(x) := \mathbf{I} - \tilde{\mathbf{n}}_h(x) \tilde{\mathbf{n}}_h(x)^T, \quad x \in \Gamma_h$$

where

$$\tilde{\mathbf{n}}_h(x) := \frac{\nabla \phi_h(x)}{\|\nabla \phi_h(x)\|}.$$

The modified localized force term $\tilde{f}_{\Gamma_h}(\mathbf{v}_h)$ is defined as follows

$$\tilde{f}_{\Gamma_h}(\mathbf{v}_h) := \tau \int_{\Gamma_h} \tilde{\mathbf{P}}_h \nabla \operatorname{id}_{\Gamma_h} \cdot \nabla_{\Gamma_h} \mathbf{v}_h \, ds \;=\; \tau \sum_{i=1}^{3} \int_{\Gamma_h} \tilde{\mathbf{P}}_h \mathbf{e}_i \cdot \nabla_{\Gamma_h} (\mathbf{v}_h)_i \, ds \tag{4.6}$$

for all $\mathbf{v}_h \in \mathbf{V}_h$.

The analysis in [GR07b] gives the estimate

$$\sup_{\mathbf{v}_h \in \mathbf{V}_h} \frac{|f_\Gamma(\mathbf{v}_h) - \tilde{f}_{\Gamma_h}(\mathbf{v}_h)|}{\|\mathbf{v}_h\|_1} \leq c \, h_\Gamma.$$

4.2 Discretization of $f_\Gamma(\mathbf{v})$ with variable surface tension coefficient

We consider the case where the surface tension coefficient τ is not necessarily constant. The localized surface force $f_\Gamma(\mathbf{v})$ then has the form

$$f_\Gamma(\mathbf{v}) = \int_\Gamma (\tau\kappa\mathbf{n} - \nabla_\Gamma\tau)\cdot\mathbf{v}ds. \tag{4.7}$$

Using the result from Theorem 4.1 and integration by part, we rewrite (4.7) for all $\mathbf{v}_h \in \mathbf{V}_h$ as follows

$$\begin{aligned}
f_\Gamma(\mathbf{v}_h) &= \int_\Gamma (\tau\kappa\mathbf{n} - \nabla_\Gamma\tau)\cdot\mathbf{v}_h ds \\
&= \int_\Gamma (\tau(-\Delta_\Gamma \mathrm{id}_\Gamma) - \nabla_\Gamma\tau)\cdot\mathbf{v}_h ds \\
&= \int_\Gamma (-\Delta_\Gamma \mathrm{id}_\Gamma)\cdot(\tau\mathbf{v}_h)\, ds - \int_\Gamma \nabla_\Gamma\tau\cdot\mathbf{v}_h\, ds \\
&= \int_\Gamma \nabla_\Gamma \mathrm{id}_\Gamma \cdot\nabla_\Gamma(\tau\mathbf{v}_h)\, ds - \int_\Gamma \nabla_\Gamma\tau\cdot\mathbf{v}_h\, ds \\
&= \sum_{i=1}^{3}\int_\Gamma \nabla_\Gamma(\mathrm{id}_\Gamma)_i\,\nabla_\Gamma(\tau\cdot(\mathbf{v}_h)_i)\, ds - \int_\Gamma \nabla_\Gamma\tau\cdot\mathbf{v}_h\, ds \\
&= \sum_{i=1}^{3}\Big(\int_\Gamma \nabla_\Gamma(\mathrm{id}_\Gamma)_i\,[(\nabla_\Gamma\tau)\,(\mathbf{v}_h)_i + \tau\,(\nabla_\Gamma(\mathbf{v}_h)_i)]\; ds\Big) \\
&\quad - \int_\Gamma \nabla_\Gamma\tau\cdot\mathbf{v}_h\, ds \\
&= \sum_{i=1}^{3}\Big(\int_\Gamma \tau\nabla_\Gamma(\mathrm{id}_\Gamma)_i\,\nabla_\Gamma(\mathbf{v}_h)_i\, ds + \sum_{i=1}^{3}\int_\Gamma (\mathbf{v}_h)_i\,\nabla_\Gamma(\mathrm{id}_\Gamma)_i\,\nabla_\Gamma\tau\, ds\Big) \\
&\quad - \int_\Gamma \nabla_\Gamma\tau\cdot\mathbf{v}_h\, ds.
\end{aligned} \tag{4.8}$$

We assume that $\tau = \tau(x)$, which is defined for $x \in \Gamma$, has an extension to $x \in \Gamma_h$. Applying the improved Laplace-Beltrami discretization in Section

4.1 to the last expression in (4.8), we obtain the approximation

$$\tilde{f}_{\Gamma_h}(\mathbf{v}_h) \approx \sum_{i=1}^{3} \Big(\int_{\Gamma_h} \tau\, \tilde{\mathbf{P}}_h \mathbf{e}_i \cdot \nabla_{\Gamma_h} (\mathbf{v}_h)_i \, ds + \int_{\Gamma_h} (\mathbf{v}_h)_i \, \tilde{\mathbf{P}}_h \mathbf{e}_i \cdot \nabla_{\Gamma_h} \tau \, ds \Big) - \int_{\Gamma_h} \tilde{\mathbf{P}}_h \nabla \tau \cdot \mathbf{v}_h \, ds. \tag{4.9}$$

Note that if τ is constant, the approximations in (4.9) and (4.6) are identical. An error analysis of this discretization scheme is not available, yet.

4.3 Implementation issues

In our implementation, we consider a model in which a smooth extensions τ^e of the surface tension coefficient τ is given in a (small) neighbourhood of Γ. The piecewise polygonal approximation Γ_h of the interface Γ is constructed as in section 3.2.4. For each tetrahedron T which is intersected by Γ_h, let T' be one of the 8 regular children of T. The planar segment $\Gamma_{h,T'} = T' \cap \Gamma_h$ is either a triangle or a quadrilateral, the latter can be subdivided into 2 triangles. Without loss of generality, we can assume that $\Gamma_{h,T'}$ is a triangle. Thus local integrals over $\Gamma_{h,T'}$ of smooth functions can be computed with high accuracy using a Gauss quadrature rule on a triangle. We construct a data structure which allows fast evaluations of the approximate level set function ϕ_h on the tetrahedron T. With this structure, the normal vector $\tilde{\mathbf{n}}_h$, and thus the projection $\tilde{\mathbf{P}}_h$, at the Gauss quadrature nodes (in barycentric coordinates) on $\Gamma_{h,T'}$ can be easily determined.

In chapter 7 we consider a model in which the surface tension coefficient τ depends on the restriction to the interface of the concentration c of a dissolved species in the continuous phase Ω_2, cf. (7.2). In this model, the concentration is discontinuous across the interface and is approximated by a function in the XFEM space Q_h^Γ. Let T be a tetrahedron defined as above. We determine the linear extension c_2^e of c_2 in T and evaluate the extension τ^e of τ at the Gauss quadrature nodes on $\Gamma_{h,T'}$ using (7.2). The gradient of τ^e on T is computed by the chain rule

$$\nabla \tau^e = \frac{\partial \tau^e}{\partial c_2^e} \cdot \nabla c_2^e.$$

The term ∇c_2^e is easy to determine, since c_2^e is a linear function in T, while $\frac{\partial \tau^e}{\partial c_2^e}$ is derived from (7.2).

4.4 Numerical experiment

In this section, we present results of numerical simulations for problems with a variable surface tension coefficient. These simulations are performed by the research group at the Chair of Thermal Process Engineering (RWTH Aachen), cf. [BKP09, BP09], using the DROPS package. In this package we implemented the discretization method for the localized surface tension force as discussed in Sections 4.2 and 4.3. A similar simulation has been addressed in [EGR08], which describes the dynamics of a levitated toluene droplet in a downward going water flow using a simple model for the variable surface tension τ. The simulation is motivated by a measurement using the fast NMR (nuclear magnetic resonance) technique, cf. [ASB05], which is displayed in Figure 4.1. In this NMR image, a velocity field inside the droplet at the equilibrium state is shown and a so-called "stagnant cap" can be recognized, with very low velocity in the lower half of the droplet. This effect is considered to be a consequence of the variable surface tension due to the appearance of surfactants. The "stagnant cap" occurs in the region where the contaminant tends to accumulate, cf. [Ama06], i. e. where the surface tension coefficient is lower.

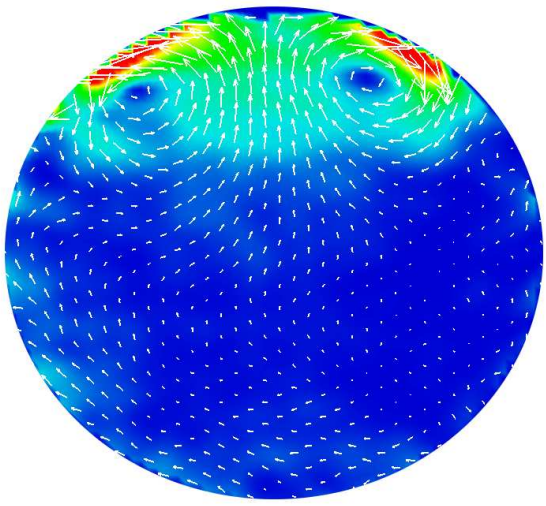

Figure 4.1: Stagnant cap in experiment.

As the exact surface tension coefficient τ is not known, we construct a model in which the value of τ in the lower part of the droplet is smaller than

that in the upper part. A smoothed piecewise constant function τ which depends on the height of the droplet is considered for simplicity. First we map the current vertical coordinate of the droplet to the interval $[0, 2]$, with 0 corresponding to the highest point and 2 to the lowest point of the droplet. For all $z \in [0, 2]$, we define a piecewise constant function which has a jump at $z_{jump} \in (0, 2)$

$$t(z) = \begin{cases} \tau_0 & \text{if } 0 \leq z < z_{jump}, \\ a \cdot \tau_0 & \text{if } z_{jump} \leq z \leq 2. \end{cases}$$

with some value $\tau_0 > 0$ and a factor $a \in (0, 1]$, and regularize this function in the neighbourhood of the jump position as follows:

$$\tau(z) = \begin{cases} \tau_0 & \text{if } 0 \leq z < z_{jump} - \epsilon, \\ s(z) & \text{if } z_{jump} - \epsilon \leq z \leq z_{jump} + \epsilon, \\ a \cdot \tau_0 & \text{if } z_{jump} + \epsilon < z \leq 2. \end{cases}$$

The function $s(z)$ is chosen such that $\tau(z)$ is smooth in the interval $[0, 2]$. Thus, the surface tension coefficient is determined by three parameters:

- A factor $a \in (0, 1]$,
- The jump position $z_{jump} \in (0, 2)$,
- The width ϵ of the region in which the function t is smoothed.

In Figure 4.2 the colour coding indicates the magnitude of the surface tension coefficient. The material coefficients are given in Table 4.1. The diameter of the droplet is $d = 4\,\text{mm}$. The surface tension in the upper part of the droplet is $\tau_0 = 34.31 \cdot 10^{-3}\,\text{N/m}$. The jump position $z_{jump} = 0.5$ and the jump width $2 \cdot 10^{-3}$ are used in the simulations.

For the spatial discretization, the finite element pair $(\mathbf{V}_h, Q_h^\gamma)$ for the velocity and pressure is used. For the level set equation, the piecewise quadratic finite elements are used. The surface force f_Γ is approximated by (4.9). The problem is discretized in time using the linearized θ-scheme (3.33) ($\theta = 1$) in Section 3.3.2 with the time step size $\Delta t = 2 \cdot 10^{-4}\,\text{s}$.

In the first simulation, the factor $a = 0.95$ is used. The constant downward inflow velocity is $80\,\text{mm/s}$. In Figure 4.3, the velocity distribution at $t = 0.1$ is shown, which exhibits a similar "stagnant cap" as in the experimental one in Figure 4.1. Small counter vortices below the jump position can also be seen.

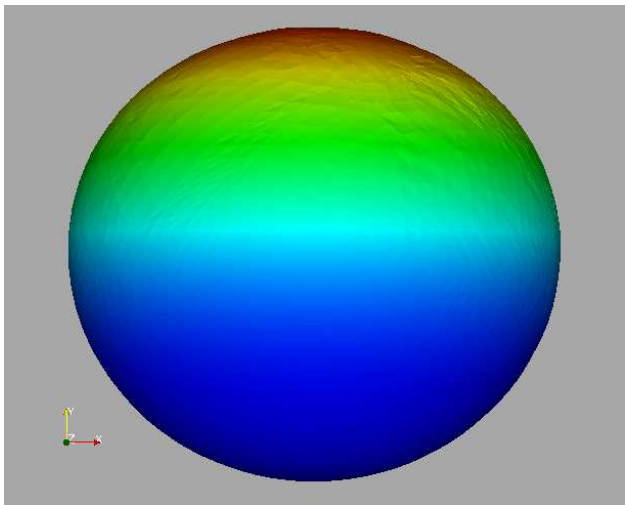

Figure 4.2: Distribution of the variable surface tension τ on the interface.

toluene-water		
	$\mu[Pa \cdot s]$	$\rho[kg/m^3]$
Ω_1	5.96e-4	867
Ω_2	1.03e-3	999

Table 4.1: Material properties

In the second simulation, a small change of the surface tension in the lower part is considered, with $a = 0.94$. The downward inflow velocity for this case is 83 mm/s, which is chosen such that the droplet quickly reaches its equilibrium position. The velocity distribution for this simulation is shown in Figure 4.4. In this case, the influence of Marangoni convection due to the concentration difference is significantly larger: the vortices in the upper part almost disappear while the counter vortices are dominant. In reality, the assumption that the ratio of the surface tension coefficient between the lower and upper parts of the droplet remains unchanged is not valid, since the surfactant in the lower part will be transported upwards due to the Marangoni convection, and thus the difference of the surfactant concentration will be reduced. Hence, such a velocity field can not be observed in experiments.

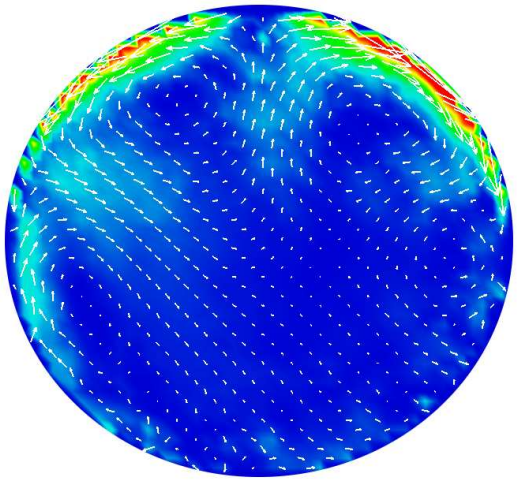

Figure 4.3: Stagnant cap in simulation for $a = 0.95$.

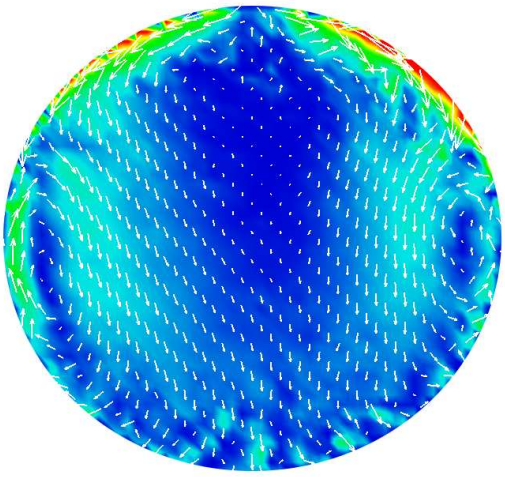

Figure 4.4: Velocity field in simulation for $a = 0.94$.

Chapter 5

Two-phase mass transport problem with a stationary interface

The results in this chapter are new and were recently published in [RN09]. We consider the mass transport equation (2.2)-(2.4) in the *stationary* case, in which the interface Γ does not depend on time. A model example is a droplet at a stationary position in a flow field. For simplicity, we assume that the surface tension coefficient τ in the two-phase flow Navier-Stokes equations (3.1) is independent of the concentration of the dissolved species. Hence the mass transport equations have no effect upon the two-phase flow problem. For the sake of convenience, in this chapter as well as in Chapter 6, we rewrite the equations (2.2)-(2.4) using some new notations, with $u(\mathbf{x}, t)$ denoting the concentration and $\mathbf{w}$ the divergence-free velocity field resulting from (3.1). The Dirichlet boundary condition on $\partial\Omega$ is taken to simplify the analysis.

$$\frac{\partial u}{\partial t} + \mathbf{w} \cdot \nabla u - \operatorname{div}(\alpha \nabla u) = f \quad \text{in } \Omega_i,\ i = 1, 2,\ t \in [0, T], \tag{5.1}$$

$$[\alpha \nabla u \cdot \mathbf{n}]_\Gamma = 0, \tag{5.2}$$

$$[\beta u]_\Gamma = 0, \tag{5.3}$$

$$u(\cdot, 0) = u_0 \quad \text{in } \Omega_i,\ i = 1, 2, \tag{5.4}$$

$$u(\cdot, t) = 0 \quad \text{on } \partial\Omega, \quad t \in (0, T]. \tag{5.5}$$

For the special case $\beta_1 = \beta_2$ (no discontinuity) and with a triangulation

which is *fitted* to the interface, standard finite element spaces have (close to) optimal approximation properties. In [CZ98] it is proved that in this special case for standard linear finite elements an L^2-discretization error bound of the order $h^2 \log h$ holds.

We allow $\beta_1 \neq \beta_2$ and use triangulations that are *un*fitted (as in level set or VOF approaches), i.e. the interface crosses the elements. We will analyze a variant of Nitsche's method [Nit71] for the spatial discretization of this problem. From this semi-discrete problem a full discretization is obtained by using a standard θ-scheme for time discretization. We use the same Nitsche method as presented and analyzed in [HH02], cf. also [HH04, HHL03, Han05]. In that paper this method is applied to a *stationary* heat conduction problem with a conductivity that is discontinuous across the interface ($\alpha_1 \neq \alpha_2$) but with a solution that is continuous across the interface ($\beta_1 = \beta_2$). We apply this method to the *instationary* problem described above, with $\beta_1 \neq \beta_2$ (discontinuous solution), and furthermore allow a convection term in (2.2) (in [HH02] only pure diffusion is considered). We consider, however, only the diffusion dominated case. For convection dominated problems additional stabilization terms in the Nitsche method are needed, which will be studied in future work. In the error analysis that we present some key results from [HH02] are used.

We also mention the papers [HJ07a, HJ07b, HN03, HP02, HP05] in which a similar Nitsche method is applied and analyzed in a different setting, namely as a mortar method, which allows the use of non-matching meshes, for the discretization of elliptic and parabolic problems with smooth solutions.

Remark 5.1. The discontinuity of u across the interface can be avoided by introducing transformed quantities $\tilde{u} := \beta u,\ \tilde{\alpha} := \alpha/\beta,\ \tilde{\mathbf{w}} := \mathbf{w}/\beta$. Then (2.2)-(2.4) can be reformulated as

$$\beta^{-1}\frac{\partial \tilde{u}}{\partial t} + \tilde{\mathbf{w}} \cdot \nabla \tilde{u} - \operatorname{div}(\tilde{\alpha}\nabla \tilde{u}) = f \quad \text{in } \ \Omega_i,\ i = 1, 2,\ t \in [0, T], \tag{5.6}$$

$$[\tilde{\alpha}\nabla \tilde{u} \cdot \mathbf{n}]_\Gamma = 0, \tag{5.7}$$

$$[\tilde{u}]_\Gamma = 0. \tag{5.8}$$

In this formulation we have continuity of $\tilde{u}$ across Γ but, compared to (2.2), a subdomain dependent scaling factor β^{-1} in front of the time derivative. The scaled velocity $\tilde{\mathbf{w}}$ is also discontinuous across the interface.

We will consider the model in the formulation (5.1)-(5.5). The discretization method obtained for this model immediately yields an analogon for the

transformed model (5.6)-(5.8), cf. remark 5.5.

The chapter is organized as follows. In Section 5.1 we discuss a weak formulation of the problem (5.1)-(5.5). Nitsche's finite element method for the spatial discretization is presented in Section 5.2 . In Section 5.3 optimal discretization error bounds are derived. In Section 5.4 the issue of time discretization is briefly addressed. Finally, in section 5.5 we present results of numerical experiments with a three-dimensional transport problem of the form (5.1)-(5.5).

5.1 Weak formulation

In this section we give a weak formulation of the problem (5.1)-(5.5) which, under reasonable assumptions on the data f, u_0 (and $\mathbf{w}$), has a unique solution. We assume that for the function u_0 in the initial condition (5.4) the conditions in (5.2), (5.3) are satisfied. For simplicity we only consider homogeneous Dirichlet boundary conditions in (5.5). Note that this boundary condition is given (only) on $\partial\Omega$ and thus if $\partial\Omega_1 \cap \partial\Omega = \emptyset$, then it does not prescribe values for $u_1 = u_{|\Omega_1}$.

Due to the fact that the underlying two-phase fluid dynamics concerns two incompressible immiscible phases it is reasonable to make the following assumption about the velocity field $\mathbf{w}$:

$$\operatorname{div} \mathbf{w} = 0 \quad \text{in} \quad \Omega_i,\ i = 1,2, \ \text{and} \quad \mathbf{w}\cdot\mathbf{n} = 0 \quad \text{at} \quad \Gamma, \quad \|\mathbf{w}\|_{L^\infty(\Omega)} \le c < \infty. \tag{5.9}$$

In the remainder of the chapter we assume that (5.9) holds.

For a weak formulation we introduce suitable Hilbert spaces. We define $H_0^1(\Omega_1 \cup \Omega_2) := \{\, v \in L^2(\Omega) : \ v_i \in H^1(\Omega_i),\ i = 1,2,\ v_{|\partial\Omega} = 0 \,\}$, where $v_i := v_{|\Omega_i}$, and

$$H := L^2(\Omega), \quad V := \{\, v \in H_0^1(\Omega_1 \cup \Omega_2) : \ [\beta v]_\Gamma = 0 \,\}.$$

On H we use the scalar product

$$(u,v)_0 := \int_\Omega \beta u v \, dx,$$

which clearly is equivalent to the standard scalar product on $L^2(\Omega)$. The corresponding norm on H is denoted by $\|\cdot\|_0$. For $u, v \in H^1(\Omega_1 \cup \Omega_2)$ we define $(u_i, v_i)_{1,\Omega_i} := \beta_i \int_{\Omega_i} \nabla u_i \cdot \nabla v_i \, dx$ and

$$(u, v)_{1,\Omega_1\cup\Omega_2} := (u, v)_{1,\Omega_1} + (u, v)_{1,\Omega_2}, \quad u, v \in V.$$

The corresponding norm on V is denoted by $|\cdot|_{1,\Omega_1\cup\Omega_2}$. This norm is equivalent with

$$\big(\|\cdot\|_0^2 + |\cdot|_{1,\Omega_1\cup\Omega_2}^2\big)^{\frac{1}{2}} =: \|\cdot\|_{1,\Omega_1\cup\Omega_2}.$$

The space $\big(V, (\cdot,\cdot)_{1,\Omega_1\cup\Omega_2}\big)$ is a Hilbert space. We obtain a Gelfand triple $V \hookrightarrow H \equiv H' \hookrightarrow V'$, with dense and continuous embeddings $\hookrightarrow$.

We now introduce the bilinear form

$$a(u, v) := (\alpha u, v)_{1,\Omega_1\cup\Omega_2} + (\mathbf{w} \cdot \nabla u, v)_0, \quad u, v \in V.$$

This bilinear form is continuous on V and using (5.9) we get, for $u \in V$,

$$\begin{aligned}(\mathbf{w} \cdot \nabla u, u)_0 &= \sum_{i=1,2} \beta_i \int_{\Omega_i} \mathbf{w} \cdot \nabla u_i \, u_i \, dx \\ &= \int_\Gamma \mathbf{w} \cdot \mathbf{n} [\beta u^2]_{|\Gamma} \, ds - \sum_{i=1,2} \beta_i \int_{\Omega_i} \operatorname{div} \mathbf{w} \, u_i^2 \, dx - (\mathbf{w} \cdot \nabla u, u)_0 \\ &= -(\mathbf{w} \cdot \nabla u, u)_0.\end{aligned} \tag{5.10}$$

Hence, $(\mathbf{w} \cdot \nabla u, u)_0 = 0$ holds. This yields ellipticity of $a(\cdot,\cdot)$:

$$a(u, u) \geq \big(\min_{i=1,2} \alpha_i\big) |u|_{1,\Omega_1\cup\Omega_2}^2 \quad \text{for all} \;\; u \in V. \tag{5.11}$$

We introduce some further standard notation. If X is a Banach space then $L^2(0, T; X)$ is the space of L^2 functions from $(0, T)$ into X, which is a Banach space for the norm

$$\|f\|_{L^2(0,T;X)} = \Big(\int_0^T \|f(t)\|_X^2 \, dt \Big)^{\frac{1}{2}}.$$

Furthermore $C([0, T]; X)$ denotes the space of continuous functions from $[0, T]$ into X, which is a Banach space for the norm

$$\|f\|_{C([0,T];X)} = \sup_{t\in[0,T]} \|f(t)\|_X.$$

Now consider the following weak formulation of (5.1)-(5.5). Given $f \in V'$, $u_0 \in H$, determine $u \in L^2(0,T;V)$ such that

$$u(0) = u_0, \quad \langle \frac{\partial u}{\partial t}, v \rangle + a(u,v) = \langle f, v \rangle \quad \text{for all} \quad v \in V. \tag{5.12}$$

Here $\langle \cdot, \cdot \rangle$ denotes the duality pairing on $V' \times V$. The derivative $\frac{\partial u}{\partial t}$ is defined in a distributional sense, cf. for example [LM72, Tem84]. In particular $\frac{\partial u}{\partial t} \in L^2(0,T;V')$. It can be shown ([LM72, Tem84]) that $u \in C([0,T];H)$ holds and thus the initial condition $u(0) = u_0$ is well-defined. It is proved in [LM72, Tem84] that the weak formulation (5.12) *has a unique solution.*

Remark 5.2. This existence and uniqueness result still holds (cf. [Tho97, EG04]) if instead of ellipticity of the bilinear form $a(\cdot,\cdot)$, cf. (5.11), one has the weaker property

$$a(u,u) \geq c_0 |u|^2_{1,\Omega_1 \cup \Omega_2} - c_1 \|u\|^2_0 \quad \text{for all} \quad u \in V,$$

with constants $c_0 > 0$ and c_1 independent of u. Using

$$|(\mathbf{w} \cdot \nabla u, u)_0| \leq c |u|_{1,\Omega_1 \cup \Omega_2} \|u\|_0$$

it easily follows that this property holds *without* using the first two assumptions in (5.9). We introduce these assumptions because they simplify the presentation of the analysis for the continuous problem and we need them in our analysis of Nitsche's method in Section 5.3.

The duality pairing in (5.12) can be replaced by the scalar product $(\cdot,\cdot)_0$ on H if one assumes additional regularity of the data f and u_0. Related to this regularity issue we first consider the stationary problem: for $f \in H$,

$$\text{find} \quad w \in V \quad \text{such that} \quad a(w,v) = (f,v)_0 \quad \text{for all} \quad v \in V. \tag{5.13}$$

The unique solution w of this problem satisfies

$$w \in V_{\text{reg}} := \{\, v \in V : \, v_i \in H^2(\Omega_i), \quad i = 1, 2. \,\}, \tag{5.14}$$

and

$$\|w\|_{2,\Omega_1 \cup \Omega_2} := \left(\|w\|^2_{1,\Omega_1 \cup \Omega_2} + |w|^2_{2,\Omega_1 \cup \Omega_2} \right)^{\frac{1}{2}} \leq c \, \|f\|_0 \tag{5.15}$$

holds, with a constant c independent of f. For the stationary problem it is no restriction to assume $\beta_1 = \beta_2$, since the general case can be reduced to that by a transformation as in (5.6)-(5.8). For the symmetric case $\mathbf{w} = 0$, this regularity result is given in [CZ98]. For the general case such regularity results are derived in Chapter 3 of [LU68] (cf. also [LRU66]). The space V_{reg} is a Banach space with respect to the norm $\|\cdot\|_{2,\Omega_1\cup\Omega_2}$. Using this regularity result it follows from Theorem 3.2 in [Tem88] that the following holds:

Lemma 5.1. *Take $f \in H$, $u_0 \in V_{\mathrm{reg}}$ There exists a unique $u \in C([0,T];V_{\mathrm{reg}})$ such that $u(0) = u_0$ and*

$$(\frac{\partial u}{\partial t}, v)_0 + a(u,v) = (f,v)_0 \quad \textit{for all} \;\; v \in V. \tag{5.16}$$

Moreover, the distributional time derivative satisfies

$$\frac{\partial u}{\partial t} \in L^2(0,T;V) \cap C([0,T];H). \tag{5.17}$$

We now show that the variational problem (5.16) is indeed a correct weak formulation of the problem (5.1)-(5.5).

Lemma 5.2. *Take $f \in H$, $u_0 \in V_{\mathrm{reg}}$. Assume that (5.1)-(5.5) has a solution $u(x,t)$ which is sufficiently smooth such that for $u : t \to u(\cdot,t)$ we have $u \in C([0,T];V_{\mathrm{reg}})$ and $\frac{\partial u}{\partial t} \in L^2(0,T;H)$. This u solves the variational problem (5.16).*
Conversely, if $u \in C([0,T];V_{\mathrm{reg}})$ with $u(0) = u_0$ solves the variational problem (5.16) then u satisfies (5.1) in a weak $L^2(\Omega_i)$ sense and (5.2), (5.3), (5.5) in trace sense.

Proof. Take $u \in C([0,T];V_{\mathrm{reg}})$ with $\frac{\partial u}{\partial t} \in L^2(0,T;H)$, and $v \in V$. Using $[\beta v] = 0$ we get

$$\begin{aligned}
[\alpha\nabla u \cdot \mathbf{n}\beta v]_\Gamma &= [\alpha\nabla u \cdot \mathbf{n}]_\Gamma \frac{1}{2}\big((\beta_1 v_1)_{|\Gamma} + (\beta_2 v_2)_{|\Gamma}\big) \\
&\quad + \frac{1}{2}\big((\alpha_1\nabla u_1 \cdot \mathbf{n})_{|\Gamma} + (\alpha_2 \nabla u_2 \cdot \mathbf{n})_{|\Gamma}\big)[\beta v]_{|\Gamma} \\
&= [\alpha\nabla u \cdot \mathbf{n}]_\Gamma \frac{1}{2}\big((\beta_1 v_1)_{|\Gamma} + (\beta_2 v_2)_{|\Gamma}\big).
\end{aligned}$$

Using this we obtain

$$
\begin{aligned}
&(\frac{\partial u}{\partial t}, v)_0 + a(u,v) \\
&= (\frac{\partial u}{\partial t}, v)_0 + (\mathbf{w}\cdot\nabla u, v)_0 - \sum_{i=1,2}\int_{\Omega_i} \operatorname{div}(\alpha_i \nabla u)\beta_i v\, dx + \int_\Gamma [\alpha\nabla u\cdot\mathbf{n}\beta v]_\Gamma\, ds \\
&= \sum_{i=1,2}\int_{\Omega_i} \big(\frac{\partial u}{\partial t} + \mathbf{w}\cdot\nabla u - \operatorname{div}(\alpha_i\nabla u)\big)\beta_i v\, dx \\
&\quad + \int_\Gamma [\alpha\nabla u\cdot\mathbf{n}]_\Gamma \frac{1}{2}\big((\beta_1 v_1)_{|\Gamma} + (\beta_2 v_2)_{|\Gamma}\big)\, ds.
\end{aligned}
\tag{5.18}
$$

If u satisfies (5.1), (5.2) we thus obtain

$$
(\frac{\partial u}{\partial t}, v)_0 + a(u,v) = (f,v)_0 \quad \text{for all} \quad v \in V,
$$

i.e., (5.16) holds. Conversely, if $u \in C([0,T]; V_{\mathrm{reg}})$ with $u(0) = u_0$ solves the variational problem (5.16) we obtain

$$
\begin{aligned}
&\sum_{i=1,2}\int_{\Omega_i} \big(\frac{\partial u}{\partial t} + \mathbf{w}\cdot\nabla u - \operatorname{div}(\alpha_i\nabla u) - f\big)\beta_i v\, dx \\
&\quad + \int_\Gamma [\alpha\nabla u\cdot\mathbf{n}]_\Gamma \frac{1}{2}\big((\beta_1 v_1)_{|\Gamma} + (\beta_2 v_2)_{|\Gamma}\big)\, ds = 0
\end{aligned}
$$

for all $v \in V$. This implies that $\frac{\partial u}{\partial t} + \mathbf{w}\cdot\nabla u - \operatorname{div}(\alpha_i\nabla u) = f$ in $L^2(\Omega_i)$ sense and $[\alpha\nabla u\cdot\mathbf{n}]_\Gamma = 0$ in trace sense. The properties in (5.3) and (5.5) hold due to $u \in V$. □

For the result in (5.18) it is essential that we multiply the equation (2.2) by βv and not by v. This explains why in the scalar products $(\cdot,\cdot)_0$ and $(\cdot,\cdot)_{1,\Omega_1\cup\Omega_2}$ we use the weighting with the (piecewise constant) function β.

5.2 Nitsche's method

We present Nitsche's method for the *two*-dimensional case, $\Omega \subset \mathbb{R}^2$, along the same lines as in [HH02]. Both the method and its convergence analysis

can be extended to the three-dimensional case, cf. Remark 5.4 below. For ease of presentation we decided to consider the 2D case. In our numerical experiments in Section 5.5.3 we consider three-dimensional problems.

Let $\{\mathcal{T}_h\}_{h>0}$ be a family of shape regular triangulations of Ω. A triangulation $\mathcal{T}_h$ consists of triangles T, with $h_T := \operatorname{diam}(T)$ and $h := \max\{ h_T \mid T \in \mathcal{T}_h\}$. For any triangle $T \in \mathcal{T}_h$ let $T_i := T \cap \Omega_i$ be the part of T in Ω_i. For any T with $T \cap \Gamma \neq \emptyset$ we define $\Gamma_T := T \cap \Gamma$. Related to the triangulation we formulate the same assumptions as in [HH02]:

Assumption 1. Consider a T with $T \cap \Gamma \neq \emptyset$. We assume that the interface Γ intersects ∂T exactly twice and each edge of T at most once. Let $\Gamma_{T,h}$ be the straight line connecting the points of intersection between Γ and ∂T. We assume that Γ_T is a function of length on $\Gamma_{T,h}$:

$$\Gamma_{T,h} = \{\, (\xi,\eta) :\ 0 < \xi < |\Gamma_{T,h}|,\ \eta = 0 \,\},$$
$$\Gamma_T = \{\, (\xi,\eta) :\ 0 < \xi < |\Gamma_{T,h}|,\ \eta = \delta(\xi) \,\}.$$

The assumptions formulated in Assumption 1 are satisfied on sufficiently fine meshes. We now introduce the finite element space

$$V_h^\Gamma := \{\, v \in H_0^1(\Omega_1 \cup \Omega_2) :\ v_{|T_i} \ \text{ is linear for all } \ T \in \mathcal{T}_h,\ i = 1, 2. \,\} \quad (5.19)$$

Note that $V_h^\Gamma \subset H_0^1(\Omega_1 \cup \Omega_2)$, but $V_h^\Gamma \not\subset V$, since the Henry interface condition $[\beta v_h] = 0$ does not necessarily hold for $v_h \in V_h^\Gamma$.

Define

$$(\kappa_i)_{|T} = \frac{|T_i|}{|T|}, \quad T \in \mathcal{T}_h,\ i = 1, 2,$$

hence, $\kappa_1 + \kappa_2 = 1$. For v sufficiently smooth such that $(v_i)_{|\Gamma}$, $i = 1, 2$, are well-defined, we define the weighted average

$$\{v\} := \kappa_1 (v_1)_{|\Gamma} + \kappa_2 (v_2)_{|\Gamma}.$$

For the average and jump operators the following identity holds for all f, g such that these operators are well-defined:

$$[fg] = \{f\}[g] + [f]\{g\} - (\kappa_1 - \kappa_2)[f][g]. \quad (5.20)$$

Let $(f, g)_\Gamma := \int_\Gamma f g \, ds$ be the $L^2(\Gamma)$ scalar product. We introduce the bilinear form

$$\begin{aligned} a_h(u, v) := {} & (\alpha u, v)_{1,\Omega_1 \cup \Omega_2} + (\mathbf{w} \cdot \nabla u, v)_0 - ([\beta u], \{\alpha \nabla v \cdot \mathbf{n}\})_\Gamma \\ & - (\{\alpha \nabla u \cdot \mathbf{n}\}, [\beta v])_\Gamma + \lambda h^{-1} ([\beta u], [\beta v])_\Gamma, \end{aligned} \quad (5.21)$$

with $\lambda > 0$ a parameter. This bilinear form is well-defined on the space V_h^Γ but also on

$$W_{\text{reg}} := \{\, v \in H_0^1(\Omega_1 \cup \Omega_2) : \, v_i \in H^2(\Omega_i),\ i = 1, 2. \,\}.$$

The space W_{reg} is larger than the space V_{reg} in (5.14). The interface condition $[\beta v] = 0$ is fulfilled for all $v \in V_{\text{reg}}$ but not necessarily for $v \in W_{\text{reg}}$.

Using this bilinear form we define a method of lines discretization of (5.16). Let $u_{0,h} \in V_h^\Gamma$ be an approximation of u_0. For $t \in [0, T]$ let $u_h(t) \in V_h^\Gamma$ be such that $u_h(0) = u_{0,h}$ and

$$(\frac{\partial u_h}{\partial t}, v_h)_0 + a_h(u_h, v_h) = (f, v_h)_0 \quad \text{for all} \quad v_h \in V_h^\Gamma. \tag{5.22}$$

Opposite to the weak formulation in (5.16), in this discretization method the Henry interface condition $[\beta u_h] = 0$ is *not* treated as an "essential" interface condition in the finite element space V_h^Γ. The discrete problem is consistent (cf. Lemma 5.3 below) and the bilinear form $a_h(\cdot, \cdot)$ is stable. For the discrete solution the Henry interface condition is satisfied only approximately. As we will show in the following sections, this approach leads to optimal order error bounds (Section 5.3) and satisfactory results in numerical experiments (Section 5.5).

5.3 Analysis of Nitsche's method

In this section we present an error analysis of the method of lines discretization given in (5.22). We start with a consistency result:

Lemma 5.3. *Let $u = u(t) \in V_{\text{reg}}$ be the solution defined in Lemma 5.1. Then $u(t)$ satisfies*

$$(\frac{\partial u}{\partial t}, v_h)_0 + a_h(u, v_h) = (f, v_h) \quad \textit{for all} \quad v_h \in V_h^\Gamma, \quad t \in [0, T]. \tag{5.23}$$

Proof. From Lemma 5.2 we have that $u = u(t)$ satisfies $[\alpha \nabla u \cdot \mathbf{n}] = 0,\ [\beta u] = 0$. Using this and (5.20) we obtain:

$$\begin{aligned}
&- \sum_{i=1,2} \int_{\Omega_i} \operatorname{div}(\alpha_i \nabla u) \beta v_h \, dx + (\mathbf{w} \cdot \nabla u, v_h)_0 \\
&= - \int_\Gamma [\alpha \nabla u \cdot \mathbf{n} \beta v_h] \, ds + (\alpha u, v_h)_{1, \Omega_1 \cup \Omega_2} + (\mathbf{w} \cdot \nabla u, v_h)_0 \\
&= -(\{\alpha \nabla u \cdot \mathbf{n}\}, [\beta v_h])_\Gamma + (\alpha u, v_h)_{1, \Omega_1 \cup \Omega_2} + (\mathbf{w} \cdot \nabla u, v_h)_0 = a_h(u, v_h).
\end{aligned}$$

Furthermore, u solves (5.1) (in the sense as in Lemma 5.2). Multiplication of (5.1) by βv_h and integration over Ω results in

$$\begin{aligned}(f, v_h)_0 &= (\frac{\partial u}{\partial t}, v_h)_0 + (\mathbf{w}\cdot\nabla u, v_h)_0 - \sum_{i=1,2}\int_{\Omega_i} \operatorname{div}(\alpha_i \nabla u)\beta v_h \, dx \\ &= (\frac{\partial u}{\partial t}, v_h)_0 + a_h(u, v_h),\end{aligned}$$

and thus the consistency result holds. □

For the error analysis we introduce a suitable norm, as in [HH02]. Let G_h denote the set of all triangles that are intersected by Γ. We define

$$\|v\|^2_{1/2,h,\Gamma} := \sum_{T\in G_h} h_T^{-1}\|v\|^2_{L^2(\Gamma_T)}, \tag{5.24}$$

$$\|v\|^2_{-1/2,h,\Gamma} := \sum_{T\in G_h} h_T\|v\|^2_{L^2(\Gamma_T)}, \tag{5.25}$$

$$|\!|\!| v |\!|\!|^2 := |v|^2_{1,\Omega_1\cup\Omega_2} + \|\{\nabla v\cdot\mathbf{n}\}\|^2_{-1/2,h,\Gamma} + \|[\beta v]\|^2_{1/2,h,\Gamma}. \tag{5.26}$$

Note that different from [HH02] we have a scaling with β in the terms $|v|_{1,\Omega_1\cup\Omega_2}$ and $\|[\beta v]\|_{1/2,h,\Gamma}$. The bilinear form $a_h(\cdot,\cdot)$ has the following continuity and ellipticity properties with respect to the norm $|\!|\!|\cdot|\!|\!|$.

Lemma 5.4. *There exist constants c_1, $c_2 > 0$ such that for λ sufficiently large (independent of h) the following holds:*

$$|a_h(u,v)| \le c_1 |\!|\!| u |\!|\!| \, |\!|\!| v |\!|\!| \quad \textit{for all} \;\; u, v \in V_h^\Gamma + W_{\mathrm{reg}}, \tag{5.27}$$

$$a_h(v_h, v_h) \ge c_2 |\!|\!| v_h |\!|\!|^2 \quad \textit{for all} \;\; v_h \in V_h^\Gamma. \tag{5.28}$$

Proof. First note that $|(f,g)_\Gamma| \le \|f\|_{1/2,h,\Gamma}\|g\|_{-1/2,h,\Gamma}$ holds. Take $u, v \in V_h^\Gamma + W_{\mathrm{reg}}$. Using the Cauchy-Schwarz inequality and the definitions of the norms we obtain

$$\begin{aligned}|a_h(u,v)| \le{}& c\,|u|_{1,\Omega_1\cup\Omega_2}|v|_{1,\Omega_1\cup\Omega_2} + c\,|u|_{1,\Omega_1\cup\Omega_2}\|v\|_0 \\ &+ \|[\beta u]\|_{1/2,h,\Gamma}\|\{\alpha\nabla v\cdot\mathbf{n}\}\|_{-1/2,h,\Gamma} + \|\{\alpha\nabla u\cdot\mathbf{n}\}\|_{-1/2,h,\Gamma}\|[\beta v]\|_{1/2,h,\Gamma} \\ &+ \lambda\|[\beta u]\|_{1/2,h,\Gamma}\|[\beta v]\|_{1/2,h,\Gamma} \le c\,|\!|\!| u |\!|\!| \, |\!|\!| v |\!|\!|,\end{aligned}$$

which proves the continuity. Using the assumptions (5.9) we obtain for $v_h \in V_h^\Gamma$, cf. (5.10), $(\mathbf{w}\cdot\nabla v_h, v_h)_0 = 0$. Hence,

$$\begin{aligned} a_h(v_h,v_h) &\geq |\alpha^{\frac{1}{2}} v_h|^2_{1,\Omega_1\cup\Omega_2} - 2|(\{\alpha\nabla v_h\cdot\mathbf{n}\},[\beta v_h],)_\Gamma| + \lambda c\|[\beta v_h]\|^2_{1/2,h,\Gamma} \\ &\geq |\alpha^{\frac{1}{2}} v_h|^2_{1,\Omega_1\cup\Omega_2} - 2\|\{\alpha\nabla v_h\cdot\mathbf{n}\}\|_{-1/2,h,\Gamma}\|[\beta v]\|_{1/2,h,\Gamma} + \lambda c\|[\beta v_h]\|^2_{1/2,h,\Gamma}, \end{aligned}$$

with $c>0$ independent of h. From Lemma 4 in [HH02] we have

$$\|\{\alpha\nabla v_h\cdot\mathbf{n}\}\|_{-1/2,h,\Gamma} \leq c\,|\alpha^{\frac{1}{2}} v_h|_{1,\Omega_1\cup\Omega_2} \quad \text{for all} \;\; v_h\in V_h^\Gamma.$$

Using this we obtain the ellipticity result in (5.28), provided the parameter λ is chosen sufficiently large. □

In [HH02] an interpolation operator $I_h^* : H_0^1(\Omega)\cap H^2(\Omega_1\cup\Omega_2) \to V_h^\Gamma$ is introduced and an interpolation error bound is proved. This interpolation operator is defined as follows.

Let $E_i : H^2(\Omega_i) \to H^2(\Omega)$, $i=1,2$, be bounded extension operators and I_h the standard nodal linear interpolation operator corresponding to the triangulation $\mathcal{T}_h$. Define

$$I_h^* v := \big((I_h E_1 v_1)_{|\Omega_1}, (I_h E_1 v_2)_{|\Omega_2}\big).$$

This is well-defined not only for $v\in H_0^1(\Omega)\cap H^2(\Omega_1\cup\Omega_2)$ but also for v from the larger space W_{reg}. Moreover, the analysis in [HH02] (Theorem 2) does *not* use the fact that $v\in H_0^1(\Omega)\cap H^2(\Omega_1\cup\Omega_2)$ is continuous across Γ and it applies without changes to $v\in W_{\mathrm{reg}}$. The analysis of the interpolation error in [HH02] applies, with only minor changes, if in the norm $|\!|\!| \cdot |\!|\!|$ we use a scaling with β, cf.(5.26). Thus Theorem 2 in [HH02] yields the following.

Theorem 5.1. *Let $I_h^* : W_{\mathrm{reg}} \to V_h^\Gamma$ be the interpolation operator defined above. There exists a constant c such that*

$$|\!|\!| v - I_h^* v |\!|\!| \leq c\,h\|v\|_{2,\Omega_1\cup\Omega_2} \quad \textit{for all} \;\; v\in W_{\mathrm{reg}} \tag{5.29}$$

holds.

In the error analysis we use the elliptic projection $R_h : W_{\mathrm{reg}} + V_h^\Gamma \to V_h^\Gamma$, defined by

$$a_h(R_h v, w_h) = a_h(v,w_h) \quad \text{for all} \;\; w_h\in V_h^\Gamma.$$

In the following two lemmas we derive error bounds for this projection.

Lemma 5.5. *The following holds:*

$$|\!|\!| R_h v - v |\!|\!| \leq c\, h \|v\|_{2,\Omega_1\cup\Omega_2} \quad \textit{for all} \;\; v \in W_{\mathrm{reg}}.$$

Proof. For $v \in W_{\mathrm{reg}}$ define $\chi_h := R_h v - I_h^* v \in V_h^\Gamma$. Using Lemma 5.4 and Theorem 5.1 we get, with $c_2 > 0$:

$$\begin{aligned} c_2 |\!|\!| \chi_h |\!|\!|^2 &\leq a_h(\chi_h, \chi_h) = a_h(R_h v - I_h^* v, \chi_h) \\ &= a_h(v - I_h^* v, \chi_h) \leq c_1 |\!|\!| v - I_h^* v |\!|\!| \, |\!|\!| \chi_h |\!|\!| \leq ch \|v\|_{2,\Omega_1\cup\Omega_2} |\!|\!| \chi_h |\!|\!|. \end{aligned}$$

Hence, $|\!|\!| \chi_h |\!|\!| \leq c\, h \|v\|_{2,\Omega_1\cup\Omega_2}$ holds and thus

$$|\!|\!| R_h v - v |\!|\!| \leq |\!|\!| \chi_h |\!|\!| + |\!|\!| v - I_h^* v |\!|\!| \leq c\, h \|v\|_{2,\Omega_1\cup\Omega_2}$$

holds. □

Remark 5.3. The constants c_1 and c_2 in the inequalities (5.27) and (5.28) are independent of the mesh size h. However, $c_1 < \max(\|\mathbf{w}\|_\infty, \lambda)$ and c_2 depends on the diffusion coefficient α. If $\max(\alpha_1, \alpha_2) \ll \|\mathbf{w}\|_\infty$, i. e. the mass transport problem is strongly convection dominated, the discretization in this chapter is not stable.

Lemma 5.6. *The following holds:*

$$\|R_h v - v\|_0 \leq c\, h^2 \|v\|_{2,\Omega_1\cup\Omega_2} \quad \textit{for all} \;\; v \in W_{\mathrm{reg}}.$$

Proof. For $v \in W_{\mathrm{reg}}$ define $e_h := R_h v - v \in V_h^\Gamma + W_{\mathrm{reg}}$. Introduce the bilinear form

$$\tilde{a}(u, v) = (\alpha u, v)_{1,\Omega_1\cup\Omega_2} - (\mathbf{w} \cdot \nabla u, v)_0, \quad u, v \in H_0^1(\Omega_1 \cup \Omega_2).$$

Using $\mathbf{w} \cdot \mathbf{n} = 0$ on Γ and $\operatorname{div} \mathbf{w} = 0$ in Ω_i we get $-(\mathbf{w} \cdot \nabla u, v)_0 = (\mathbf{w} \cdot \nabla v, u)_0$ and thus $\tilde{a}(u, v) = a(v, u)$ for $u, v \in H_0^1(\Omega_1 \cup \Omega_2)$. Let $\tilde{u} \in V$ be the unique solution of

$$\tilde{a}(\tilde{u}, v) = (e_h, v)_0 \quad \text{for all} \;\; v \in V.$$

This dual problem has the same regularity properties as the one in (5.13), i.e., $\tilde{u} \in H^2(\Omega_1 \cup \Omega_2)$ and

$$\|\tilde{u}\|_{2,\Omega_1\cup\Omega_2} \leq c \|e_h\|_0,$$

with a constant c independent of e_h. Using this regularity property, combined with $[\beta\tilde{u}] = 0$ (since $\tilde{u} \in V$) it follows that $\tilde{u}$ solves the following problem:

$$-\operatorname{div}(\alpha\nabla\tilde{u}) - \mathbf{w}\cdot\nabla\tilde{u} = e_h \quad \text{in } \Omega_i,\ i = 1,2, \quad (\text{in } L^2 \text{ sense}), \tag{5.30}$$

$$[\alpha\nabla\tilde{u}\cdot\mathbf{n}]_\Gamma = 0, \tag{5.31}$$

$$[\beta\tilde{u}]_\Gamma = 0. \tag{5.32}$$

Multiplication of (5.30) with βe_h, integration over Ω_i and applying partial integration we obtain, using (5.31),(5.32):

$$\begin{aligned}(e_h,e_h)_0 &= (\alpha\tilde{u},e_h)_{1,\Omega_1\cup\Omega_2} - (\mathbf{w}\cdot\nabla\tilde{u},e_h)_0 - \int_\Gamma [\alpha\nabla\tilde{u}\cdot\mathbf{n}\beta e_h]\,ds\\ &= (\alpha e_h,\tilde{u})_{1,\Omega_1\cup\Omega_2} + (\mathbf{w}\cdot\nabla e_h,\tilde{u})_0 - ([\beta e_h],\{\alpha\nabla\tilde{u}\cdot\mathbf{n}\})_\Gamma\\ &\quad - (\{\alpha\nabla e_h\cdot\mathbf{n}\},[\beta\tilde{u}])_\Gamma + \lambda h^{-1}([\beta e_h],[\beta\tilde{u}])_\Gamma\\ &= a_h(e_h,\tilde{u}).\end{aligned}$$

Using this in combination with Theorem 5.1 and Lemma 5.5 we get

$$\begin{aligned}(e_h,e_h)_0 = a_h(e_h,\tilde{u}) = a_h(e_h,\tilde{u}-I_h^*\tilde{u}) &\le c_1|\!|\!|e_h|\!|\!|\,|\!|\!|\tilde{u}-I_h^*\tilde{u}|\!|\!|\\ &\le c\,h^2\|v\|_{2,\Omega_1\cup\Omega_2}\|\tilde{u}\|_{2,\Omega_1\cup\Omega_2} \le c\,h^2\|v\|_{2,\Omega_1\cup\Omega_2}\|e_h\|_0,\end{aligned}$$

which completes the proof. □

We now derive an error bound for the semi-discretization by Nitsche's method in (5.22). We require that the solution $u = u(t) \in V_{\text{reg}}$ as defined in Lemma 5.1 has sufficient regularity, in particular $\frac{\partial u}{\partial t} \in L^1\big(0,T;W_{\text{reg}}\big)$. The analysis uses standard arguments as in, for example, [Tho97].

Theorem 5.2. *Let $u = u(t) \in V_{\text{reg}}$ be the solution defined in Lemma 5.1 and $u_h = u_h(t) \in V_h^\Gamma$ the solution of (5.22) with $u_h(0) = u_{0,h}$. The following holds*

$$\begin{aligned}\|u_h(t)-u(t)\|_0 \le &\|u_{0,h}-R_hu_0\|_0 + c\,h^2\big\{\|u_0\|_{2,\Omega_1\cup\Omega_2}\\ &+ \int_0^t \left\|\frac{\partial u}{\partial t}\right\|_{2,\Omega_1\cup\Omega_2} d\tau\big\}, \quad 0\le t\le T.\end{aligned}$$

Proof. Introduce the splitting $u_h(t) - u(t) = \theta(t) + \rho(t)$, with $\theta := u_h - R_h u$, $\rho := R_h u - u$. From Lemma 5.6 we have

$$\|\rho(t)\|_0 \leq ch^2 \|u(t)\|_{2,\Omega_1\cup\Omega_2} \leq c\, h^2 \big(\|u_0\|_{2,\Omega_1\cup\Omega_2} + \int_0^t \left\| \frac{\partial u}{\partial t} \right\|_{2,\Omega_1\cup\Omega_2} d\tau \big). \quad (5.33)$$

For $\theta = \theta(t) \in V_h^\Gamma$ we have, using Lemma 5.3:

$$\begin{aligned} \|\theta\|_0 \frac{d}{dt}\|\theta\|_0 = \frac{1}{2}\frac{d}{dt}\|\theta\|_0^2 &= \big(\frac{\partial \theta}{\partial t}, \theta\big)_0 \leq \big(\frac{\partial \theta}{\partial t}, \theta\big)_0 + a_h(\theta,\theta) \\ &= \big(\frac{\partial u_h}{\partial t}, \theta\big)_0 + a_h(u_h,\theta) - \big(\frac{\partial R_h u}{\partial t}, \theta\big)_0 - a_h(R_h u, \theta) \\ &= (f,\theta)_0 - a_h(u,\theta) - \big(\frac{\partial R_h u}{\partial t}, \theta\big)_0 \\ &= \big(\frac{\partial u}{\partial t}, \theta\big)_0 - \big(\frac{\partial R_h u}{\partial t}, \theta\big)_0 = \big(w - R_h w, \theta\big)_0, \end{aligned}$$

with $w = \frac{\partial u}{\partial t}$. We assumed sufficient regularity, in particular $w \in W_{\text{reg}}$. Using Lemma 5.6 we get

$$\big(w - R_h w, \theta\big)_0 \leq c\, h^2 \left\| \frac{\partial u}{\partial t} \right\|_{2,\Omega_1\cup\Omega_2} \|\theta\|_0.$$

Thus we have

$$\frac{d}{dt}\|\theta\|_0 \leq c\, h^2 \left\| \frac{\partial u}{\partial t} \right\|_{2,\Omega_1\cup\Omega_2}.$$

Integration over $[0,t]$ and using $\|\theta(0)\|_0 = \|u_{0,h} - R_h u_0\|_0$ proves the desired result. □

Remark 5.4. We comment on the error analysis for the three-dimensional case. The Nitsche method given in (5.22) has an obvious analogon if we consider a problem as in (5.1)-(5.5) with $\Omega \subset \mathbb{R}^3$ and use the extended finite element space on a family of shape regular tetrahedral triangulations. The arguments to derive the consistency result in Lemma 5.3 are dimension independent. Results as in Lemma 5.4, Lemma 5.5 and Lemma 5.6 can be proved using results from [HH04]. In particular the key Lemma 3 from [HH02] is proved for the 3D case in Lemma 3 in [HH04]. The regularity results in (5.14), (5.15) also hold for the 3D case, cf. [LU68].

5.4 Time discretization

The semi-discretization (5.22), resulting from Nitsche's method, can be combined with standard time discretization methods. For example, the θ-scheme takes the following form. For $n = 0, 1, \ldots, N-1$, with $N\Delta t = T$, set $u_h^0 := u_{0,h} \in V_h^\Gamma$, and determine $u_h^{n+1} \in V_h^\Gamma$ such that for all $v_h \in V_h^\Gamma$

$$\left(\frac{u_h^{n+1} - u_h^n}{\Delta t}, v_h\right)_0 + a_h(\theta u_h^{n+1} + (1-\theta)u_h^n, v_h) = (\theta f(t_{n+1}) + (1-\theta)f(t_n), v_h)_0 \tag{5.34}$$

holds. In practice almost always either $\theta = 0.5$ (Crank-Nicolson) or $\theta = 1$ (implicit Euler) is used. The error analysis of this full (i.e. space and time) discretization method can be performed using standard arguments, as in [Tho97]. For completeness we derive an error bound for the implicit Euler method. Again we require that the solution $u = u(t) \in V_{\text{reg}}$ as defined in Lemma 5.1 has sufficient regularity, in particular $\frac{\partial u}{\partial t} \in L^1\big(0, T; W_{\text{reg}}\big)$ and $\frac{\partial^2 u}{\partial t^2} \in L^1\big(0, T; L^2(\Omega)\big)$.

Theorem 5.3. *Let $u = u(t) \in V_{\text{reg}}$ be the solution defined in Lemma 5.1 and $u_h^n \in V_h^\Gamma$, $n = 0, 1, \ldots, N$ the solution of the θ-scheme* (5.34) *for $\theta = 1$. The following holds:*

$$\|u_h^n - u(t_n)\|_0 \le \|u_{0,h} - R_h u_0\|_0 + c\,h^2\big\{\|u_0\|_{2,\Omega_1\cup\Omega_2} + \int_0^{t_n} \left\|\frac{\partial u}{\partial t}\right\|_{2,\Omega_1\cup\Omega_2} d\tau\big\}$$
$$+ \Delta t \int_0^{t_n} \left\|\frac{\partial^2 u}{\partial t^2}\right\|_0 d\tau.$$

Proof. We use the splitting $u_h^n - u(t_n) = \big(u_h^n - R_h u(t_n)\big) + \big(R_h u(t_n) - u(t_n)\big) =: \theta^n + \rho^n$. For $\|\rho^n\|_0 = \|\rho(t_n)\|_0$ we have a bound as in (5.33). For the backward difference quotient we introduce the notation $\bar\partial^n w := (w^n - w^{n-1})/\Delta t$. Using the definition of u_h^n in (5.34), the definition of the semi-discretization in (5.22) and the consistency result in Lemma 5.3 we obtain

$$\begin{aligned}(\bar\partial\theta^n, v_h)_0 + a_h(\theta^n, v_h) &= \frac{1}{\Delta t}(u_h^n - u_h^{n-1}, v_h)_0 + a_h(u_h^n, v_h)\\ &\quad - (\bar\partial R_h u(t_n), v_h)_0 - a_h(R_h u(t_n), v_h)\\ &= (f(t_n), v_h)_0 - a_h(u(t_n), v_h) - (\bar\partial R_h u(t_n), v_h)_0\\ &= \big(\frac{\partial u(t_n)}{\partial t}, v_h\big)_0 - (R_h \bar\partial u(t_n), v_h)_0 =: (\omega^n, v_h)_0,\end{aligned}$$

with

$$\begin{aligned}\omega^n &= \frac{\partial u(t_n)}{\partial t} - R_h \bar{\partial} u(t_n) \\ &= \left[(I - R_h)\bar{\partial} u(t_n)\right] - \left[\bar{\partial} u(t_n) - \frac{\partial u(t_n)}{\partial t}\right] \\ &=: \omega_1^n - \omega_2^n.\end{aligned}$$

Taking $v_h = \theta^n \in V_h^\Gamma$ and using $a_h(\theta^n, \theta^n) \geq 0$ we get

$$\|\theta^n\|_0^2 - (\theta^{n-1}, \theta^n) \leq \Delta t \|\omega^n\|_0 \|\theta^n\|_0.$$

Hence,

$$\|\theta^n\|_0 \leq \|\theta^{n-1}\|_0 + \Delta t \|\omega^n\|_0,$$

and

$$\begin{aligned}\|\theta^n\|_0 &\leq \|\theta^0\|_0 + \Delta t \sum_{j=1}^n \|\omega^j\|_0 \\ &\leq \|u_{0,h} - R_h u_0\|_0 + \Delta t \sum_{j=1}^n \|\omega_1^j\|_0 + \Delta t \sum_{j=1}^n \|\omega_2^j\|_0. \end{aligned} \tag{5.35}$$

For $\|\omega_1^j\|_0$ we obtain with Lemma 5.6

$$\begin{aligned}\|\omega_1^j\|_0 &= \left\| \frac{1}{\Delta t}(I - R_h) \int_{t_{j-1}}^{t_j} \frac{\partial u}{\partial t}\, d\tau \right\|_0 \leq \frac{1}{\Delta t} \int_{t_{j-1}}^{t_j} \left\| (I - R_h) \frac{\partial u}{\partial t} \right\|_0 d\tau \\ &\leq c \frac{h^2}{\Delta t} \int_{t_{j-1}}^{t_j} \left\| \frac{\partial u}{\partial t} \right\|_{2,\Omega_1 \cup \Omega_2} d\tau,\end{aligned}$$

and thus

$$\Delta t \sum_{j=1}^n \|\omega_1^j\|_0 \leq c h^2 \int_0^{t_n} \left\| \frac{\partial u}{\partial t} \right\|_{2,\Omega_1 \cup \Omega_2} d\tau. \tag{5.36}$$

For ω_2^j we have

$$\Delta t\, \omega_2^j = u(t_j) - u(t_{j-1}) - \Delta t \frac{\partial u(t_j)}{\partial t} = -\int_{t_{j-1}}^{t_j} (\tau - t_{j-1}) \frac{\partial^2 u(\tau)}{\partial t^2}\, d\tau,$$

and thus

$$\Delta t \sum_{j=1}^{n} \|\omega_2^j\|_0 \leq \sum_{j=1}^{n} \int_{t_{j-1}}^{t_j} (\tau - t_{j-1}) \left\| \frac{\partial^2 u}{\partial t^2} \right\|_0 d\tau \leq \Delta t \int_0^{t_n} \left\| \frac{\partial^2 u}{\partial t^2} \right\|_0 d\tau. \quad (5.37)$$

Using the results from (5.36), (5.37) in (5.35) in combination with the bound for $\|\rho^n\|_0$ from (5.33) we obtain the result. □

The analysis of the time discretization given in this section is essentially dimension independent. Key ingredients are sufficient smoothness of the solution u and the results in Lemma 5.4 and Lemma 5.6, cf. Remark 5.4.

Remark 5.5. Introducing the transformed variable $\tilde{u}_h^n := \beta u_h^n \in V_h^\Gamma$ the discretization in (5.34) immediately results in a discretization of the transformed equations (5.6)-(5.8), cf. Remark 5.1.

5.5 Numerical experiments

In subsection 5.5.1 we present two *three*-dimensional test problems of the form (5.1)-(5.5) on $\Omega = (0,1)^3$ with different interfaces Γ. In the first test we take a simple planar interface. Thus we avoid errors due to numerical interface approximation. In the second experiment we consider a cylindrical interface, which has to be approximated on the unfitted tetrahedral meshes that we use. In both cases, the exact solution u is smooth, known and satisfies the interface conditions (5.2)-(5.3). The velocity field $\mathbf{w}$ satisfies the assumptions (5.9).

5.5.1 Test problems

Case 1: Planar interface

The domain Ω contains two subdomains $\Omega_1 := \{(x,y,z) \in \Omega \mid z < 0.34113\}$ and $\Omega_2 := \Omega \setminus \overline{\Omega}_1$, which are separated by the interface $\Gamma := \{(x,y,z) \in \Omega \mid z = 0.34113\}$. The position of the interface is chosen to avoid grid matching.

We choose the coefficients $(\alpha_1, \alpha_2) = (1, 2)$, $(\beta_1, \beta_2) = (2, 1)$ and a stationary velocity $\mathbf{w} := (y(1-z), x, 0)^T$. The right hand side f is taken such that the exact solution is

$$u(x,y,z,t) := \begin{cases} \mathrm{e}^{-t}\cos(\pi x)\cos(2\pi y)az(z+b) & \text{for } x \text{ in } \Omega_1, \\ \mathrm{e}^{-t}\cos(\pi x)\cos(2\pi y)z(z-1) & \text{for } x \text{ in } \Omega_2, \end{cases} \tag{5.38}$$

where the parameters a and b are determined from the interface conditions (5.2)-(5.3). We take homogeneous Dirichlet boundary conditions on the segments $z = 0$ and $z = 1$ and homogeneous Neumann boundary conditions on the other boundary segments.

Case 2: Cylindrical interface

In this experiment, the domain Ω is subdivided into

$$\Omega_1 = \{(x,y,z) \in \Omega \mid x^2 + y^2 < R^2\}, \quad \Omega_2 = \Omega \setminus \Omega_1,$$

with $R = 0.1$. We take a constant velocity field $\mathbf{w} = (0, 0, 1)^T$ and coefficients $(\alpha_1, \alpha_2) = (1, 5)$, $(\beta_1, \beta_2) = (2, 1)$. The exact solution is given by

$$u(x,y,z,t) := \begin{cases} \alpha_2\big(x^2 + y^2 - R^2\big) + \beta_2 & \text{in } \Omega_1, \\ \alpha_1\big(x^2 + y^2 - R^2\big) + \beta_1 & \text{in } \Omega_2. \end{cases} \tag{5.39}$$

We take homogeneous Neumann conditions on the boundary segments $z = 0$ and $z = 1$. On the remaining part of the boundary the values of u are used as inhomogeneous Dirichlet conditions.

5.5.2 Implementation issues

Let $\mathcal{T}_h$ be a shape regular tetrahedral triangulation of Ω. On this triangulation we want to implement the Euler-Nitsche discretization as in (5.22), (5.34). For the finite element spaces and the bilinear form $a_h(\cdot,\cdot)$ we need an approximation of the interface Γ. We assume that we have a (level set) function d available such that its zero level is a sufficiently good approximation of Γ. In our second test problem, we use for d the signed distance function to Γ, for which it is easy to give an explicit formula using cylindrical coordinates. d

Let $\{\psi_k\}_{k\in\mathcal{I}}$ be the nodal basis functions of the standard linear finite element space V_h. Then the basis functions of V_h^Γ are $\{\psi_k\}_{k\in\mathcal{I}} \cup \{\psi_l^\Gamma\}_{l\in\mathcal{I}_\Gamma}$. The dimension of V_h^Γ is denoted by $N^\Gamma = |\mathcal{I}| + |\mathcal{I}_\Gamma|$. For convenience, the basis functions of V_h are indexed such that all basis functions which have the enriched counterparts are numbered first. Thus the index set $\mathcal{I}_\Gamma$ contains consecutive numbers from 1 to $|\mathcal{I}_\Gamma|$.

The solution u_h has the following representation in V_h^Γ

$$u_h = \sum_{k\in\mathcal{I}} u_k\psi_k + \sum_{l\in\mathcal{I}_\Gamma} u_l^\Gamma \psi_l^\Gamma, \quad \vec{\mathbf{u}} := (u_1, \ldots, u_{|\mathcal{I}|}, u_1^\Gamma, \ldots, u_{|\mathcal{I}_\Gamma|}^\Gamma).$$

With these basis functions, we define the matrices $\mathbf{M}$, $\mathbf{A}$ and $\mathbf{C}$ in $\mathbb{R}^{N^\Gamma\times N^\Gamma}$ which correspond to the reaction, diffusion, convection terms, respectively. A matrix $\mathbf{N}$ in $\mathbb{R}^{N^\Gamma\times N^\Gamma}$ is used for the other terms on the interface from the bilinear form $a_h(\cdot,\cdot)$. We use a 2×2-block structure for these matrices. For example, the mass matrix $\mathbf{M}$ is defined as

$$\mathbf{M} = \begin{bmatrix} M_{11} & M_{12} \\ M_{21} & M_{22} \end{bmatrix},$$

where

$$\begin{aligned}
(M_{11})_{i,j} &= (\psi_i, \psi_j)_0, && i,j \in \mathcal{I},\\
(M_{12})_{i,j} &= (\psi_i, \psi_j^\Gamma)_0, && i \in \mathcal{I},\ j \in \mathcal{I}_\Gamma,\\
(M_{21})_{i,j} &= (\psi_i^\Gamma, \psi_j)_0, && i \in \mathcal{I}_\Gamma,\ j \in \mathcal{I},\\
(M_{22})_{i,j} &= (\psi_i^\Gamma, \psi_j^\Gamma)_0, && i,j \in \mathcal{I}_\Gamma.
\end{aligned}$$

In Section 3.2.4, we discuss the assembling of the matrices for the two-phase Navier-Stokes equations, in which the discontinuities of either the coefficients or the basis functions across the interface are present. The computations of quantities like $(\phi_i^{\Gamma_h}, \psi_h)_0$ and $(\phi_i^{\Gamma_h}, \psi_h)_{1,\Omega_1\cup\Omega_2}$, with $\psi_h \in \{\phi_j, \phi_j^\Gamma\}$ deal with both kinds of discontinuities.

Let x_i, x_j be two vertices of a tetrahedron T in $\mathcal{T}_{\Gamma_h}$; assume that $x_i \in \Omega_{1,h}$. A local integral on T is assembled over all children $T' \in T$ as follows. Using $\mathrm{supp}(\phi_i^{\Gamma_h}) \cap T' = T_2'$ we obtain

$$\int_{T'} \beta\phi_i^{\Gamma_h}\psi_h dx = \int_{T_2'} \beta_2\, \phi_i^{\Gamma_h}\, \psi_h dx. \tag{5.40}$$

The latter integral is easy to determine. The other volume integrals in $a_h(\phi_i^\Gamma, \psi_h)$ can be computed in a similar way. In our test problems a Gauss quadrature rule of degree three on a tetrahedron is sufficient to compute the volume integrals in the bilinear form $a_h(\cdot,\cdot)$, with Γ replaced by Γ_h, exactly. The scalar product $(f, \psi_h)_0$ in the right hand side of (5.22) is approximated with high accuracy (using the same assembling process as described above) by a Gauss quadrature rule of degree five on tetrahedra. The interfacial integrals over Γ_h (instead of Γ) in $a_h(\phi_i^{\Gamma_h}, \psi_h)$ are approximated by summing the local integrals on each planar segment $\Gamma_{h,T'}$ of Γ_h using a Gauss quadrature rule of degree five on a triangle.

5.5.3 Numerical results

Case 1

For the spatial discretization, we first create a uniform grid with mesh size $h = \frac{1}{N}$, where $N = 8, 16, 32$. Starting from this uniform grid the elements near the interface are refined two times further, i. e. the local mesh size close to the interface is $h_\Gamma = \frac{1}{4N}$. For the case $N = 32$ this results in a problem with 1293754 tetrahedra and 226087 unknowns. The approximation of the initial value $u_{0,h}$ is chosen as $I_h^*(u(\cdot, 0))$, with I_h^* the interpolation operator as in Theorem 5.1. For the parameter λ in the bilinear form $a_h(\cdot,\cdot)$ we take the value $\lambda = 100$. This choice is based on numerical experiments. It turns out that the error behaviour is not very sensitive with respect to the choice of the parameter value. The results are essentially the same for all $10^1 \leq \lambda \leq 10^3$.

The semi-discretization $u_h(t)$ is not known. We computed an accurate approximation of $u_h(t)$ using the implicit Euler time-stepping scheme with a time step size Δt which is sufficiently small (in our experiments: $\Delta t = 10^{-4}$) such that the error due to the time discretization is negligible compared to the space discretization error. The resulting reference solution is denoted by $u_h^*(t)$. In Table 5.1, the errors $\|u_h^*(T) - u(T)\|_{L^2}$ at $T = 0.15$ are displayed. These results are consistent with the theoretical bound $\mathcal{O}(h^2)$ given in Theorem 5.2.

The exact solution satisfies $[\beta u]_\Gamma = 0$. In the Nitsche discretization this interface condition is satisfied only approximately. For a *stationary* elliptic problem it is shown in [HH02] that for the discretization u_h the error in this interface condition is bounded by $\|[\beta u_h]\|_{L^2(\Gamma)} \leq c h^{\frac{3}{2}} \|u\|_{2,\Omega_1\cup\Omega_2}$. For the *in*stationary case we were not able to derive a theoretical bound for this error

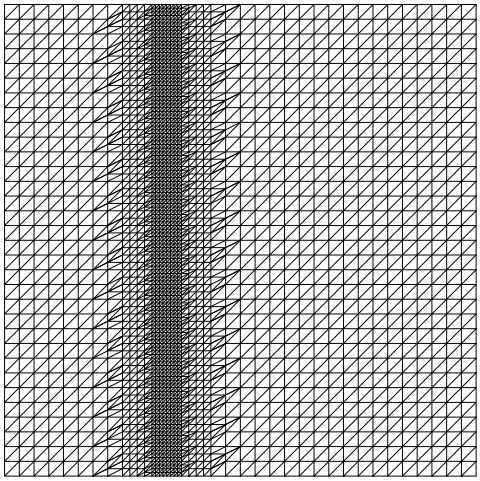

Figure 5.1: Case 1: A slice of the tetrahedral mesh at $x = 0.25$, for the case $N = 16$.

N	$\|u_h^*(T) - u(T)\|_{L^2}$	order
8	0.00738506	-
16	0.00202308	1.87
32	0.0005228	1.95

Table 5.1: Case 1: Spatial discretization error in L^2-norm and convergence order at $T = 0.15$

quantity. We computed the errors $\|[\beta u_h^*]\|_{L^2(\Gamma)}$ for our problem; the results are given in Table 5.2. It can be observed that the interface condition (5.3) is satisfied only approximately and the error $\|[\beta u_h^*]\|_{L^2(\Gamma)}$ seems to behave like $\mathcal{O}(h)$.

N	$\|[\beta u_h^*(T)]\|_{L^2(\Gamma)}$	order
8	$1.565e-4$	-
16	$7.975e-05$	0.972
32	$3.900e-05$	1.03

Table 5.2: Case 1: L^2-norm of the jump $[\beta u_h^*(T)]_\Gamma$ and convergence order at $T = 0.15$

The numerical solution for $N = 16$ at $T = 0.15$ on the plane $x = 0.25$ is

shown in Figure 5.2.

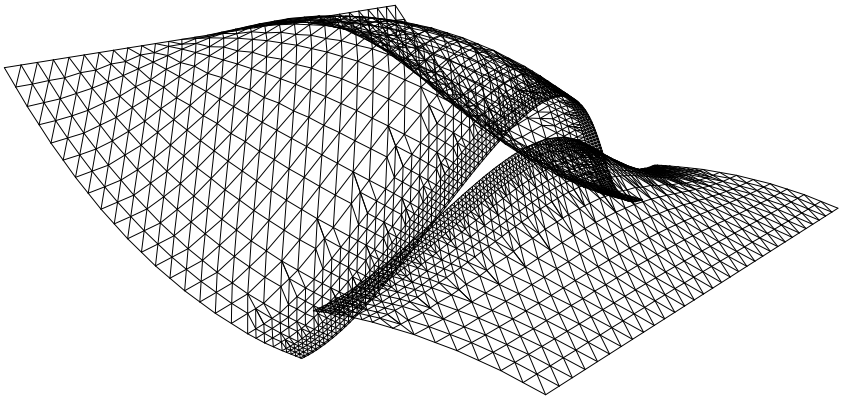

Figure 5.2: Case 1: Numerical solution at $T = 0.15$ in the plane $x = 0.25$.

Now we study the time discretization error bound for the implicit Euler method in Theorem 5.3. We use the fixed mesh with $N = 16$ as described above and compute a reference solution with $\Delta t = 10^{-4}$ in the time interval $[0, T]$, $T = 0.2$, which is denoted by $u_h^*(t)$. The Euler discretization, i.e. (5.34) with $\theta = 1$, with time step $\Delta t = \frac{T}{n}$ results in approximations $u_h^n(T)$ of $u_h^*(T)$. For the cases $n = 5, 10, 20$ the temporal errors in the L^2-norm, i.e. $\|u_h^n(0.2) - u_h^*(0.2)\|_{L^2}$, are given in Table 5.3. We observe the expected first order of convergence in Δt.

n	$\|u_h^n - u_h^*(0.2)\|_{L^2}$	order
5	$1.254e-05$	-
10	$6.092e-06$	1.04
20	$3.011e-06$	1.02

Table 5.3: Case 1: Time discretization error in L^2 norm and convergence order at $T = 0.2$ (implicit Euler).

The time discretization errors $\|u_h^n(0.2) - u_h^*(0.2)\|_{L^2}$ for the Crank-Nicolson method are presented in Table 5.4. The second order of convergence is obtained for smaller time steps sizes w. r. t. $n = 40, 80, 160$. However, since the factor between the time step size $1.25 \cdot 10^{-4}$ w. r. t. to $n = 160$ and the time step size $\Delta t = 10^{-4}$ for the reference solution is not large, it is difficult to determine the correct order of convergence for the Crank-Nicolson method.

n	$\|u_h^n - u_h^*(0.2)\|_{L^2}$	order
40	$7.21e-05$	-
80	$1.864e-05$	1.95
160	$3.77e-06$	2.29

Table 5.4: Case 1: Time discretization error in L^2 norm and convergence order at $T = 0.2$ (Crank-Nicolson).

Case 2

For the spatial discretization we proceed as in case 1. A difference is that we now have an approximation Γ_h of Γ which is constructed as explained in subsection 5.5.2. We use uniform grids with mesh size $h = \frac{1}{N}$, $N = 10, 20, 40$, and refine the elements near the interface (only) one time further, due to the memory limitation. For the case $N = 40$, the grid already contains 1043040 tetrahedra which leads to a problem with 166059 unknowns. The implicit Euler method with $\Delta t = 10^{-4}$ is used to compute the reference solution $u_h^*(t)$ for $t \in [0, 0.1]$. The error $\|u_h^*(T) - u(T)\|_{L^2}$ at $T = 0.1$ given in Table 5.5 is in good agreement with the $\mathcal{O}(h^2)$ error bound derived in Theorem 5.2. The $L^2(\Gamma_h)$-norm of the jump $[\beta u_h^n]$ at the approximated interface Γ_h again appears to have a numerical convergence order 1, cf. Table 5.6.

N	$\|u_h^*(T) - u(T)\|_{L^2}$	order
10	0.00327273	-
20	0.00080687	2.02
40	0.000206194	1.968

Table 5.5: Case 2: Spatial discretization error in L^2-norm and convergence order at $T = 0.1$

Figure 5.3 shows the numerical solution on the plane $z = 0.5$ at $T = 0.1$.

N	$\|[\beta u_h^n]\|_{L^2(\Gamma_h)}$	order
10	0.00103106	-
20	0.000500593	1.04
40	0.00022014	1.185

Table 5.6: Case 2: $L^2(\Gamma_h)$-norm of the jump $[\beta u_h^n]$ and convergence order at $T = 0.1$

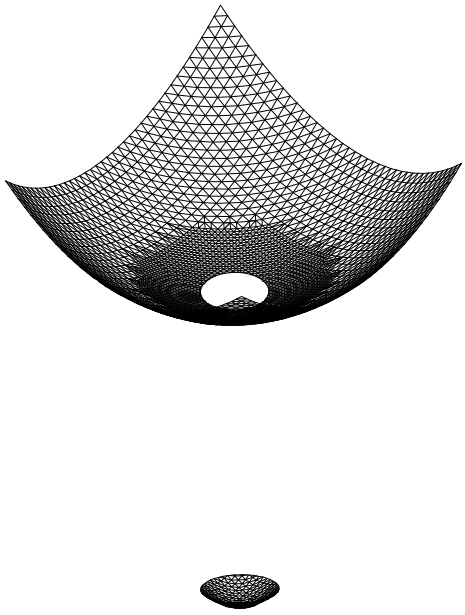

Figure 5.3: Case 2: Numerical solution at $T = 0.1$ in the plane $z = 0.5$.

Chapter 6

Two-phase mass transport problem with a moving interface

In Chapter 5 we analyzed the discretization of the mass transport equations (5.1)-(5.5) with a *stationary* interface. We employed the "method of lines" approach, in which the spatial discretization by Nitsche's finite element method is done first. After that, a standard time stepping θ-scheme was applied to the semi-discrete problem. This approach uses the fact that, if the interface is stationary, the XFEM space V_h^Γ is time-independent. This approach is not applicable in the case of a moving interface $\Gamma(t)$. Even when a fixed mesh is used and the standard finite element basis functions are unchanged, the extended finite element basis functions are defined depending on the position of the interface. In the setting of the moving interface, it is more natural to apply the time discretization first, cf. [FZ09]. This is the so-called Rothe method. In each time step, the reaction-convection-diffusion problem obtained from the θ-scheme is discretized in space by Nitsche's method.

6.1 Time discretization

The equation (5.1) can be written as

$$\frac{\partial u}{\partial t} = F(u,t), \tag{6.1}$$

where $F(u,t) = \nabla \cdot (\alpha \nabla u) + f(t) - \mathbf{w} \cdot \nabla u$.

For $\theta \in [0,1]$, the θ-scheme for (6.1) gives

$$\frac{u^{n+1}-u^n}{\Delta t} = \theta F(u^{n+1}, t_{n+1}) + (1-\theta)F(u^n, t_n). \tag{6.2}$$

The stationary PDE in (6.2) is a reaction-convection-diffusion equation. Note that, in the strong form, ∇u and $\nabla \cdot (\alpha \nabla u)$ in $F(u,t)$ are well-defined only in two separate subdomains ($\Omega_1(t)$ and $\Omega_2(t)$), due to the discontinuities of u and of the diffusion coefficient α across $\Gamma(t)$. If $\theta \in (0,1)$, both terms $F(u^n, t_n)$ and $F(u^{n+1}, t_{n+1})$ appear in (6.2). As the interface evolves, the terms ∇u and $\nabla \cdot (\alpha \nabla u)$ at two different time levels t_n and t_{n+1} are well-defined in different subdomains. Hence the right hand side of (6.2) is only well-defined in each part of the intersections $\Omega_i(t_n) \cap \Omega_j(t_{n+1})$, $(i,j = 1,2)$, which makes the spatial discretization more complicated. A space-time variational approach would be more appropriate and does not have this difficulty for $\theta \neq 1$.

We want to avoid the space-time formulation and restrict ourselves to the (simpler) Rothe approach. The difficulty outlined above does *not* occur if we take $\theta = 1$ (implicit Euler). Therefore, in the remainder of this chapter, we restrict ourselves to the case $\theta = 1$. We then obtain the following problem for the numerical solution at the time level t_{n+1}

$$\begin{aligned} &\frac{1}{\Delta t}u^{n+1} - \nabla \cdot (\alpha^{n+1} \nabla u^{n+1}) + \mathbf{w}^{n+1} \cdot \nabla u^{n+1} \\ &= \frac{1}{\Delta t}u^n + f(t_{n+1}). \end{aligned} \tag{6.3}$$

6.2 Nitsche's method for spatial discretization

We consider the time discretization (6.3) of (5.1)-(5.5) at one fixed time level $t_k = k\Delta t\,(k > 0)$. Here the notation k is used instead of $n+1$ for convenience. The fixed subdomains and the interface at this time level are denoted by $\Omega_1 = \Omega_1(t_k)$, $\Omega_2 = \Omega_2(t_k)$ and $\Gamma = \Gamma(t_k)$, respectively. We define $\sigma = (\Delta t)^{-1}$, $g^k := \frac{1}{\Delta t}u^{k-1} + f(t_k)$ and drop the superscript k. We rewrite (6.3) in the form of a *stationary* reaction-convection-diffusion problem as

follows:

$$\begin{aligned} \sigma u + \mathbf{w} \cdot \nabla u - \nabla \cdot (\alpha \nabla u) &= g \quad \text{in } \Omega, \\ [\alpha \nabla u \cdot \mathbf{n}] &= 0 \quad \text{on } \Gamma, \\ [\beta u] &= 0 \quad \text{on } \Gamma, \\ u &= 0 \quad \text{in } \partial\Omega. \end{aligned} \tag{6.4}$$

Note that σ is a constant in the problem (6.4) but is a parameter in the time discretization (6.3).

We assume that the velocity $\mathbf{w}$ is divergence-free and bounded, namely

$$\operatorname{div} \mathbf{w} = 0 \quad \text{in } \ \Omega_i, \ i = 1, 2, \ \text{and} \quad \|\mathbf{w}\|_{L^\infty(\Omega)} \le c < \infty. \tag{6.5}$$

The assumption $\mathbf{w} \cdot \mathbf{n} = 0$, however, is not satisfied any more.

Corresponding to the subdomains Ω_1 and Ω_2, the Hilbert spaces H, V and V_{reg} and their norms are defined similarly to those in Chapter 5. Using the extended finite element space V_h^Γ, we define the bilinear form

$$\begin{aligned} a_h(u, v) := (\sigma u, v)_0 + (\alpha u, v)_{1,\Omega_1 \cup \Omega_2} + (\mathbf{w} \cdot \nabla u, v)_0 - ([\beta u], \{\alpha \nabla v \cdot \mathbf{n}\})_\Gamma \\ - (\{\alpha \nabla u \cdot \mathbf{n}\}, [\beta v])_\Gamma + \lambda h^{-1} ([\beta u], [\beta v])_\Gamma, \quad u, v \in V_h^\Gamma. \end{aligned} \tag{6.6}$$

The Nitsche discretization of (6.4) reads: Find $u_h \in V_h^\Gamma$ such that

$$a_h(u_h, v_h) = (g, v_h)_0 \quad \text{for all } \ v_h \in V_h^\Gamma. \tag{6.7}$$

The following consistency property of the problem (6.7) is a consequence of Lemma 5.3.

Lemma 6.1. *Let $u \in V_{\text{reg}}$ be the solution of the problem (6.4). Then u satisfies*

$$a_h(u, v_h) = (g, v_h) \quad \textit{for all } \ v_h \in V_h^\Gamma, \quad t \in [0, T]. \tag{6.8}$$

Thus we have the *Galerkin orthogonality*

$$a_h(u - u_h, v) = 0, \qquad \forall\, v \in V_h^\Gamma. \tag{6.9}$$

Note that u_h is only consistent with the solution of (6.4), i. e. the time approximation $u := u^k$ of the exact solution $u(t_k)$ in (5.1)-(5.5) at $t = t_k$.

To obtain the continuity and coercivity of $a_h(\cdot,\cdot)$ we define the following norm in V_h^Γ

$$|\!|\!| v |\!|\!|^2 := \|v\|_0^2 + |v|_{1,\Omega_1\cup\Omega_2}^2 + \|\{\nabla v\cdot\mathbf{n}\}\|_{-1/2,h,\Gamma}^2 + \|[\beta v]\|_{1/2,h,\Gamma}^2 \tag{6.10}$$

using the same definitions for $\|\cdot\|_{-\frac{1}{2},h,\Gamma}$ and $\|\cdot\|_{\frac{1}{2},h,\Gamma}$ as in (5.24) and (5.25).

Below we derive optimal approximation property of V_h^Γ w. r. t. the $|\!|\!|\cdot|\!|\!|$ norm, using arguments similar to those in [HH02].

Theorem 6.1. *Let $I_h^* : W_{\mathrm{reg}} \to V_h^\Gamma$ be the interpolation operator defined in section 5.3. There exists a constant c such that*

$$|\!|\!| v - I_h^* v |\!|\!| \le c\, h \|v\|_{2,\Omega_1\cup\Omega_2} \quad \textit{for all} \;\; v \in W_{\mathrm{reg}} \tag{6.11}$$

holds.

In the following lemma, we show the continuity and coercivity of the bilinear form $a_h(\cdot,\cdot)$ w. r. t. the $|\!|\!|\cdot|\!|\!|$ norm. Unlike the case with the stationary interface, the assumption $\mathbf{w}\cdot\mathbf{n} = 0$ at Γ does not hold. Due to this, the parameters λ and σ must be chosen sufficiently large to obtain the coercivity. For convenience, we introduce the notations $\alpha_{\max} = \max(\alpha_1,\alpha_2)$ and $\alpha_{\min} = \min(\alpha_1,\alpha_2)$.

Lemma 6.2. *There exist constants c_1, $c_2 > 0$ such that for λ and σ sufficiently large (independent of h) the following holds:*

$$|a_h(u,v)| \le c_1 |\!|\!| u |\!|\!| \, |\!|\!| v |\!|\!| \quad \textit{for all} \;\; u, v \in V_h^\Gamma + W_{\mathrm{reg}}, \tag{6.12}$$

$$a_h(v_h, v_h) \ge c_2 |\!|\!| v_h |\!|\!|^2 \quad \textit{for all} \;\; v_h \in V_h^\Gamma. \tag{6.13}$$

Proof. The continuity can be proven from the definitions of the norms and the Cauchy-Schwarz inequality as in Lemma 5.4. We have

$$\begin{aligned} |a_h(u,v)| \le{}& \sigma\|u\|_0\|v\|_0 + \alpha_{\max}\,|u|_{1,\Omega_1\cup\Omega_2}|v|_{1,\Omega_1\cup\Omega_2} \\ &+ \|\mathbf{w}\|_\infty\,|u|_{1,\Omega_1\cup\Omega_2}\|v\|_0 + \|[\beta u]\|_{1/2,h,\Gamma}\|\{\alpha\nabla v\cdot\mathbf{n}\}\|_{-1/2,h,\Gamma} \\ &+ \|\{\alpha\nabla u\cdot\mathbf{n}\}\|_{-1/2,h,\Gamma}\|[\beta v]\|_{1/2,h,\Gamma} \\ &+ c\lambda\|[\beta u]\|_{1/2,h,\Gamma}\|[\beta v]\|_{1/2,h,\Gamma} \le c_1\, |\!|\!| u |\!|\!| \, |\!|\!| v |\!|\!|, \end{aligned}$$

Then we obtain (6.12) using the same arguments as in the proof of Lemma 5.4 and by choosing $c_1 > 2\max(\sigma, \alpha_{\max}, \|\mathbf{w}\|_\infty, c\lambda)$, with a constant $c > 0$ independent of h.

The difference to the proof of the coercivity in Lemma 5.4 is that we need an upper bound for $|(\mathbf{w}\cdot\nabla u, u)_0|$, which vanishes when $\mathbf{w}\cdot\mathbf{n} = 0$ at Γ. Indeed, for sufficiently large σ, this term is bounded by the sum of the reaction and diffusion terms. Using the Cauchy-Schwarz inequality, we obtain

$$\begin{aligned}
|(\mathbf{w}\cdot\nabla v_h, v_h)_0| &\leq \|\mathbf{w}\|_\infty |v_h|_{1,\Omega_1\cup\Omega_2}\|v_h\|_0 \\
&\leq \frac{1}{2}\big(\alpha|v_h|^2_{1,\Omega_1\cup\Omega_2} + \frac{\|\mathbf{w}\|^2_\infty}{\alpha}\|v_h\|^2_0\big) \\
&\leq \frac{1}{2}\big(\alpha|v_h|^2_{1,\Omega_1\cup\Omega_2} + \sigma\|v_h\|^2_0\big),
\end{aligned}$$

provided $\sigma \geq \frac{\|\mathbf{w}\|^2_\infty}{\alpha}$.

With this result, we have

$$\begin{aligned}
a_h(v_h, v_h) \geq\, & \sigma\|v_h\|^2_0 + |\alpha^{\frac{1}{2}} v_h|^2_{1,\Omega_1\cup\Omega_2} + (\mathbf{w}\cdot\nabla v_h, v_h)_0 \\
& - 2([\beta v_h], \{\alpha\nabla v_h\cdot\mathbf{n}\})_\Gamma + \lambda h^{-1}\|[\beta v_h]\|^2_{0,\Gamma} \\
\geq\, & \sigma\|v_h\|^2_0 + |\alpha^{\frac{1}{2}}\nabla v_h|^2_{1,\Omega_1\cup\Omega_2} - |(\mathbf{w}\cdot\nabla v_h, v_h)_0| \\
& - 2\|\{\alpha\nabla v_h\cdot\mathbf{n}\}\|_{-1/2,h,\Gamma}\|[\beta v]\|_{1/2,h,\Gamma} + c\lambda\|[\beta v_h]\|^2_{1/2,h,\Gamma} \\
\geq\, & \frac{\sigma}{2}\|v_h\|^2_0 + \frac{1}{2}|\alpha^{\frac{1}{2}}\nabla v_h|^2_{1,\Omega_1\cup\Omega_2} \\
& - 2\|\{\alpha\nabla v_h\cdot\mathbf{n}\}\|_{-1/2,h,\Gamma}\|[\beta v]\|_{1/2,h,\Gamma} + c\lambda\|[\beta v_h]\|^2_{1/2,h,\Gamma}
\end{aligned}$$

with a constant c independent of h. From Lemma 4 in [HH02] we have

$$\|\{\alpha\nabla v_h\cdot\mathbf{n}\}\|_{-1/2,h,\Gamma} \leq c_I\,|\alpha^{\frac{1}{2}} v_h|_{1,\Omega_1\cup\Omega_2} \quad \text{for all} \quad v_h \in V_h^\Gamma.$$

Thus, we obtain

$$\begin{aligned}
a_h(v_h, v_h) \geq & \frac{\sigma}{2}\|v_h\|_0^2 + \frac{1}{4}|\alpha^{\frac{1}{2}}\nabla v_h|^2_{1,\Omega_1\cup\Omega_2} + \frac{1}{4c_I^2}\|\{\alpha\nabla v_h\cdot\mathbf{n}\}\|^2_{-1/2,h,\Gamma} \\
& + \frac{c\lambda}{2}\|[\beta v_h]\|^2_{0,\Gamma} - 2\|\{\alpha\nabla v_h\cdot\mathbf{n}\}\|_{-1/2,h,\Gamma}\|[\beta v]\|_{1/2,h,\Gamma} \\
& + \frac{c\lambda}{2}\|[\beta v_h]\|^2_{1/2,h,\Gamma} \\
\geq & \Big(\frac{\sigma}{2}\|v_h\|_0^2 + \frac{1}{8}|\alpha^{\frac{1}{2}}\nabla v_h|^2_{1,\Omega_1\cup\Omega_2} + \frac{1}{4c_I^2}\|\{\alpha\nabla v_h\cdot\mathbf{n}\}\|^2_{-1/2,h,\Gamma} \\
& + \frac{c\lambda}{2}\|[\beta v_h]\|^2_{0,\Gamma}\Big) + \frac{1}{8}|\alpha^{\frac{1}{2}}\nabla v_h|^2_{1,\Omega_1\cup\Omega_2} + \frac{c\lambda}{2}\|[\beta v_h]\|^2_{1/2,h,\Gamma} \\
& - 2\|\{\alpha\nabla v_h\cdot\mathbf{n}\}\|_{-1/2,h,\Gamma}\|[\beta v]\|_{1/2,h,\Gamma} \\
\geq & \, c_2|\!|\!|v_h|\!|\!|^2 + \Big(\frac{1}{8}|\alpha^{\frac{1}{2}}\nabla v_h|^2_{1,\Omega_1\cup\Omega_2} + \frac{c\lambda}{2}\|[\beta v_h]\|^2_{1/2,h,\Gamma} \\
& - \frac{2}{c_I}|\alpha^{\frac{1}{2}}\nabla v_h|_{1,\Omega_1\cup\Omega_2}\|[\beta v]\|_{1/2,h,\Gamma}\Big),
\end{aligned}$$

with a positive constant c_2 independent of h such that

$$c_2 < \min(\frac{\sigma}{2}, \frac{\alpha_{\min}}{8}, \frac{\alpha_{\min}^2}{4c_I^2}, \frac{c\lambda}{2}).$$

Using again the Cauchy-Schwarz inequality, we obtain

$$a_h(v_h, v_h) \geq c_2|\!|\!|v_h|\!|\!|^2 \quad \text{for all} \;\; v_h \in V_h^\Gamma,$$

provided the parameters σ and λ are sufficiently large, namely $\sigma \geq \frac{\|\mathbf{w}\|_\infty^2}{\alpha}$ and $\lambda > \frac{16}{c\cdot c_I^2}$. □

Remark 6.1. The value of the parameter λ must be chosen sufficiently large, but is independent of σ, the inverse of the time step size Δt.

We obtain the following error estimate:

Lemma 6.3. *Let $u \in V_{\text{reg}}$ solve the problem (6.4) and $u_h \in V_h^\Gamma$ solve (6.7). The following holds:*

$$|\!|\!|u - u_h|\!|\!| \leq c\, h\|u\|_{2,\Omega_1\cup\Omega_2}.$$

Proof. Define $\chi_h := u_h - I_h^* u \in V_h^\Gamma$. Combining the Galerkin orthogonality (6.9), the interpolation property (6.11) and the results of Lemma 6.2 with $c_1, c_2 > 0$, we have:

$$\begin{aligned} c_2 |\!|\!| \chi_h |\!|\!|^2 &\leq a_h(\chi_h, \chi_h) = a_h(u_h - I_h^* u, \chi_h) \\ &= a_h(u - I_h^* u, \chi_h) \leq c_1 |\!|\!| u - I_h^* u |\!|\!| |\!|\!| \chi_h |\!|\!| \leq ch \|u\|_{2,\Omega_1 \cup \Omega_2} |\!|\!| \chi_h |\!|\!|. \end{aligned}$$

Hence, $|\!|\!| \chi_h |\!|\!| \leq c\, h \|v\|_{2,\Omega_1 \cup \Omega_2}$ holds and thus

$$|\!|\!| u - u_h |\!|\!| \leq |\!|\!| \chi_h |\!|\!| + |\!|\!| u - I_h^* u |\!|\!| \leq c\, h \|u\|_{2,\Omega_1 \cup \Omega_2}.$$

holds. □

Note that without assumption $\mathbf{w} \cdot \mathbf{n} = 0$, the relation

$$-(\mathbf{w} \cdot \nabla u, v)_0 = (\mathbf{w} \cdot \nabla v, u)_0$$

does not hold. Hence we cannot use the duality argument to obtain a bound in the L^2-norm as in Chapter 5.

6.3 Implementation issues

In this section, we combine the time integration and spatial discretization in Sections 6.1 and 6.2. Let Γ^k denote the interface at the time level t_k ($k = 1, 2, \ldots$) and $V_h^{\Gamma^k}$ be the XFEM space in the corresponding subdomains. Note that at different time levels, we have different XFEM spaces depending on the positions of the moving interface. The dimensions of these XFEM spaces are in general different.

We use the notations as in Section 5.5.2. Let $\{\psi_l\}_{l \in \mathcal{I}}$ be the nodal basis functions of the standard linear finite element space V_h. Then the basis functions of $V_h^{\Gamma^k}$ are $\{\psi_l\}_{l \in \mathcal{I}} \cup \{\psi_m^{\Gamma^k}\}_{m \in \mathcal{I}_{\Gamma^k}}$. The dimension of $V_h^{\Gamma^k}$ is $N^{\Gamma^k} = |\mathcal{I}| + |\mathcal{I}_{\Gamma^k}|$.

The solution u_h^k has the following representation in $V_h^{\Gamma^k}$

$$u_h^k = \sum_{l \in \mathcal{I}} u_l^k \psi_l + \sum_{m \in \mathcal{I}_{\Gamma^k}} u_m^{\Gamma^k} \psi_m^{\Gamma^k}.$$

We introduce the vector

$$\vec{u^k} := (u_1^k, \ldots, u_{|\mathcal{I}|}^k, u_1^{\Gamma^k}, \ldots, u_{|\mathcal{I}_{\Gamma^k}|}^{\Gamma^k}).$$

The matrices $\mathbf{M}$, $\mathbf{A}$, $\mathbf{C}$ and $\mathbf{N}$ in $\mathbb{R}^{N^{\Gamma^k} \times N^{\Gamma^k}}$ for the reaction, diffusion, convection terms and the Nitsche's term w. r. t. the XFEM space $V_h^{\Gamma^k}$ are also defined and assembled similar to those in section 5.5.2. However, in the right hand side of (6.7) we have the term $\sigma \cdot (u_h^{k-1}, v_h)_0$. This term needs an additional treatment, since the numerical solution u_h^{k-1} at t_{k-1} belongs to the XFEM space $V_h^{\Gamma^{k-1}}$, while the test function v_h belongs to $V_h^{\Gamma^k}$. In general, the elements of the index sets $\mathcal{I}_{\Gamma^k}$ and $\mathcal{I}_{\Gamma^{k-1}}$ are not consecutive. For $k \geq 1$ we introduce the bijective mapping

$$\pi_k : \mathcal{I}_{\Gamma^k} \mapsto \{1, \ldots, |\mathcal{I}_{\Gamma^k}|\}$$

and define another matrix $\tilde{\mathbf{M}} \in \mathbb{R}^{N^{\Gamma^k} \times N^{\Gamma^{k-1}}}$ for the scalar products relating the basis functions in both spaces $V_h^{\Gamma^{k-1}}$ and $V_h^{\Gamma^k}$ as follows:

$$\tilde{\mathbf{M}} = \begin{bmatrix} \tilde{M}_{11} & \tilde{M}_{12} \\ \tilde{M}_{21} & \tilde{M}_{22} \end{bmatrix},$$

where

$$\begin{aligned}
(\tilde{M}_{11})_{i,j} &= (\psi_i, \psi_j)_0, && i, j \in \mathcal{I}, \\
(\tilde{M}_{12})_{i,\pi_{k-1}(j)} &= (\psi_i, \psi_j^{\Gamma^{k-1}})_0, && i \in \mathcal{I},\ j \in \mathcal{I}_{\Gamma^{k-1}}, \\
(\tilde{M}_{21})_{\pi_k(i),j} &= (\psi_i^{\Gamma^k}, \psi_j)_0, && i \in \mathcal{I}_{\Gamma^k},\ j \in \mathcal{I}, \\
(\tilde{M}_{22})_{\pi_k(i),\pi_{k-1}(j)} &= (\psi_i^{\Gamma^k}, \psi_j^{\Gamma^{k-1}})_0, && i \in \mathcal{I}_{\Gamma^k},\ j \in \mathcal{I}_{\Gamma^{k-1}}.
\end{aligned}$$

The blocks $\tilde{M}_{11}$ and $\tilde{M}_{21}$ are the same as the counter parts in the mass matrix $\mathbf{M}$. The computations of $\tilde{M}_{12}$ can be done in a similar way, using the XFEM space corresponding to the subdomains at $t = t_{k-1}$. The local integrals of $\tilde{M}_{22}$ in an element T is more complicated. For simplicity, we consider a two-dimensional case, as illustrated in Figure 6.2. In this case, the element T, which is a triangle with vertices x_i, x_j and x_l, is intersected by both interfaces Γ^{k-1} and Γ^k. The extended basis functions $\psi_i^{\Gamma^k}$ and $\psi_j^{\Gamma^{k-1}}$ are discontinuous in T. Moreover, the positions of the discontinuities of $\psi_i^{\Gamma^k}$ and $\psi_j^{\Gamma^{k-1}}$ are different. The domain of integration, which is the intersection of $\mathrm{supp}(\psi_{\mathrm{i}}^{\Gamma^{\mathrm{k}}})$ and $\mathrm{supp}(\psi_{\mathrm{j}}^{\Gamma^{\mathrm{k-1}}})$, is determined as follows. (Note that if $T \notin \mathcal{T}_{\Gamma_h^k} \cap \mathcal{T}_{\Gamma_h^{k-1}}$, this intersection is an empty set). Firstly, each regular child T' of T is divided into two polygonal parts $T'_{1,k}$ and $T'_{2,k}$ w. r. t. the interface

Γ^k at t_k. We assume that $x_i \in \Omega_1^k$ and thus $\mathrm{supp}(\psi_{\mathrm{i}}^{\Gamma^{\mathrm{k}}})_{|\mathrm{T}'} = \mathrm{T}'_{2,\mathrm{k}}$, which can be partitioned into at most 2 triangles. Then the support of $\psi_j^{\Gamma^{k-1}}$ in each triangle of T_2' can be determined w. r. t. the interface Γ^{k-1} at t_{k-1}. This implementation can be applied also for the three-dimensional case.

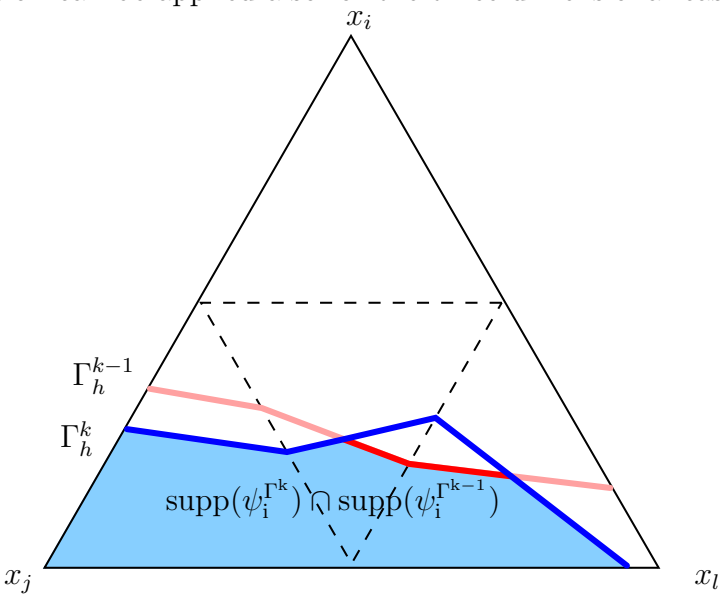

Figure 6.1: Domain of integration.

We also need the vector

$$\vec{\mathbf{f}} = (f_1^k, \ldots, f_{|\mathcal{I}|}^k, f_1^{\Gamma^k}, \ldots, f_{|\mathcal{I}_{\Gamma^k}|}^{\Gamma^k}),$$

where

$$\begin{aligned} f_i^k &= (\psi_i, f)_0, & i &\in \mathcal{I}, \\ f_j^{\Gamma^k} &= (\psi_j^{\Gamma^k}, f)_0, & j &\in \mathcal{I}_{\Gamma^k}. \end{aligned}$$

With the above notations, the Galerkin discretization (6.7) leads to the following linear system:

$$\big[\mathbf{M} + \Delta t(\mathbf{A} + \mathbf{C} + \mathbf{N})\big]\,\vec{\mathbf{u}}^k = \tilde{\mathbf{M}}\vec{\mathbf{u}}^{k-1} + \Delta t\,\vec{\mathbf{f}}^k. \tag{6.14}$$

6.4 Numerical experiment

We consider the problem (5.1)-(5.3) in the unit cube Ω and with $\Omega_1(0)$ a sphere of radius $R = 0.2$ centered at the barycenter of Ω. This sphere is

moving with a constant velocity $\mathbf{w} = (0, 1, 0)^T$, i.e. $\Omega_1(t) = \Omega_1(0) + t\mathbf{w}$. Let $d(\mathbf{x}, t)$ be the distance from the point $\mathbf{x} \in \Omega$ to the center of $\Omega_1(t)$. We take the piecewise quadratic solution

$$u(\mathbf{x}, t) := \begin{cases} \alpha_2\big(d(x,t)^2 - R^2\big) + 0.1 \cdot \beta_2 & \text{in } \Omega_1, \\ \alpha_1\big(d(x,t)^2 - R^2\big) + 0.1 \cdot \beta_1 & \text{in } \Omega_2, \end{cases} \tag{6.15}$$

with coefficients $(\alpha_1, \alpha_2) := (1, 5)$, $(\beta_1, \beta_2) := (2, 1)$. The values of u on $\partial\Omega$ are used as inhomogeneous Dirichlet conditions. We discretize the problem first in time using the implicit Euler method with the time step size $\Delta t = 10^{-4}$. The resulting convection-diffusion-reaction problem is discretized with the Nitsche method. We first create a uniform grid with the mesh size $h = \frac{1}{N}$, where $N = 8, 16, 32$, then locally refine the elements near the interface two times further. After 1000 time steps, we obtain the approximation u_h^{1000} of $u(0.1)$. The errors $\|u_h^{1000} - u(0.1)\|_{L^2}$ for $N = 8, 16, 32$ are displayed in Table 6.1. The results show the expected convergence order 2. Note that $\|u_h^{1000} - u(0.1)\|_{L^2}$ contain both time and spatial discretization errors, but for coarser grids, the spatial discretization error is dominant.

N	$\|u_h^{1000} - u(0.1)\|_{L^2}$	order
8	0.007896	-
16	0.001995	1.984
32	0.0005002	1.996

Table 6.1: Spatial discretization error in L^2-norm and convergence order at $T = 0.1$.

Remark 6.2. Since the interface evolves and adaptive grids are used, the XFEM space $V_h^\Gamma(t)$ is in general time-dependent. Hence a reference solution is not available and we cannot obtain the order of convergence for the time discretization.

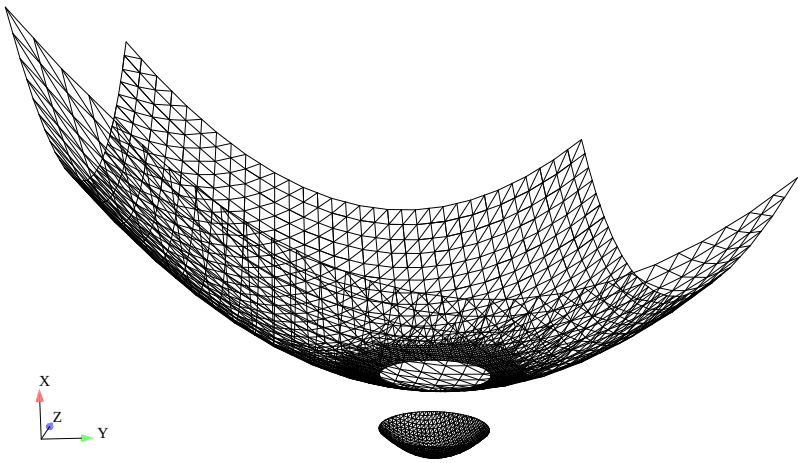

Figure 6.2: Numerical solution for $N = 16$ at $T = 0.1$ on the plane $x = 0.5$.

Chapter 7

Numerical simulations of two-phase flow with mass transport

7.1 Numerical simulations

In this chapter we study the numerical simulations of a single butanol droplet rising in water due to gravity. At the initial time, the water phase contains a dissolved species. We assume isothermal conditions and no surfactant transport on the interface. The dynamics of the droplet is determined by the Navier-Stokes equations (3.1). The transport of the mass concentration is described by the equations (2.2)-(2.4).

The model is as follows

$$
\begin{aligned}
\rho(\phi)\Big(\frac{\partial \mathbf{u}}{\partial t} + (\mathbf{u}\cdot\nabla)\mathbf{u}\Big) - \operatorname{div}(\mu(\phi)\mathbf{D}(\mathbf{u})) + \nabla p &= \rho(\phi)\mathbf{g} + f_\Gamma \\
\operatorname{div}\mathbf{u} &= 0 \\
\phi_t + \mathbf{u}\cdot\nabla\phi &= 0 \qquad (7.1)\\
\frac{\partial c}{\partial t} + \mathbf{u}\cdot\nabla c - \operatorname{div}(\alpha\nabla c) &= 0 \\
[\alpha\nabla c\cdot\mathbf{n}]_\Gamma &= 0, \\
[\beta c]_\Gamma &= 0,
\end{aligned}
$$

with suitable boundary conditions and initial conditions for the velocity and mass concentration, which will be discussed later.

We conduct simulations with two different assumptions on the surface tension coefficient τ:

- In the first case, we assume that the surface tension coefficient τ is constant and is independent of the mass concentration of the solute. Thus there is only the coupling in one direction between the Navier-Stokes problem and the mass transport problem. In each time step, after the level set and Navier-Stokes equations are solved, we use the velocity and the level set function as input for the mass transport equation. In fact, the dynamics of the droplet can be determined once and be used for different numerical simulations of the mass transport problem.

- In the second case, we use a model from [MBS85], where the surface tension coefficient depends on the mass concentration of the dissolved component in the continuous phase. With this assumption, the flow variables, the level set function and the mass concentration are fully coupled.

In both cases, we consider the *n-butanol - water - succinic acid* system, in which an *n*-butanol droplet is rising in water due to the gravity. The computational domain is $\Omega = [0, 0.02] \times [0, 0.04] \times [0, 0.02]\,\mathrm{m}^3$. The dispersed phase (droplet) and continuous phase are contained in the subdomains Ω_1 and Ω_2, respectively. At $t = 0$, the droplet is at rest and has a spherical shape, with a diameter 2mm and centered at $(0.001, 0.001, 0.001)^T\,\mathrm{m}$. The size and the initial position of the droplet are chosen such that its dynamics is not affected by the wall. We take a homogeneous Dirichlet boundary condition for the velocity and a homogeneous Neumann boundary condition for the concentration. The right hand side function $\mathbf{g}$ is taken as $\mathbf{g} = (0, -g, 0)^T$, with $g = 9.81\,\mathrm{m/s}^2$. The viscosity μ and density ρ for each phase at 20°C are given in Table 7.1.

butanol-water		
	$\mu[Pa \cdot s]$	$\rho[kg/m^3]$
Ω_1	3.28e-3	845
Ω_2	1.39e-3	987

Table 7.1: Material properties

x_{CP}	C_0	C_1	C_2	C_3	C_4
0	1.625	28.078	222.786	0	0

Table 7.2: Model parameters for the variable surface tension (*n*-butanol - water - succinic acid).

The concentrations in Ω_1 and Ω_2 are denoted by c_1 and c_2, respectively. At $t = 0$, the water phase contains a solute of succinic acid with initial concentration $c_2(0) > 0$ while the dispersed phase is clean. The initial condition for the mass transport problem is

$$c(\mathbf{x}, 0) := c_0 = \begin{cases} 0 & \text{in } \Omega_1, \\ c_2(0) & \text{in } \Omega_2. \end{cases}$$

Thus, this initial condition doesn't satisfy the Henry condition.

The Henry constant for the system at 20°C is $\beta = (1.2143, 1)$. The real diffusion coefficient $\alpha_r = (2.29 \cdot 10^{-10}, 5.8345 \cdot 10^{-10})\,\mathrm{m}^2/\mathrm{s}$ is extremely small and the mass transport equation is strongly convection dominated. In this case, Nitsche's discretization of the mass transport in Chapter 6 is not suitable for a stable discretization of this problem. A suitable stabilization for the Nitsche's discretization is not available, yet. Moreover, the thin concentration boundary layer requires a very high resolution at the interface, which leads to high computational cost. Thus, in our simulation, we use the (much) larger values $\alpha_F = F \cdot \alpha_r$ with different large factors $F \gg 1$ for the diffusion coefficient in order to obtain reliable numerical results, which are however not physically realistic and thus cannot be verified by experiments.

In [MBS85] the surface tension coefficient τ based on the experimental data for different systems has the form

$$\tau = \frac{1}{1 - C_4 x_C} \sum_{n=0}^{3} C_n (x_C - x_{CP})^n \quad [10^{-3}\,\mathrm{N/m}], \tag{7.2}$$

where $x_C = c_2|_\Gamma$ is the restriction to the interface of the weight fraction of the solute in the continuous phase. The coefficients x_{CP} and $C_i (i = 1, \ldots, 4)$ depend on the specific system. For the *n-butanol - water - succinic acid* system, these coefficients (at 20°C) are given in Table 7.2. In this case, τ is a quadratic function of x_C. For other systems, for example *toluene-water - acetone*, the coefficients C_2, C_3, C_4 and x_{CP} are non-zero. Due to

the limited solubility of succinic acid in water, which is 5.8% at 20°C , the model (7.2) for the surface tension coefficient τ is valid for x_C in the interval $[0, 0.058]$, as shown in Figure 7.1. In simulations with a constant τ, we take $\tau = 1.625 \cdot 10^{-3}\,\mathrm{N/m}$.

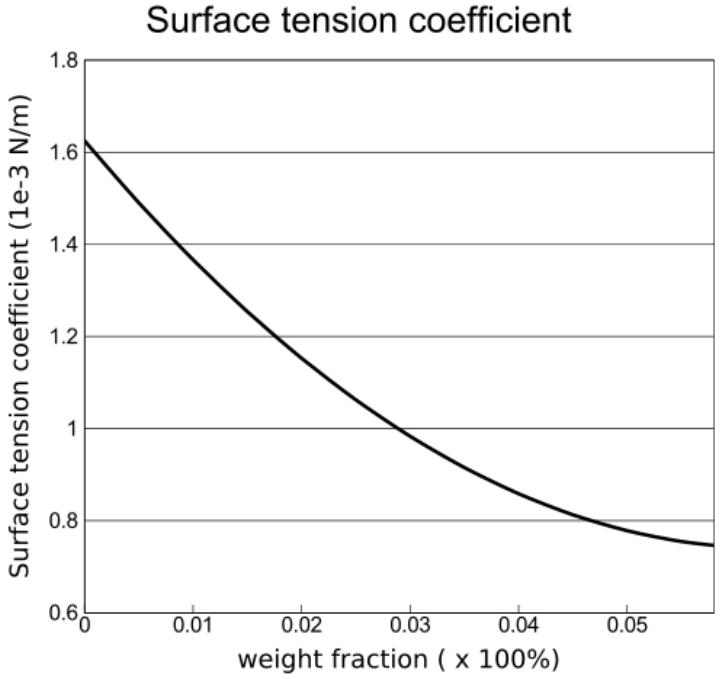

Figure 7.1: Surface tension coefficient τ vs. x_C.

In our simulations, we study the effects of the initial concentration $c_2(0)$ and the size of the convection (relative to the diffusion) on the rising velocity of the droplet and the steady state concentration. For the first case, we choose a fixed diffusion coefficient α_F with $F = 10^5$ and perform simulations with different values of the initial concentration $c_2(0)$. Numerical results for $c_2(0) = 1\%, 2.5\%$ and 5% will be presented.

Since the real diffusion coefficient cannot be used, we also perform simulations with different values of the diffusion coefficient α_F for the same initial concentration $c_2(0) = 1\%$. The smaller the diffusion coefficient is, the more convection dominated the mass transport problem becomes.

7.2 Numerical methods

In this section we briefly discuss important methods needed for numerically solving systems resulting from the discretization of the Navier-Stokes and mass transport equations and for maintaining the level set function. We give an overview of the methods used for our simulations.

7.2.1 Iterative solvers

Decoupling and linearization

In the time discretization of the Navier-Stokes and level set equations, if the generalized θ-scheme in Section 3.3.1 is used, we have a nonlinear coupling between the flow variables and the level set function. In [RFG+, Reu09], a fixed point iteration method is used for the decoupling of the flow variables and the level set function. This technique can also be applied for the case of a mass concentration dependent surface tension coefficient.

However, we take a simpler approach, although in general less accurate, using the linearized θ-scheme time integration presented in section 3.3.2. As discussed in Section 3.3.2, in this time-stepping scheme, the Navier-Stokes and the level set equations are decoupled. Moreover, since the surface force f_Γ in the right-hand side of the Navier-Stokes equations (cf. (3.33)) is only evaluated at the old time step (using the old concentration), the mass transport can be solved after the Navier-Stokes equations. Hence, the fixed point iteration to linearize the couplings between the Navier-Stokes, level set and mass transport equations can be avoided.

In both cases, we obtain a nonlinear system resulting from the Navier-Stokes equations, which has the form

$$\begin{aligned} \mathbf{A}\mathbf{x} + \mathbf{N}(\mathbf{x})\mathbf{x} + \mathbf{B}^T\mathbf{y} &= \mathbf{b} \\ \mathbf{B}\mathbf{x} &= \mathbf{c}. \end{aligned} \tag{7.3}$$

Using an adaptive fixed point defect correction method from cf. [Tur99], the nonlinear system can be linearized. In each iteration, we obtain a discrete Oseen problem of the form:

$$\mathbf{K}\begin{pmatrix}\mathbf{x}\\ \mathbf{y}\end{pmatrix} := \begin{pmatrix}\hat{\mathbf{A}} & \mathbf{B}^T\\ \mathbf{B} & 0\end{pmatrix}\begin{pmatrix}\mathbf{x}\\ \mathbf{y}\end{pmatrix} = \begin{pmatrix}\mathbf{f}_1\\ \mathbf{f}_2\end{pmatrix}, \quad \hat{\mathbf{A}} := \mathbf{A} + \mathbf{N}(\mathbf{x}^{\text{old}}) + \beta\mathbf{M}. \tag{7.4}$$

This linear system can be solved by the iterative linear solvers presented in the next subsection.

Iterative linear solvers

The large, sparse linear systems resulting from the discretization and linearization of the Navier-Stokes, level set and mass transport equations are in general non-symmetric and will be solved by iterative methods. In our simulations we use preconditioned Krylov subspace methods, cf. [Saa03]. For systems obtained from the level set and mass transport problems, the GMRES method is used.

The saddle point system (7.4) is solved by preconditioned GCR (Generalized Conjugate Residual) or FGMRES (Flexible GMRES) methods , cf. [Saa03]. The main reason for using these methods is that they can be used with a variable preconditioner. We use a block-preconditioner in [EHS+06] of the form

$$\begin{pmatrix} \mathbf{Q}_A & \mathbf{B}^T \\ 0 & -\mathbf{Q}_S \end{pmatrix}. \tag{7.5}$$

Here $\mathbf{Q}_A$ and $\mathbf{Q}_S$ are preconditioners of the matrix $\mathbf{A}$ and the Schur complement $\mathbf{S} = \mathbf{B}\mathbf{A}^{-1}\mathbf{B}^T$, respectively. These preconditioners are briefly addressed below.

7.2.2 Reparametrization and mass conservation

Reparametrization

During the evolution of the level set function ϕ, its shape may become distorted. Thus, a reinitialization of the level set function is needed to keep it close to an approximate signed distance function. The new level set function should satisfy following properties, cf. [Gro08, Reu09]:

- The zero level of ϕ should be preserved.
- The norm of its gradient should be close to 1.
- The reparametrization can be used to smooth ϕ (close to the interface) and thus stabilize the evolution of the level set function.

Popular reparametrization methods are the re-initialization based on a pseudo time-stepping scheme for the Eikonal equation $\|\nabla\psi\| = 1$, cf. [SSO94, SF99] and the Fast Marching method, cf. [Set96a, KS98, Set99].

In our simulations we use the Fast Marching method. For discussion of the method, we refer to [Hup06, RFG+, Gro08].

Mass conservation

The loss of mass by discretizations of the level set function can be reduced if the grid is refined. However, this will lead to higher computational costs. We use another method, cf. [RFG+, Gro08], in which the level set method is shifted over a distance δ in the normal direction, such that the volumes of both phases remain unchanged. Since the level set function is close to the signed distance function, it can be done by subtracting δ from the level set function.

7.2.3 Overview of numerical methods

We summarize the main components used in our numerical simulations:

- A multilevel triangulation is used for the spatial discretization, cf. Section 3.2.1. For the initial triangulation, we partition the domain into $10 \times 20 \times 10$ cubes and then each of them is subdivided into six tetrahedra. The grid is then refined three times further near the interface, which results in the smallest mesh size about $2.5 \cdot 10^{-4}\,\mathrm{m}$. When the interface evolves, the grid will be adaptively refined and coarsened. In Figure 7.2 the grid on the plane $x = 0.01$ and the interface at $t = 0$ and $t = 0.4\,\mathrm{s}$ is shown.

- The finite element pair $(\mathbf{V}_h, Q_h^\gamma)$ for velocity and pressure in the Navier-Stokes equations. For the level set, we use piecewise quadratics with SDFEM stabilization, cf. section 3.2.4. The XFEM space Q_h^γ is also use for the mass concentration. The cut-off parameter $\tilde{c} = 0.1$ is chosen.

- The improved Laplace-Beltrami discretization (4.6) is used for the surface force f_Γ for the case τ is constant. In the variable surface tension coefficient case, the generalized Laplace-Beltrami discretization (4.9) is used.

- The Fast Marching Method and a volume correction technique in Section 7.2.2 are used to correct the level set function.

- The mass transport equation is discretized first in time using the implicit Euler scheme. The obtained problem is discretized in space using the Nitsche's method cf. Chapter 6. We choose the parameter $\lambda = 100$.

- The linearized θ-scheme (3.33) for the time integration for the Navier-Stokes and level set equation is used to avoid the nonlinear coupling between the variables. The time step size $\Delta t = 5 \cdot 10^{-4}\,\mathrm{s}$ is used.

- In each time step, we use the adaptive fixed point defect correction method cf. [Tur99] for the linearization of the Navier-Stokes equations.

- The linear system

$$\begin{pmatrix} \hat{\mathbf{A}} & \mathbf{B}^T \\ \mathbf{B} & 0 \end{pmatrix} \begin{pmatrix} \mathbf{v} \\ \mathbf{q} \end{pmatrix} = \begin{pmatrix} \mathbf{r}_1 \\ \mathbf{r}_2 \end{pmatrix}.$$

  of the Oseen problem is solved by the GCR method with a block preconditioner of the form

$$\mathbf{P} = \begin{pmatrix} \mathbf{Q}_A & 0 \\ \mathbf{B} & -\mathbf{Q}_S \end{pmatrix}$$

  Here $\mathbf{Q}_A$ and $\mathbf{Q}_S$ are the preconditioners of the matrix $\mathbf{A}$ and the Schur complement $\mathbf{S} = \mathbf{B}\mathbf{A}^{-1}\mathbf{B}^T$, respectively. An application of $\mathbf{Q}_A^{-1}$ to a vector $\mathbf{b}$ is done by one multigrid V-cycle iteration to approximate $\mathbf{A}^{-1}\mathbf{b}$. For $\mathbf{Q}_S$ the BFB^T-preconditioner in [Elm99, EHS+06] is used.

All of the above-mentioned components have been implemented in the software package DROPS, cf. [DRO, GPRR02, RFG+].

7.3 Numerical results

7.3.1 Effects of the initial concentration

First we present numerical results for the case $c_2(0) = 1\%$. The mean concentration $\bar{c}$ in the droplet is shown in Figure 7.3. From $t \geq 0.3$, the value of $\bar{c}$ is almost constant and steady state concentration is obtained. We obtain $\bar{c} = 1.215\%$, which is approximately equal to $\beta_1 \cdot c_2(0)$, where $c_2(0)$ is the value of the initial concentration in the water phase. This value seems to be reasonable, since the volume of the droplet is very small in comparison to the volume of water and the problem is not strongly convection dominated. Note that if the convection is absent, the concentration at steady state is piecewise constant, with the droplet concentration approximate $\bar{c}^* = \beta_1 \cdot c_2(0)$.

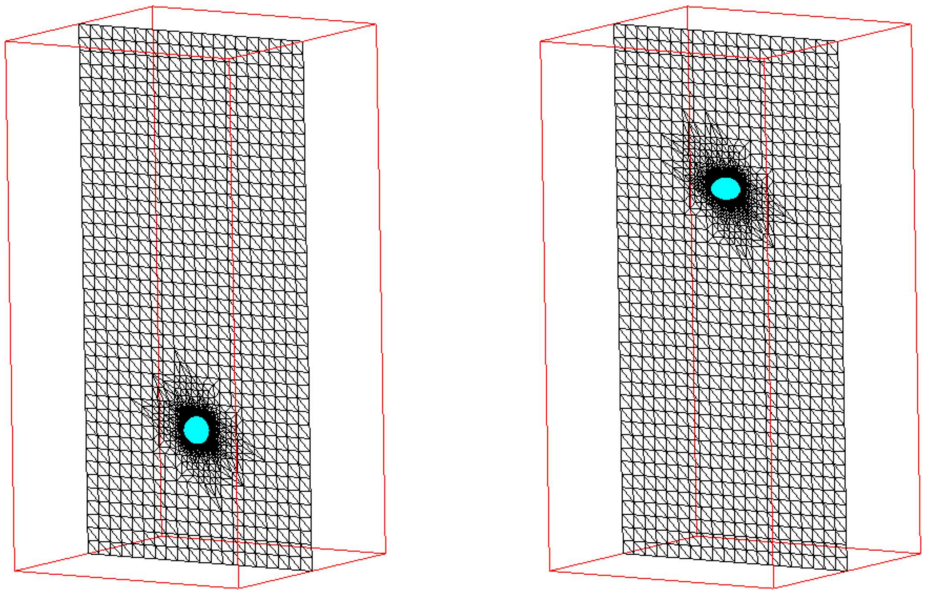

Figure 7.2: Part of the grid on the plane $x = 0.01$ at $t = 0$ (left) and $t = 0.4$ (right).

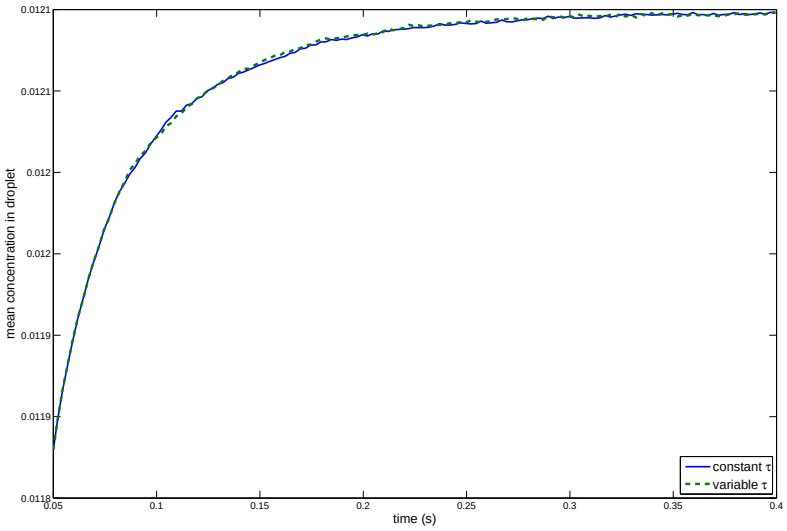

Figure 7.3: Mean concentration in the droplet: $c_2(0) = 1\%$, $F = 10^5$.

The concentrations on the plane $x = 0.01$ inside and outside of the droplet at different time steps are displayed in Figure 7.4 for constant τ, and in Figure 7.5 for variable τ. The values of the concentrations are not very different in these two cases. At the first stage, the velocity is very low and the mass transport is mainly due to diffusion. At the interface the concentration satisfies the Henry condition instantaneously, but in the middle of the droplet, the concentration is still very low due to the small diffusivity. After a short time ($t = 0.05\,\mathrm{s}$), as the droplet is accelerated, the role of the convection becomes larger. Then the concentration profile in the droplet is almost linear, cf. Figures 7.6. The maximal and minimal values are attained at the lower and upper part of the droplet, respectively. At the interface a boundary layer appears inside the elements intersected by the interface, since the numerical solution weakly satisfies the interface condition $[\alpha \nabla c \cdot \mathbf{n}]_\Gamma = 0$. These boundary layer are visualized in Figure 7.6. The width of the boundary layer may vary, depending on the position of the interface with respect to the grid. The concentration difference becomes larger until the steady state of the vertical velocity is obtained. Due to large diffusion, the concentration in the continuous phase far from the droplet remains approximately constant with the value of $c_2(0)$.

For the cases with larger initial concentrations, $c_2(0) = 2.5\%$ and $c_2(0) = 5\%$, we obtain similar behaviour of the concentration. The mean concentrations are displayed in Figures 7.7 and 7.8 while the concentration on the plane $x = 0.01$ are shown in Figure 7.9. The larger the initial concentration $c_2(0)$ is, the steeper the slope of the steady state droplet concentration becomes. Note that the high value of the slope is due to the small size of the droplet in comparison to the values of the concentration. However, for all cases we have approximately the same ratio $\frac{\max(c_1)}{\min(c_1)} = 1.15$ on the plane $x = 0.01$. For higher initial concentrations, the mean concentration in case of variable τ is slightly higher than that for constant τ, cf. Figure 7.8. This concentration difference might be the netto result of the following two phenomena which have opposite effects. On the one hand, the rising velocity in case of variable τ becomes smaller, which *reduces* the mass transport by convection in each phase. On the other hand, however, for higher concentrations, the corresponding variable surface tension coefficient is smaller (e. g. for the case $c_2(0) = 5\%$, $\tau_c \approx \tau_c(5\%) = 0.778 \cdot 10^{-3}\,\mathrm{N/m}$) than the constant value $\tau = 1.625 \cdot 10^{-3}\,\mathrm{N/m}$ and (due to this) the droplet becomes flatter. As the consequence, the interfacial area becomes larger, which *increases* the diffusive mass transport between two phases. The netto effect of these two

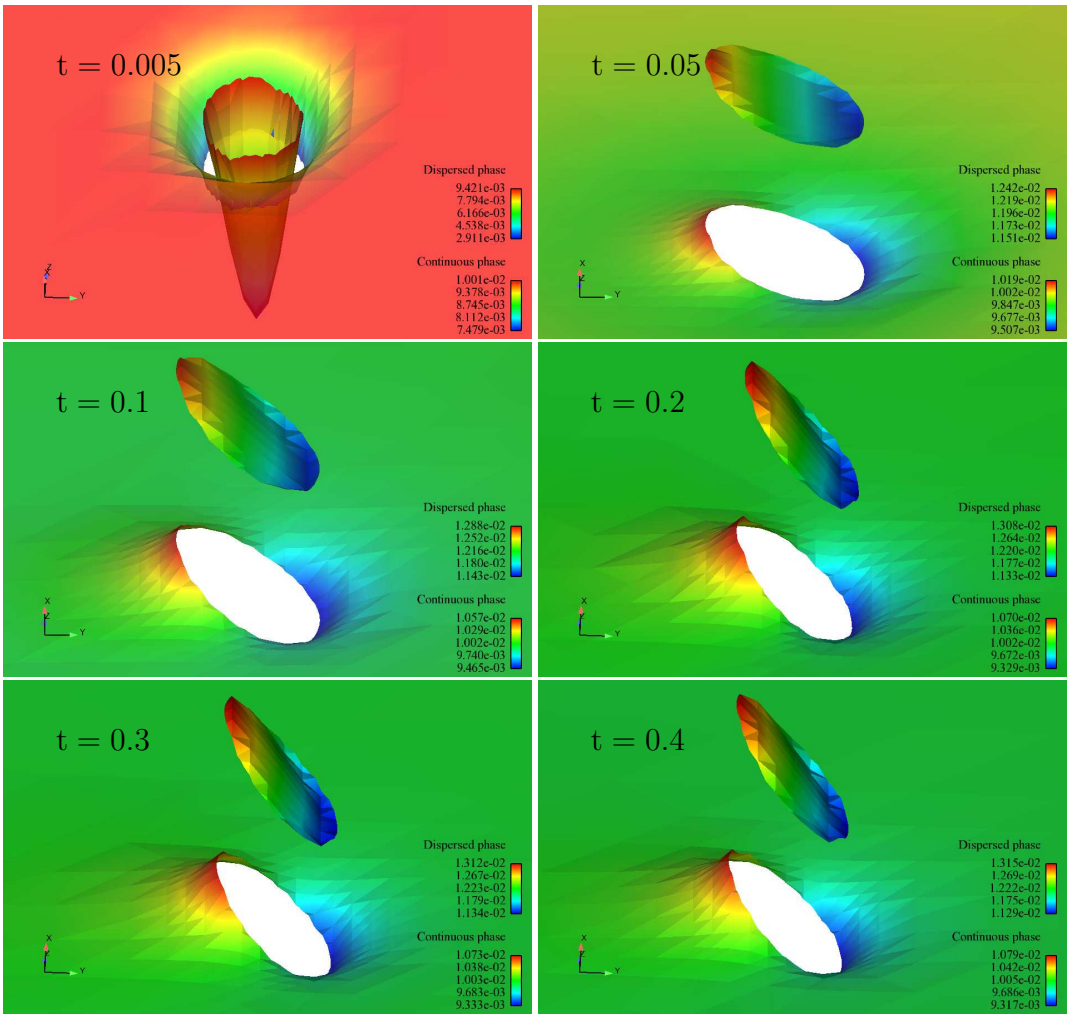

Figure 7.4: Concentration distribution around the droplet with constant τ on plane $x = 0.01$: $c_2(0) = 1\%$, $F = 10^5$.

phenomena may lead to a slightly higher transport rate for the case of variable τ.

Although the variable surface tension coefficient appears to have little effect on the concentration in droplet it does *have a significant effect on the dynamics of the droplet*. In Figure 7.10, the vertical velocity of the droplet with respect to different initial concentrations is plotted over the time. Note that for constant τ, the dynamics of the droplet is independent of the mass transport. After the same initial phase, due to Marangoni effects, the droplet

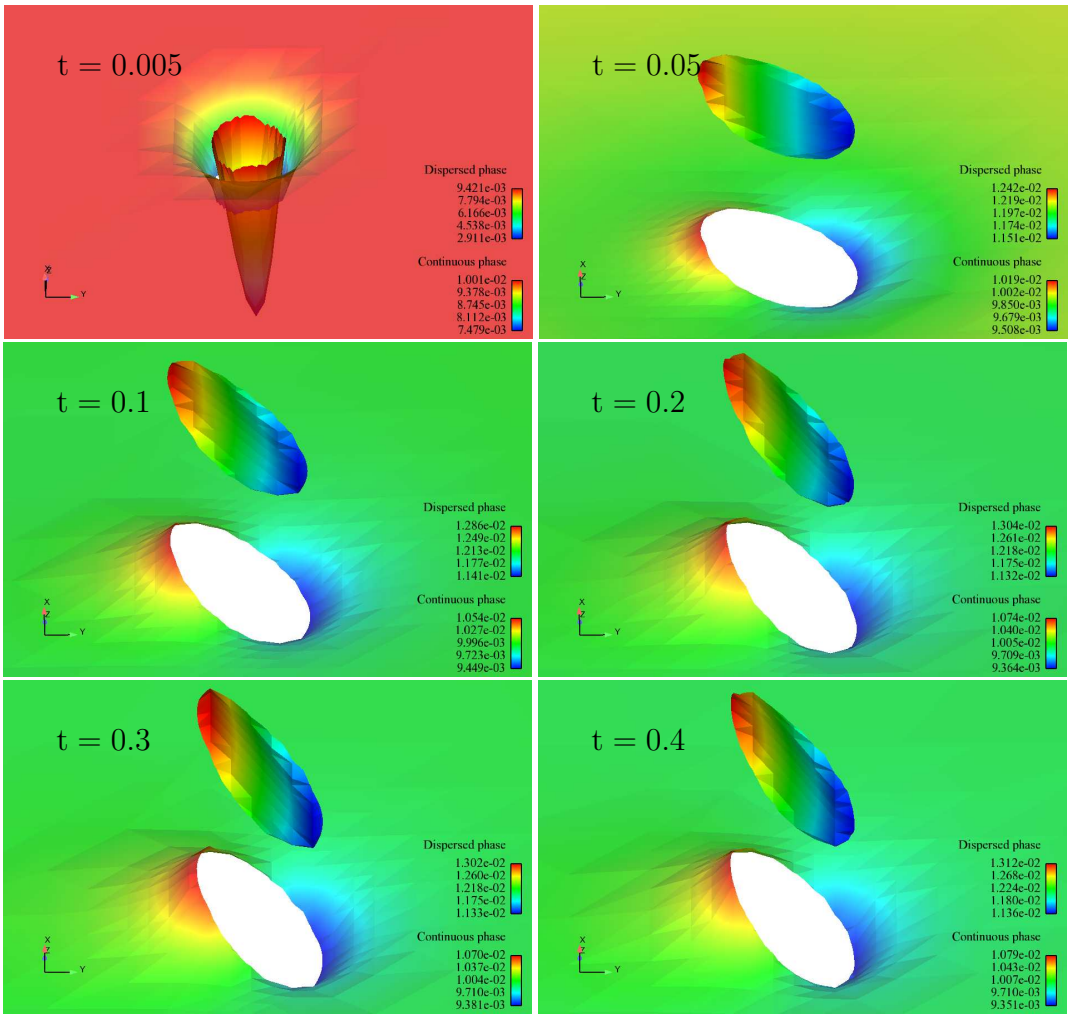

Figure 7.5: Concentration distribution around the droplet with variable τ on plane $x = 0.01$: $c_2(0) = 1\%$, $F = 10^5$.

velocity with variable τ is lower than the one with constant τ. Note that the variable surface tension τ is monotone decreasing in the interval $[0, 5.8\%]$. At the lower part of the interface, the higher concentration results in a lower value of the surface tension coefficient. Marangoni convection occurs, which retards the motion of the droplet. The larger the initial concentration $c_2(0)$ is, the stronger the Marangoni convection becomes. As a consequence, a lower value of the terminal droplet velocity is obtained. The values of the terminal velocity $\mathbf{v}_{sed}$ with respect to different initial concentrations are given

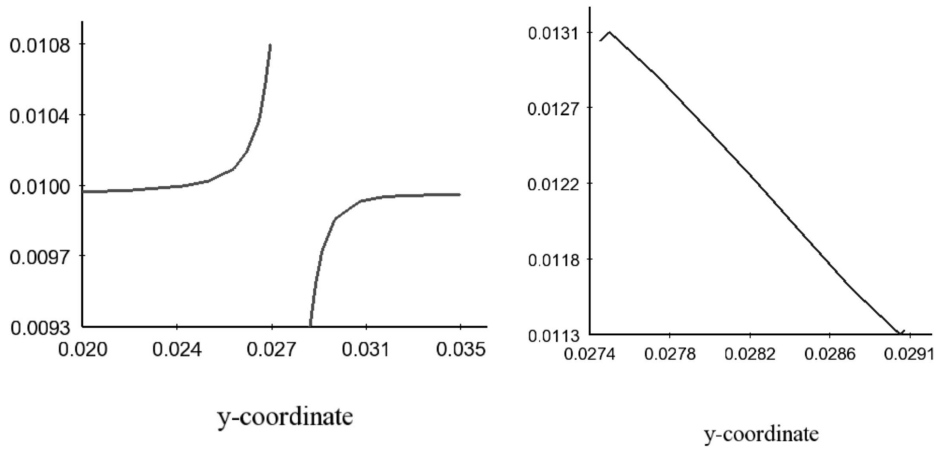

Figure 7.6: Concentration profile in the vicinity of the droplet along the symmetry axis at $t = 0.4$ in the water phase (left) and in the droplet (right): $c_2(0) = 1\%$, $F = 10^5$. Note that different scales are used for each picture and each axis.

in Table 7.3, which qualitatively agree with the results in [PW06, WFW$^+$07]. Moreover, for higher initial concentrations, the droplet becomes flatter, which also results in a slower rising velocity.

$\tau = const$	$c_2(0) = 1\%$	$c_2(0) = 2.5\%$	$c_2(0) = 5\%$
0.0532	0.0512	0.0488	0.0460

Table 7.3: Terminal velocity (m/s) of the droplet ($F = 10^5$).

In Figure 7.12 we show the vector fields of the relative velocity $\mathbf{v}_{rel} := \mathbf{v} - \mathbf{v}_{sed}$ with respect to the barycenter of the droplet (i. e. velocity in a Lagrangian reference system attached to the droplet) at steady state for the case $c_2(0) = 5\%$.

7.3.2 Effects of the convection term

In Section 7.3.1, we have shown results for simulations with $c_2(0) = 1\%$ for the case $F = 10^5$. In this section, we perform simulations using this initial concentration but with different diffusion coefficients to study the effects of the size of the convection term on the terminal velocity of the droplet and the steady state concentration. First we take a larger diffusion coefficient α_F with

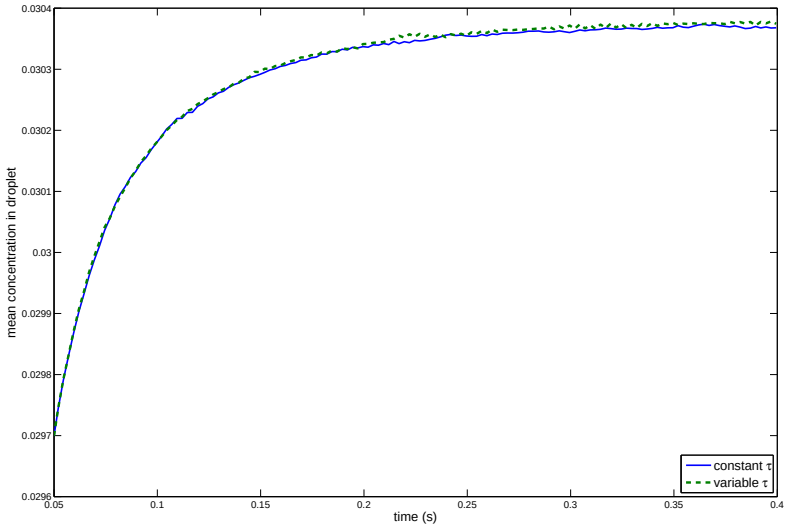

Figure 7.7: Mean concentration in the droplet: $c_2(0) = 2.5\%$, $F = 10^5$.

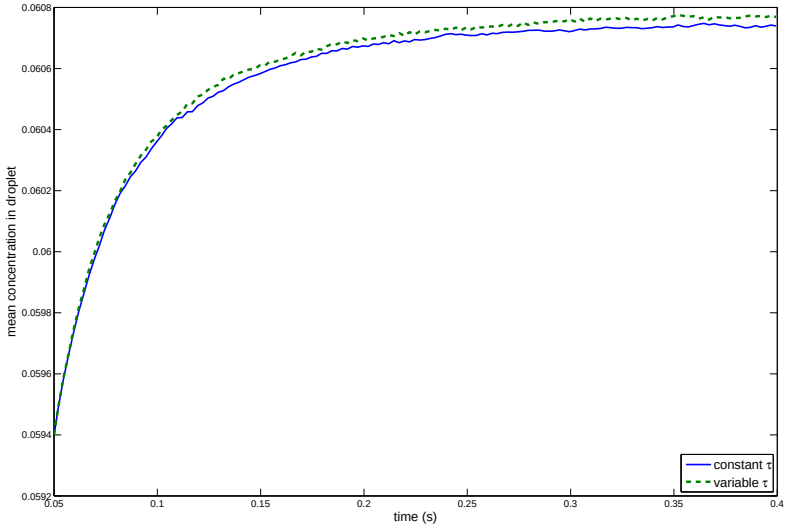

Figure 7.8: Mean concentration in the droplet: $c_2(0) = 5\%$, $F = 10^5$.

$F = 10^6$. Results for the concentration on the plane $x = 0.01$ are displayed in Figure 7.13. In this case, the diffusion dominates the mass transport. The steady state concentration is reached in a very short time, before the steady state velocity. In both cases, the steady state is obtained after less than 0.1 s, which is not very different from the concentration at $t = 0.01$ s. The steady state concentrations in both cases are almost identical. Due to convection, the concentration in the lower part of the droplet is still slightly higher than that in the upper one, but the slope of the droplet concentration is much smaller than that in the case with $F = 10^5$. In this case we have $\frac{\max(c_1)}{\min(c_1)} = 1.015$ on $x = 0.01$.

Simulations with a smaller diffusion coefficient α_F ($F = 10^4$) is also considered. In this case, the mass transport process is more dominated by convection. We use a finer grid in order to obtain a good approximation of the concentration. The domain is partitioned into $8 \times 16 \times 8$ cubes and then the grid near the interface is refined four times further. Since a different grid is used, the results for this case should be qualitatively (rather than quantitatively) compared with the ones in other cases. The distribution of the droplet concentration (shown in Figures 7.14-7.15) is very much different from those with higher diffusivities (i. e. $F = 10^5$ and $F = 10^6$). Since the diffusion is much weaker, the difference in concentration is not reduced as fast as in the case of larger diffusivities. Thus, the concentration below the droplet is much higher (compared to the case of larger diffusivity) than that in the upper part. At $t = 0.5$ s, the steady state concentration is not obtained, yet. The ratio $\frac{\max(c_1)}{\min(c_1)}$ (on $x = 0.01$) is 3.508 (constant τ) and 3.095 (variable τ), respectively. In a relatively large region below the droplet, the value of the concentration is not constant. The droplet mean concentration $\bar{c}$ is also larger than the value $\bar{c}^*$, as shown in Figure 7.16. At $t = 0.5$, the value of $\bar{c}$ is equal to 1.57% for constant τ, which is larger than the droplet mean concentration 1.538% for variable τ.

In Figure 7.17, the rising velocity of the droplet over time for different values of the diffusion coefficient is displayed. In the case of variable τ, Marangoni convection reduces the droplet velocity. For smaller diffusivity (i. e. larger Marangoni convection), the value of the velocity is also lower. The difference between the velocities in the cases of $F = 10^6$ and $F = 10^5$, however, is not noticeable. In contrast, the droplet velocity with respect to $F = 10^4$ is relatively smaller, due to large Marangoni convection. The corresponding terminal velocities are given in Table 7.4.

$\tau = const$	$F = 10^6$	$F = 10^5$	$F = 10^4$
0.0532	0.0515	0.0512	0.0486

Table 7.4: Terminal velocity (m/s) of the droplet for different diffusion coefficients.

The vector fields of the velocity in the Lagrangian reference system at steady state is shown in Figure 7.18. For variable τ, the high concentration gradient on the interface results in a *stagnant cap*, as discussed in Section 4.4. However, the shapes of the droplet in both cases are similar.

We summarize the main physical phenomena that we observed in our numerical experiments:

- Rising velocity: If the surface tension coefficient is variable, Marangoni effect occurs, which slows down the droplet. The higher the initial concentration is, the stronger the Marangoni convection becomes and thus, the slower the droplet velocity is. This is also observed in other literature [PW06, WFW$^+$07]. Note that in these papers, the direction of mass transport is from the droplet to the continuous phase, and the initial concentration $c_2(0)$ is equal to 0. When the time is sufficiently large, due to the small size of the droplet, the concentration in the continuous phase around the interface becomes very small and a re-acceleration of the droplet is observed, which is not the case in our simulation.

  Moreover, by higher initial concentration, the surface tension coefficient is reduced and the droplet becomes flatter, which also decreases the rising velocity. For convection dominated problems, the velocity field in the Lagrangian reference system attached to the droplet at steady state presents a stagnant cap, due to high concentration gradient on the interface.

- Profile of the droplet concentration: Due to convection, the concentration at the lower part of the droplet is higher than that in the upper part. For diffusion dominated problems, the droplet concentration profile at steady state is almost linear and the difference between the cases of constant τ and variable τ is not noticeable. The higher the initial concentration is, the steeper the slope of the droplet concentration profile becomes. For convection dominated problems, the concentration at the lower part of the droplet is much higher.

- Mean concentration in the droplet: For diffusion dominated problems, the mean concentration in the droplet at steady state is approximately equal to the mean concentration $\bar{c}^* = \beta_1 \cdot c_2(0)$ of the pure diffusion problem, since the volume of the droplet is very small in comparison to that of the water phase. For convection dominated problems, the mean concentration is relatively higher than $\bar{c}^*$.

- Boundary layer: At the interface, a boundary layer appears such that the interface condition $[\alpha \nabla c \cdot \mathbf{n}]_\Gamma = 0$ is satisfied. For convection dominated problems, a steep boundary layer in the water phase presents below the droplet.

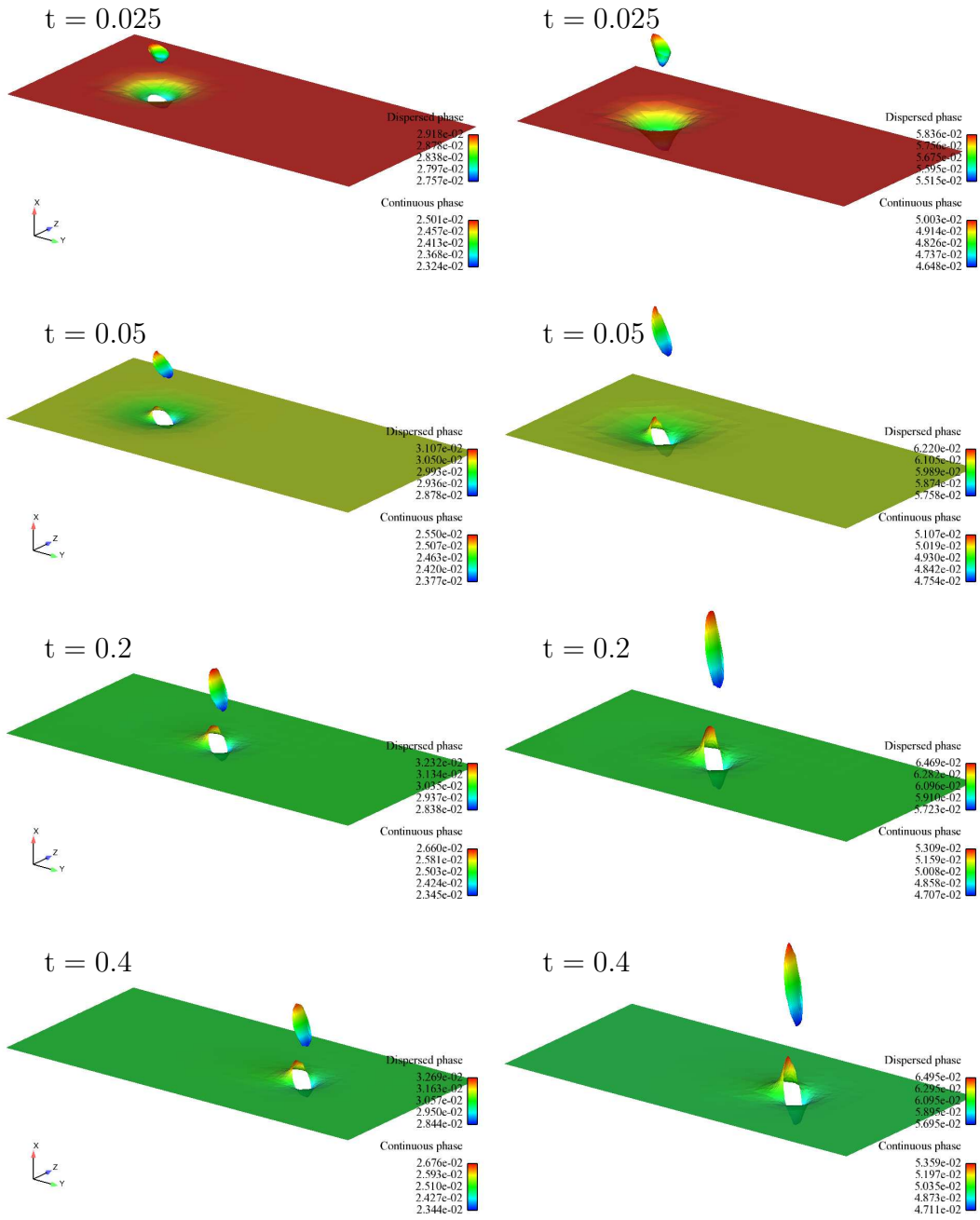

Figure 7.9: Concentration distribution with variable τ on plane $x = 0.01$: $c_2(0) = 2.5\%$ (left) and $c_2(0) = 5\%$ (right), $F = 10^5$.

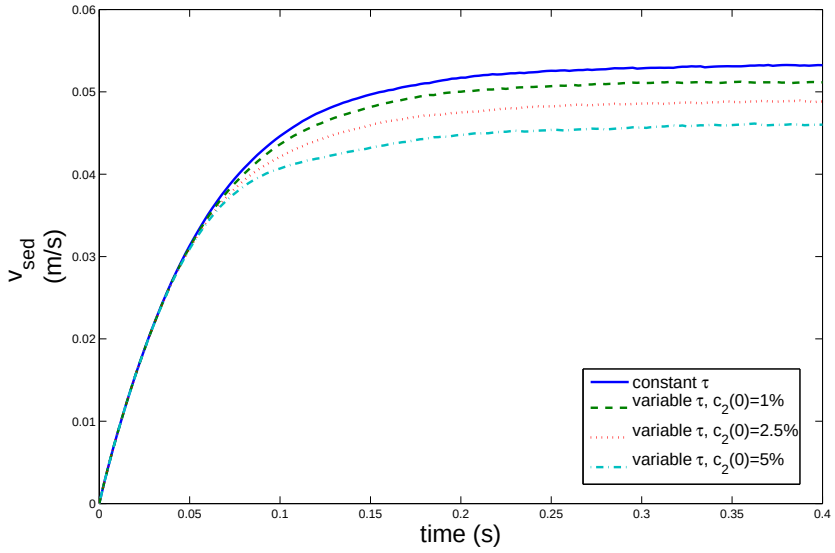

Figure 7.10: Rising velocity of the droplet ($F = 10^5$).

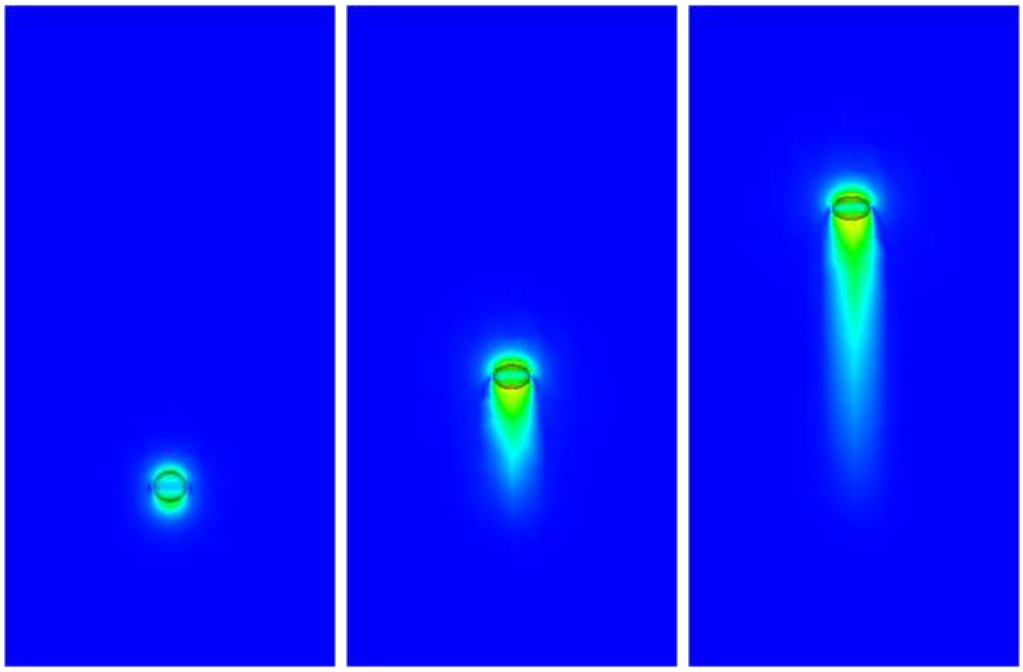

Figure 7.11: Dynamics of the rising droplet at $t = 0.05, 0.2, 0.4$, colour coding indicates velocity magnitude: $c_2(0) = 1\%$, $F = 10^5$.

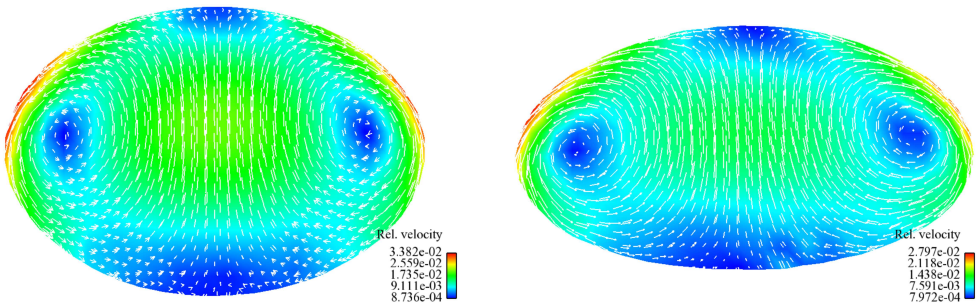

Figure 7.12: Velocity field in Lagrangian reference system at steady state : constant τ (left) and variable τ (right), $c_2(0) = 5\%$, $F = 10^5$.

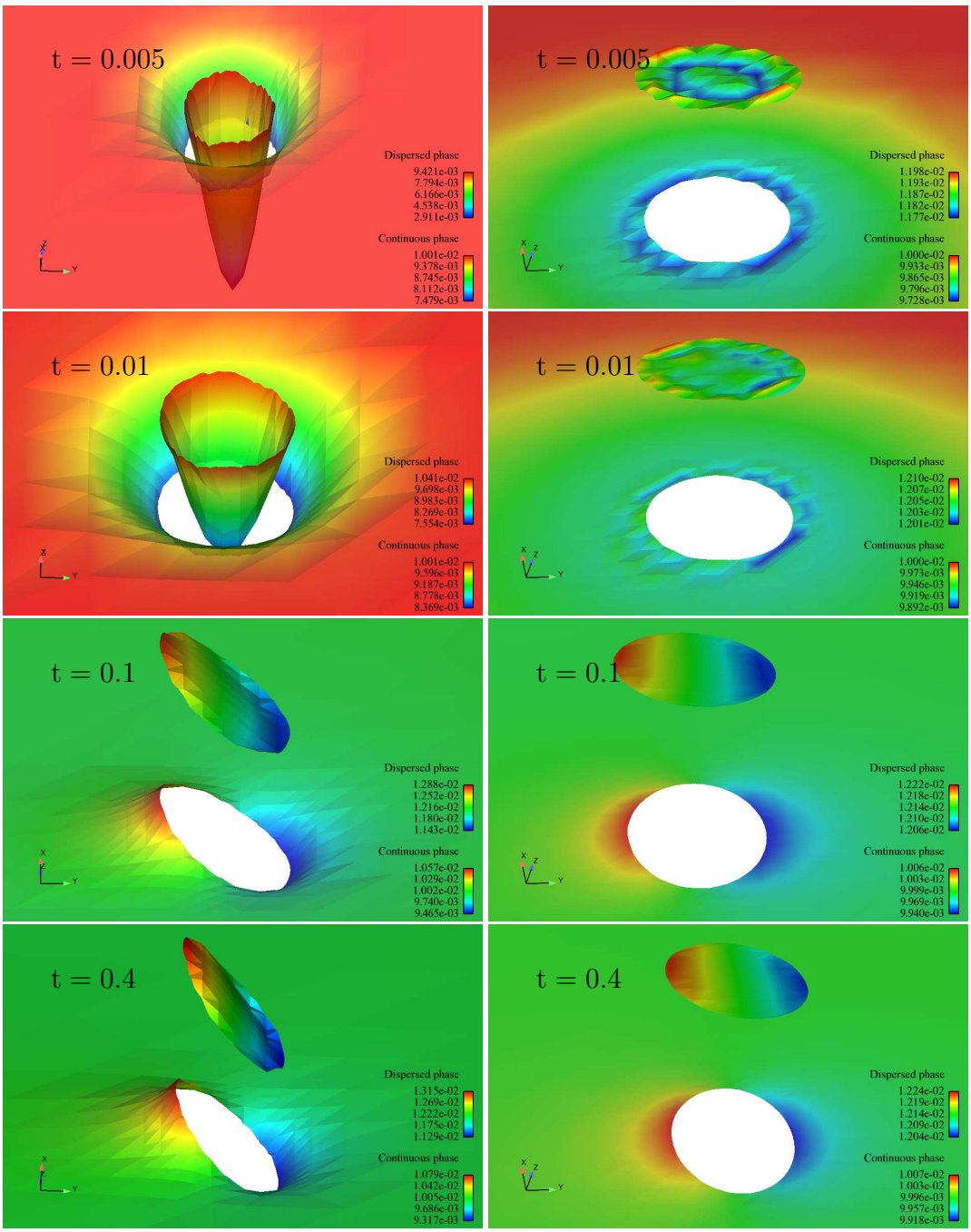

Figure 7.13: Concentration distribution around the droplet with constant τ on plane $x = 0.01$: $c_2(0) = 1\%$, $F = 10^5$ (left) and $F = 10^6$ (right).

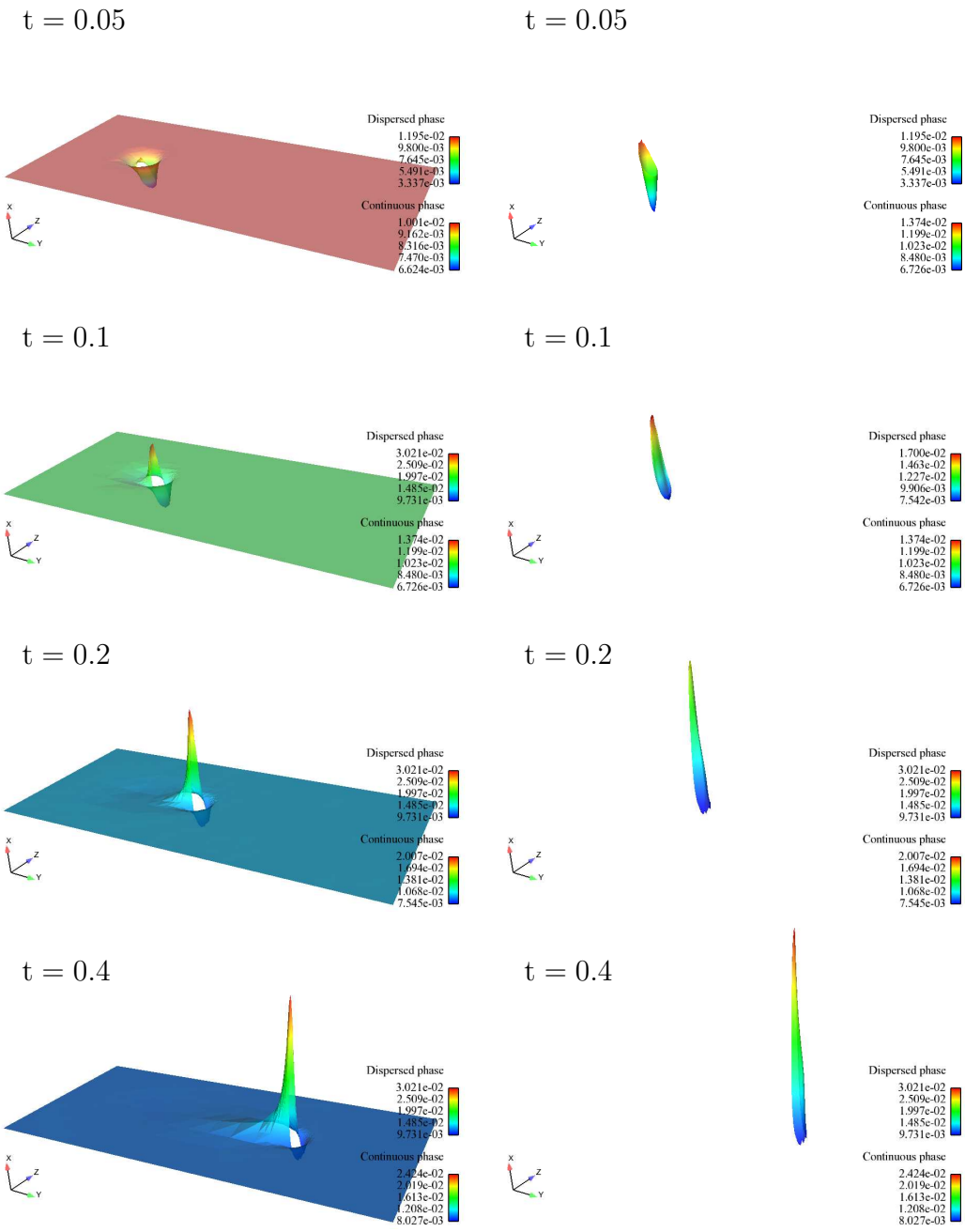

Figure 7.14: Concentration distribution in the water phase (left) and in the droplet (right) with constant τ on plane $x = 0.01$: $c_2(0) = 1\%$, $F = 10^4$.

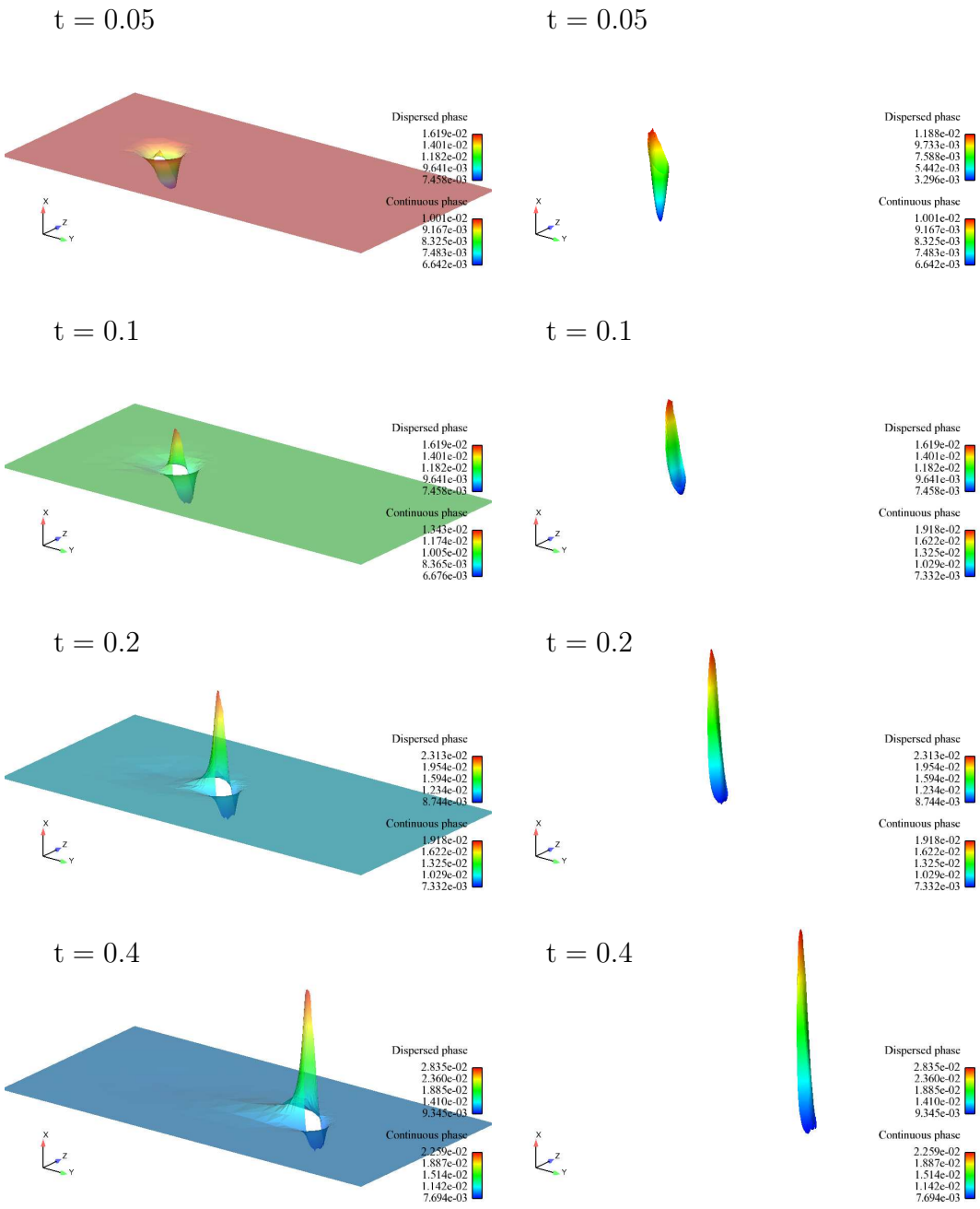

Figure 7.15: Concentration distribution in the water phase (left) and in the droplet (right) with variable τ on plane $x = 0.01$: $c_2(0) = 1\%$, $F = 10^4$.

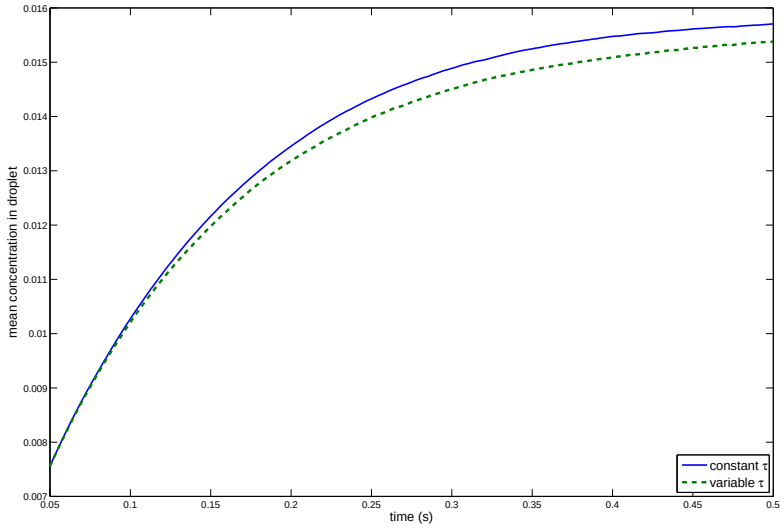

Figure 7.16: Mean concentration in the droplet: $c_2(0) = 1\%$, $F = 10^4$.

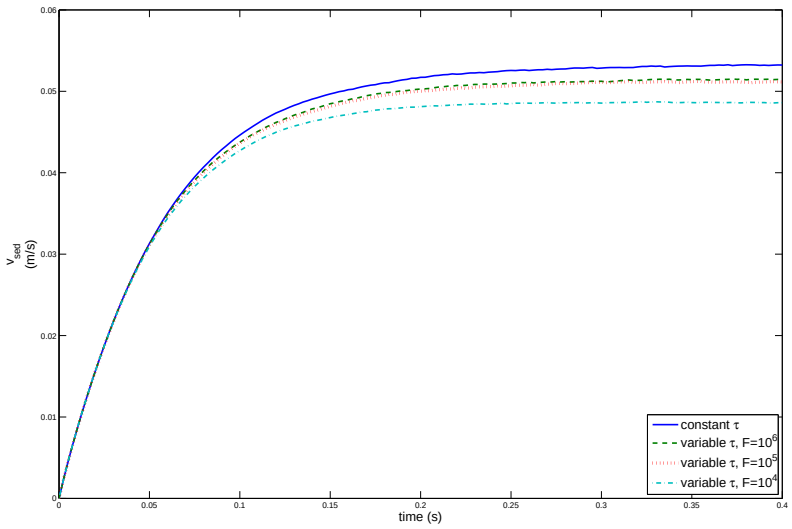

Figure 7.17: Rising velocity of the droplet for different diffusion coefficients.

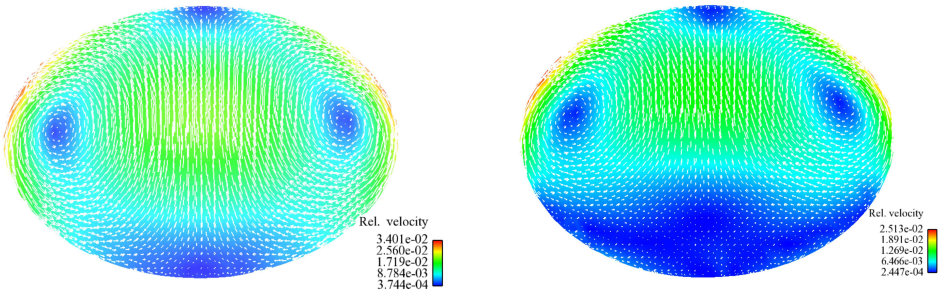

Figure 7.18: Velocity field in the Lagrangian reference system at steady state: constant τ (left) and variable τ (right), $c_2(0) = 1\%$, $F = 10^4$.

Chapter 8

Summary and Outlook

In this thesis, we presented numerical methods for discretizing and solving the mass transport problem in two-phase flows. For the two-phase Navier-Stokes equations, which model the motion of the fluid, we used known methods introduced in [Gro08, Reu09], which include

- The level set method for capturing the (in general) moving interface.
- Finite element methods for the spatial discretizations of the Navier-Stokes and the level set equations. Key components are the improved Laplace-Beltrami technique in [GR07a] for discretizing the localized surface force term and the extended finite element method for the approximation of the discontinuous pressure in [GR07b]. For the case of a constant surface tension coefficient, the combination of these two methods results in an optimal discretization error bound for the solution of a model two-phase Stokes equations.
- The θ-scheme for the time discretization of the ODE problem resulting from the spatial discretization.

For mass transport problems, however, the surface tension coefficient often depends on the mass concentration, which causes Marangoni effects. In Chapter 4 we presented a new discretization of the localized surface force term for the case of a *variable* surface tension coefficient based on the improved Laplace-Beltrami method in [GR07a]. Numerical simulations in Chapter 4 and Chapter 7 using this discretization showed that different phenomena were observed when the surface tension coefficient is variable, such as the

occurrence of the so-called *stagnant cap* in the velocity field and a significant change in the droplet rising velocity. The results are qualitatively in agreement with the results from experiments in [ASB05] and numerical simulations in [PW06, WFW$^+$07].

The discretization of the mass transport equations treated in this thesis is *new*. The Henry's condition at the interface implies that the concentration is discontinuous across the interface. In the literature often a transformation technique is used that eliminates this discontinuity of the solution but leads to a suboptimal spatial discretization error bound. We used the Nitsche-XFEM method introduced in [HH02] to handle the Henry condition and obtained an optimal error estimate $\mathcal{O}(h^2)$ in the L^2-norm for the spatial discretization in the case of a *stationary* interface. This method can also be applied for problem with moving interface but a full error analysis is not available. In Chapter 7, we performed numerical simulations of a rising droplet problem for both cases of constant and concentration-dependent surface tension coefficients. For the latter case, Marangoni effects appear and the flow is also affected by the mass transport. Since the Nitsche-XFEM method presented in this thesis is not suitable for convection-dominated problems and the real diffusion coefficient for the considered system is extremely small, we used (much) larger diffusion coefficients and the numerical results cannot be compared to experiments.

We mention several open problems, which are necessary for the effectiveness and the improvements of the presented methods:

- An error analysis for the discretization of the localized surface force term for the case of a *variable* surface tension coefficient is not available, yet. Similar to the case of a constant surface tension coefficient, an error bound $\mathcal{O}(h)$ for the term $\sup_{\mathbf{v}_h \in \mathbf{V}_h} \frac{|f_\Gamma(\mathbf{v}_h) - \tilde{f}_{\Gamma_h}(\mathbf{v}_h)|}{\|\mathbf{v}_h\|_1}$ is expected to hold.

- The Nitsche-XFEM discretization is not stable for convection-dominated mass transport problems. In this case, a stabilization technique is needed in order to obtain reliable numerical solution.

- For the case of moving interfaces, a full error analysis of the Nitsche-XFEM is not known, yet.

- In our simulations, a simple variant of the θ-scheme is used to avoid the complicated couplings between the flow variables, the level set function and the solution of the mass transport equations. The method has,

however, only first order of accuracy. Higher order time discretizations are desirable.

- If a stabilization of the Nitsche-XFEM method has been developed and implemented then a system with physically correct diffusion coefficient can be simulated. The results of these simulations should be compared with experimental results in order to validate these simulations.

- Although the simulations in [BGG$^+$08, EGR08] have shown the superiority of XFEM method to the standard finite element discretization of the two-phase Navier-Stokes equations, the analysis of the LBB-stability for the $P2 - P1X$ pair is still an open question.

Bibliography

[Ama06] A. Amar. *Fluid dynamics of single levitated drops by fast NMR techniques*. PhD thesis, RWTH Aachen, 2006.

[ASB05] A. Amar, S. Stapf, and B. Blumich. Internal fluid dynamics in levitated drops by fast magnetic resonance velocimetry. *Physical Review E (Statistical, Nonlinear, and Soft Matter Physics)*, 72(3):030201, 2005.

[Bän01] E. Bänsch. Finite element discretization of the Navier-Stokes equations with a free capillary surface. *Numer. Math.*, 88:203–235, 2001.

[Bas96] P. Bastian. *Parallele adaptive Mehrgitterverfahren*. Teubner, Stuttgart, 1996.

[BBJ+97] P. Bastian, K. Birken, K. Johannsen, S. Lang, N. Neuß, H. Rentz-Reichert, and C. Wieners. UG – a flexible software toolbox for solving partial differential equations. *Comput. Vis. Sci.*, 1:27–40, 1997.

[Bey95] J. Bey. Tetrahedral grid refinement. *Computing*, 55:355–378, 1995.

[BGG+08] E. Bertakis, S. Groß, J. Grande, O. Fortmeier, A. Reusken, and A. Pfennig. Validated simulation of droplet sedimentation with finite-element and level-set methods. *Comp. Eng. Sci.*, 2008. submitted.

[BKP09] E. Bertakis, M. Kalem, and A. Pfennig. Experimental investigation and theoretical modeling of mass-transfer induced effects at interfaces of sedimenting droplets. In *5th International Berlin*

Workshop on Transport Phenomena with Moving Boundaries (IBW5), Berlin, Germany, October 2009. extended abstract.

[BKW+04] D. Bothe, M. Koebe, K. Wielage, J. Prüss, and H.-J. Warnecke. Direct numerical simulation of mass transfer between rising gas bubbles and water. In M. Sommerfeld, editor, *Bubbly Flows: Analysis, Modelling and Calculation*, Heat and Mass Transfer. Springer, 2004.

[BKWW03] D. Bothe, M. Koebe, K. Wielage, and H.-J. Warnecke. VOF-simulations of mass transfer from single bubbles and bubble chains rising in aqueous solutions. In *Proceedings 2003 ASME joint U.S.-European Fluids Eng. Conf.*, Honolulu, 2003. ASME. FEDSM2003-45155.

[BKZ92] J. U. Brackbill, D. B. Kothe, and C. Zemach. A continuum method for modeling surface tension. *J. Comput. Phys.*, 100:335–354, 1992.

[BMUP01] T. Belytschko, N. Moës, S. Usui, and C. Parimi. Arbitrary discontinuities in finite elements. *Int. J. Num. Meth. Eng.*, 50:993–1013, 2001.

[BP09] E. Bertakis and A. Pfennig. Modellierung von Tensideffekten an Einzeltropfen mit einer ortsabhngigen Grenzflchenspannung: Implementierung in CFD-Simulationen und Validierung durch NMR-Untersuchungen. In *ProcessNet-Fachausschuss Kristallisation und Fluidverfahrenstechnik*, Dortmund, Germany, March 2009. Poster.

[BSW83] R. E. Bank, A. H. Sherman, and A. Weiser. Refinement algorithms and data structures for regular local mesh refinement. In R. Stepleman, editor, *Scientific Computing*, pages 3–17. North-Holland, Amsterdam, 1983.

[CZ98] Z. Chen and J. Zou. Finite element methods and their convergence for elliptic and parabolic interface problems. *Numer. Math.*, 79:175–202, 1998.

[DRO] DROPS package for simulation of two-phase flows. `http://www.igpm.rwth-aachen.de/DROPS/`.

[Dzi91] G. Dziuk. An algorithm for evolutionary surfaces. *Numer. Math.*, 58:603–611, 1991.

[EG04] A. Ern and J.-L. Guermond. *Theory and practice of finite elements*. Springer, New York, 2004.

[EGR08] P. Esser, J. Grande, and A. Reusken. An extended finite element method applied to a levitated droplet problem. Preprint 291, IGPM, RWTH Aachen, 2008. Submitted.

[EHS+06] Howard Elman, Victoria E. Howle, John Shadid, Robert Shuttleworth, and Ray Tuminaro. Block preconditioners based on approximate commutators. *SIAM J. Sci. Comput.*, 27(5):1651–1668 (electronic), 2006.

[Elm99] Howard C. Elman. Preconditioning for the steady-state Navier-Stokes equations with low viscosity. *SIAM Journal on Scientific Computing*, 20:1299–1316, 1999.

[FZ09] T. P. Fries and A. Zilian. On time integration in the XFEM. *Int. J. Num. Meth. Eng.*, 79:69 – 93, 2009.

[GMT07] S. Ganesan, G. Matthies, and L. Tobiska. On spurious velocities in incompressible flow problems with interfaces. *Comp. Meth. Appl. Mech. Engng.*, 196:1193–1202, 2007.

[GPRR02] S. Groß, J. Peters, V. Reichelt, and A. Reusken. The DROPS package for numerical simulations of incompressible flows using parallel adaptive multigrid techniques. Preprint 227, IGPM, RWTH Aachen University, 2002.

[GR86] V. Girault and P. A. Raviart. *Finite Element Methods for Navier-Stokes Equations*, volume 5 of *Springer Series in Computational Mathematics*. Springer, Berlin, 1986.

[GR05] S. Groß and A. Reusken. Parallel multilevel tetrahedral grid refinement. *SIAM J. Sci. Comput.*, 26(4):1261–1288, 2005.

[GR07a] S. Groß and A. Reusken. An extended pressure finite element space for two-phase incompressible flows with surface tension. *J. Comput. Phys.*, 224:40–58, 2007.

[GR07b] S. Groß and A. Reusken. Finite element discretization error analysis of a surface tension force in two-phase incompressible flows. *SIAM J. Numer. Anal.*, 45(4):1679–1700, 2007.

[Gro08] S. Groß. *Numerical methods for three-dimensional incompressible two-phase flow problems*. PhD thesis, RWTH Aachen, 2008.

[GRR06] S. Groß, V. Reichelt, and A. Reusken. A finite element based level set method for two-phase incompressible flows. *Comp. Visual. Sci.*, 9(4):239–257, 2006.

[GW01] I. Ginzburg and G. Wittum. Two-phase flows on interface refined grids modeled with VOF, staggered finite volumes, and spline interpolants. *J. Comput. Phys.*, 166:302–335, 2001.

[Han05] P. Hansbo. Nitsche's method for interface problems in computational mechanics. *GAMM-Mitt.*, 28(2):183–206, 2005.

[HH02] A. Hansbo and P. Hansbo. An unfitted finite element method, based on Nitsche's method, for elliptic interface problems. *Comput. Methods Appl. Mech. Engrg.*, 191:5537–5552, 2002.

[HH04] A. Hansbo and P. Hansbo. A finite element method for the simulation of strong and weak discontinuities in solid mechanics. *Comput. Methods Appl. Mech. Engrg.*, 193:3523–3540, 2004.

[HHL03] A. Hansbo, P. Hansbo, and M.G. Larson. A finite element method on composite grids based on Nitsche's method. *Math. Model. Numer. Anal.*, 37:495–514, 2003.

[HJ07a] B. Heinrich and B. Jung. The Fourier-Nitsche-mortaring for elliptic problems with reentrant edges. *Computing*, 80:221–246, 2007.

[HJ07b] B. Heinrich and B. Jung. Nitsche finite element method for parabolic problems. Preprint, Department of Mathematics, Technical University Chemnitz, 2007.

[HN81] C. W. Hirt and B. D. Nichols. Volume of fluid (VOF) method for the dynamics of free boundaries. *J. Comput. Phys.*, 39:201–22, 1981.

[HN03] B. Heinrich and S. Nicaise. The Nitsche mortar finite-element method for transmission problems with singularities. *IMA J. Numer. Anal.*, 23:331–358, 2003.

[HP02] B. Heinrich and K. Pietsch. Nitsche type mortaring for some elliptic problem with corner singularities. *Computing*, 68:217–238, 2002.

[HP05] B. Heinrich and K. Pönitz. Nitsche type mortaring for singularly perturbed reaction-diffusion problems. *Computing*, 75:257–279, 2005.

[Hup06] M. Huppertz. Reparametrization techniques for level set methods. Diploma thesis, IGPM, RWTH Aachen University, 2006.

[Ish75] M. Ishii. *Thermo-Fluid Dynamic Theory of Two-Phase Flow.* Eyrolles, Paris, 1975.

[JL04] A. J. James and J. Lowengrub. A surfactant-conserving volume-of-fluid method for interfacial flows with insoluble surfactant. 201(2):685–722, 2004.

[KAT07] M. N. Kashid, D. W. Agar, and S. Turek. Cfd modelling of mass transfer with and without chemical reaction in the liquid-liquid slug flow microreactor. *Chemical Engineering Science*, 62:5102–5109, 2007.

[KS98] R. Kimmel and J. A. Sethian. Computing geodesic paths on manifolds. *Proc. Natl. Acad. Sci. USA*, 95(15):8431–8435, 1998.

[LM72] J.L. Lions and E. Magenes. *Nonhomogeneous boundary value problems and applications.* Springer-Verlag, New York, 1972.

[LRU66] O. Ladyzenskaya, V. Rivkind, and N. Ural'tseva. The classical solvability of diffraction problems. In *Proc. Steklov Inst. Math.*, volume 92, pages 132–166, 1966.

[LU68] O. Ladyzenskaya and N. Ural'tseva. *Linear and Quasilinear Elliptic Equations.* Academic Press, New York, 1968.

[MBS85] T. Misek, R. Berger, and J. Schröter. *Standard Test Systems for Liquid Extraction.* The Institution of Chemical Engineers, Warwickshire, second edition, 1985.

[MC04] Z. S. Mao and J. Chen. Numerical simulation of the Marangoni effect on mass transfer to single slowly moving drops in the liquid-liquid system. *Chemical Engineering Science*, 59:1815–1828, 2004.

[MDB99] N. Moës, J. Dolbow, and T. Belytschko. A finite element method for crack growth without remeshing. *Int. J. Num. Meth. Eng.*, 46:131–150, 1999.

[Nit71] J. Nitsche. Über ein Variationsprinzip zur Lösung von Dirichlet-Problemen bei Verwendung von Teilräumen, die keinen Randbedingungen unterworfen sind. *Abh. Math. Sem. Univ. Hamburg*, 36:9–15, 1971.

[OS88] S. Osher and J. A. Sethian. Fronts propagating with curvature dependent speed: algorithms based on Hamilton-Jacobi formulations. *J. Comput. Phys.*, 79:12–49, 1988.

[PW06] A. R. Paschedag and M. Wegener. Three-dimensional simulations of mass transfer at single droplets. In *Proceedings of the Fifth International Conference on Computational Fluid Dynamics in the Process Industries*, 2006.

[Reu08] A. Reusken. Analysis of an extended pressure finite element space for two-phase incompressible flows. *Comp. Visual. Sci.*, 11:293–305, 2008.

[Reu09] A. Reusken. Numerical methods for two-phase incompressible flows. Lecture notes, IGPM, RWTH Aachen, 2009.

[RFG+] A. Reusken, O. Fortmeier, J. Grande, S. Groß, M. Larin, H. Nguyen, and P. Esser. *DROPS package, User's guide.* IGPM, RWTH Aachen University.

[RN09] A. Reusken and T. H. Nguyen. Nitsche's method for a transport problem in two-phase incompressible flows. *J. Fourier Anal. Appl.*, 2009.

[Saa03] Y. Saad. *Iterative Methods for Sparse Linear Systems*. SIAM, Philadelphia, PA, USA, 2003.

[SAC97] S. S. Sadhal, P .S. Ayyaswamy, and J .N. Chung. *Transport Phenomena with Droplets and Bubbles*. Springer, New York, 1997.

[Set96a] J. A. Sethian. A fast marching level set method for monotonically advancing fronts. *Proc. Natl. Acad. Sci. USA*, 93:1591–1595, 1996.

[Set96b] J. A. Sethian. Theory, algorithms, and applications of level set methods for propagating interfaces. *Acta Numerica*, 5:309–395, 1996.

[Set99] J. A. Sethian. *Level Set Methods and Fast Marching Methods*. Cambridge University Press, 1999.

[SF99] M. Sussman and E. Fatemi. An efficient interface preserving level set re-distancing algorithm and its application to interfacial incompressible fluid flow. *SIAM J. Sci. Comput.*, 20(4):1165–1191, 1999.

[Sla99] J. C. Slattery. *Advanced Transport Phenomena*. Cambridge Universtiy Press, Cambridge, 1999.

[Smo01] A. Smolianski. *Numerical Modeling of Two-Fluid Interfacial Flows*. Phd thesis, University of Jyvaskyla, 2001.

[SSO94] M. Sussman, P. Smereka, and S. Osher. A level set approach for computing solutions to incompressible two-phase flow. *J. Comput. Phys.*, 114:146–159, 1994.

[Tem84] R. Temam. *Navier-Stokes equations, theory and numerical analysis*. North-Holland, Amsterdam, 3rd ed., 1984.

[Tem88] R. Temam. *Infinite-dimensional dynamical systems in mechanics and physics*. Springer, New York, 1988.

[Tho97] V. Thomee. *Galerkin finite element methods for parabolic problems*. Springer, Berlin, 1997.

[Tur99] S. Turek. *Efficient Solvers for Incompressible Flow Problems: An Algorithmic and Computational Approach*, volume 6 of *Lecture Notes in Computational Science and Engineering*. Springer, Berlin, Heidelberg, 1999.

[UT92] S. O. Unverdi and G. Tryggvason. A front-tracking method for viscous, incompressible multi-fluid flows. *J. Comput. Phys.*, 100:25–37, 1992.

[WFW+07] M. Wegener, M. Fevre, Z. Wang, A. R. Paschedag, and M. Kraume. Marangoni convection in single drop flow - experimental investigations and 3d-simulations. In M. Sommerfeld, editor, *Proceedings of the International Conference on Multiphase Flows (ICMF), Leipzig, Germany*, 2007.

[WLW+08] J. Wang, P. Lu, Z. Wang, C. Yang, and Z. S. Mao. Numerical simulation of unsteady mass transfer by the level set method. *Chemical Engineering Science*, 63(12):3141–3151, 2008.

[YM05] C. Yang and Z. S. Mao. Numerical simulation of interphase mass transfer with the level set approach. *Chemical Engineering Science*, 60(10):2643–2660, 2005.